Alma Mater Studiorum – Università di Bologna

in cotutela con RWTH Aachen University

DOTTORATO DI RICERCA IN

CHIMICA

Ciclo XXXIII

Settore Concorsuale: 03/C2 - CHIMICA INDUSTRIALE

Settore Scientifico Disciplinare: CHIM/04 – CHIMICA INDUSTRIALE

UPGRADING BIO-PLATFORM MOLECULES IN THE GAS-PHASE: FROM LEVULINIC ACID TO BIO-CHEMICALS

Presentata da: Paola Blair Vasquez

Coordinatore Dottorato

Prof.ssa Domenica Tonelli

Supervisori

Prof. Fabrizio Cavani

Prof.ssa Regina Palkovits

Co-supervisori

Prof.ssa Stefania Albonetti

Dr. Tommaso Tabanelli

Esame finale anno 2021

Acknowledgement

Coming to Europe to pursue my PhD was an act of love and is from here where I should start to give thanks. Firstly, it was an act of love towards myself, believing that I could pursue whichever path I wanted to choose, and for constantly reminding myself of this. I am thankful to myself for being strong and resilient not only during the good times, but also when things seemed to fall apart. Moreover, I am thankful to my husband, who has always pushed me to fly even higher and who has always believed in me. It was you who made me see that I was capable of anything and everything, I just had to believe it myself. Thank you for the constant reminder, the constant support, and your unconditional love.

The person I am today and my achievements and successes are not a matter of coincidence, it is the work of my parents, their love, their support, and everything they sacrificed and did for me and my siblings. I will be forever grateful and proud of the home they created for us. Mom and dad, thank you so much for your unconditional love and for your constant support. This thesis, this work, and these years I have spent far away from you, are entirely dedicate to you two. I love you! And along this line, I must thank my siblings, who have always taken care of me, supported me, and pushed me to pursue even my crazier ideas. Thank you for being part of my role models and for always being there for me, no matter what.

Lastly, I want to thank to my colleagues, who have become my friends and my family away from home. Thank you to all the Catalytic Globtrotters. Special mention to my "Angels": Eleonora, Laura, Lisa and Giulia, thank you so much, girls! You are truly special, and I will be forever grateful for your friendship and your support. In addition, I want to thank my SINCHEM corner: Aisha and Vale, thank you for all of our philosophical conversations, for the silliness and the laughs and for your trust and your unconditional support. I know that no matter where we are in the world, I can count on you. Faso and Tito, I thank you for accepting and loving me for who I am, for allowing me to be 100% myself and for always supporting me and making me laugh when I needed it the most. Lastly, I must give thanks to the boss: thanks you so much Tommy, you have helped

me and guided me even when I was being impossible and when it was hard to agree with me. Thank you for having the patience of teaching me everything from scratch, I don't know what I would have done without your guidance.

I would also like to thank my Professors: Prof. Cavani, Prof, Albonetti and Prof. Palkovits, for their guidance and support throughout these three years of PhD.

Abstract

Levulinic acid (LA) is a polyfunctional molecule obtained from biomass. Because of its structure, the United States Department of energy has classified LA as one of the top 12 building block chemicals. Most commonly, it is valorized through chemical reduction to obtain γ-valerolactone (GVL). It is typically done with molecular hydrogen (H_2) in batch systems, with high H_2 pressures and noble metal catalysts, making it expensive and less applicable. Hence, alternative approaches such as the catalytic transfer hydrogenation (CTH) through the Meerwein–Ponndorf–Verley (MPV) reaction using heterogeneous transition metal oxide catalysts have been studied. This uses organic molecules, such as alcohols, which are capable of acting as a hydride transfer agent (H-donor), in order to reduce molecules containing carbonyl groups. Studies have reported the batch liquid-phase CTH of levulinate esters with secondary alcohols, given the stability of the carbocationic intermediate. Remarkable results have been obtained (in terms of GVL yield) over ZrO_2, given the need of a Lewis acid and base pair in order for CTH to take place. However, there were no studies in the literature reporting the continuous gas-phase CTH of levulinate esters. Therefore, high surface area ZrO_2 was tested for the gas-phase CTH of methyl levulinate (ML) at different temperatures using ethanol, methanol and isopropanol as H-donors. Under optimized conditions with ethanol (250 °C), the reaction is selective toward the formation of GVL (yield 70%). However, the deposition of heavy compounds over the catalysts surface progressively blocked Lewis acid sites leading to a progressive change in the chemoselectivity. The *in situ* regeneration of the catalyst permitted a partial recovery of the Lewis acid sites and an almost total recovery of the initial catalytic behavior, proving that the deactivation is reversible. Results obtained with methanol were not promising (conversion of 35% and GVL yield of 4%). However, as expected, using isopropanol a complete conversion was achieved with a GVL yield of 80%. The reaction was also tested using bioethanol derived from agricultural waste. In addition, a preliminary study was performed for the hydrogenolysis of polyols for the production of bioethanol. Pd-Fe catalyst was found to be active for the hydrogenolysis of glycerol, being quite selective towards ethanol (37%).

Table of Contents

1. Introduction

1.1. Green chemistry

Over the last decades, there has been an exponential growth of the world population, which, consequently, has sprouted an increase of the industrial activity, energy demand, consumption and waste generation. This situation has created, in addition, an increment on the pollution and emission generated, which have become society's biggest challenges. Therefore, there has been an increase in the public's awareness towards environmental problems related to the anthropogenic activities, which has moved governments to stablish more restrictive and binding laws in terms of emissions of pollutants and environmental and human safety in general. This led to the introduction of the terms *"green"* and *"sustainable"*, and with the issuing of the United States Pollution Prevention Act of 1990, a platform was set for Paul Anastas were he proposed the term "green chemistry", and with John Warner in 1993 developed the twelve principles of Green Chemistry[1]. Green chemistry and its principles seek to eliminate or minimize the hazards of chemical feedstock, reagents, solvents and products. It is defined as "the design of chemical products and processes to reduce or eliminate the use and generation of hazardous substances"[1–3]. For this purpose, the 12 principles of green chemistry[2] are the following:

1. Prevention of waste
2. Atom Economy, maximize material usage
3. Less hazardous chemical synthesis
4. Designing safer chemicals
5. Safer solvents and auxiliaries
6. Design for energy efficiency
7. Use of renewable feedstock

8. Reduce Derivatives
9. Catalysis
10. Design for degradation
11. Real-time analysis for pollution prevention
12. Inherently safer chemistry for accident prevention

1.2. Renewable feedstock: biomass

As previously mentioned, pollution and waste generation are two of society's biggest challenges. The uncontrolled industrial growth has had as main drawbacks the increase in the generation of wastes and in the emissions related to the use of petrochemical feedstock. Given these issues, the scientific community has been faced with the challenge of finding a solution to switch from petrochemical feedstock to renewable, abundant, and economic alternatives. Among them, bio-based building blocks have become of great interest given their potential as "synthon" for the production of several other valuable molecules. The majority of the bio-based chemicals identified as potential building blocks are sugars, sugar-derivatives, and lignin-derivatives.[4] Lignocellulosic biomass is a valuable starting material for producing bio-based chemicals at lower prices[5,6], because of its abundance. In order to ensure the supply of lignocellulosic biomass, government have started funding several projects which seek the production and collection of this type of biomass[7]. Along this line, the European Union (EU) has stated that 1 billion tons of lignocellulosic biomass will be produced on an annual basis by 2030[8]. In addition, different biotechnological advances in the United States of America suggest that 1.3 billion dry tons of this biomass could be produced without compromising the food security of the population[9].

Lignocellulosic biomass is composed by three different biopolymers that are characterized by their different chemical structure and properties:

- Lignin (15-30wt%): rigid bio-polymer characterized by a complex structure of cross-linked phenolic compounds which give mechanical chemical resistant to legnocellulose[10].
- Hemicellulose (25-35 wt%): highly branched polymer composed primarily of five-carbon sugars (mostly xylose). It is chemically bonded to lignin and serves as an interface between lignin and cellulose.
- Cellulose (35-55wt%): linear polymer of glucose linked by β-1,4 glycosidic bonds. Hydrogen bonds occur between adjacent cellulose polymers chains leading to a high crystallinity grade structure that gives structural strength to the plants and that makes cellulose particularly difficult to be attacked by enzymes[11].

The valorisation of biomass into energy and chemicals can be performed following three general strategies: thermochemical, chemical, and biochemical processes. Thermochemical process can be divided in two:

- Pyrolysis: it uses intermediate temperatures (300-600 °C) in the absence of oxygen to convert the feedstock into bio-oil, bio-char and light gases similar to syngas[12,13]. The bio-oil obtained is usually a dark complex mixture of polar and non-polar compounds consequence of the fragmentation and depolymerization of not only lignocellulose biopolymers, but also lipids and proteins in some types of biomass. As previously mentioned, bio-oil is a complex mixture which is composed of water, phenols, guaiacols, syringols, nitrogen containing compounds, fatty acids, aldehydes, ketones, sugars, hydrocarbons, and pyrolytic lignin. Depending on its composition, some bio-oils represent a promising starting material for the production of several valuable chemicals through microbial fermentation[14]. On the other hand, bio-char is a carbon-rich, fine-grained, porous substance which contains a high proportion of aromatic carbon, specifically fused aromatic structures. It can have different forms: amorphous carbon when pyrolysis is performed at low temperature pyrolysis, and turbostratic (disordered graphitic crystallites dominate) when operating at high temperatures. Bio-char has multiple uses, however, its most relevant and studied is its used for soil amendment. It has the ability of not only mitigating climate change by sequestrating carbon from atmosphere into soil but also of improving soil properties and enhancing soil fertility by improving moisture, nutrient retention and microbial activity[15–18].
- Gasification: it consists in treating biomass at high temperature (>700 °C) with low oxygen levels to produce syngas (H_2, CO, CO_2 and CH_4). This can then be used directly as biofuel or it can be exploited as a chemical intermediate for the production of fuels (e.g. ethanol) or chemicals (e.g. alcohols, ammonia, others)[12,19].

However, lignocellulose is typically treated and valorised following the chemical and biochemical processes, which consist on firstly separating lignin, hemicellulose and cellulose by means of

chemical or fermentation process, which then are broken down into simpler molecules from which a multiple variety of chemicals can be obtained.

- Biochemical: fermentation and anaerobic digestion are the typically used processes, in which low temperatures are employed and low reaction rates are obtained. Fermentation uses microorganisms and/or enzymes and anaerobic digestion takes place in the absence of oxygen and it involves the bacterial breakdown of organic material [20].
- Chemical: the most commonly used approaches are hydrolysis and transesterification. Hydrolysis usually uses mainly inorganic acid such as HCl and H_2SO_4 to depolymerize polysaccharides and proteins into their main constituents (e.g. glucose from cellulose and amino acids from proteins) or derivate chemicals (e.g. levulinic acid from glucose). Nonetheless, organic acids such as oxalic, acetylsalicylic and salicylic acid have also been successfully used[21]. Transesterification is the most common approach employed for the production of biodiesel were vegetable oils are converted to methyl or ethyl esters of fatty acids[22]

1.3. Levulinic Acid (LA)

As previously mentioned, diverse bio-based platform molecules can be obtained from the biochemical and chemical treatment of lignocellulose[23], some of this can be seen in figure 1. These molecules are characterised by multiple functional groups and have a high potential to be transformed into new families of useful chemical molecules. Amongst them, LA is a polyfunctional molecule containing two valuable functional groups: ketonic and carboxylic. Because of this particularity, LA has become a molecule of great interested to the scientific community and it has been successfully used for the synthesis of various organic (bulk)-chemicals; for this reason the United States Department of energy has classified LA as one of the top 12 most promising bio-based building block chemicals.[24] (figure 2), and it can be obtained from cellulose.
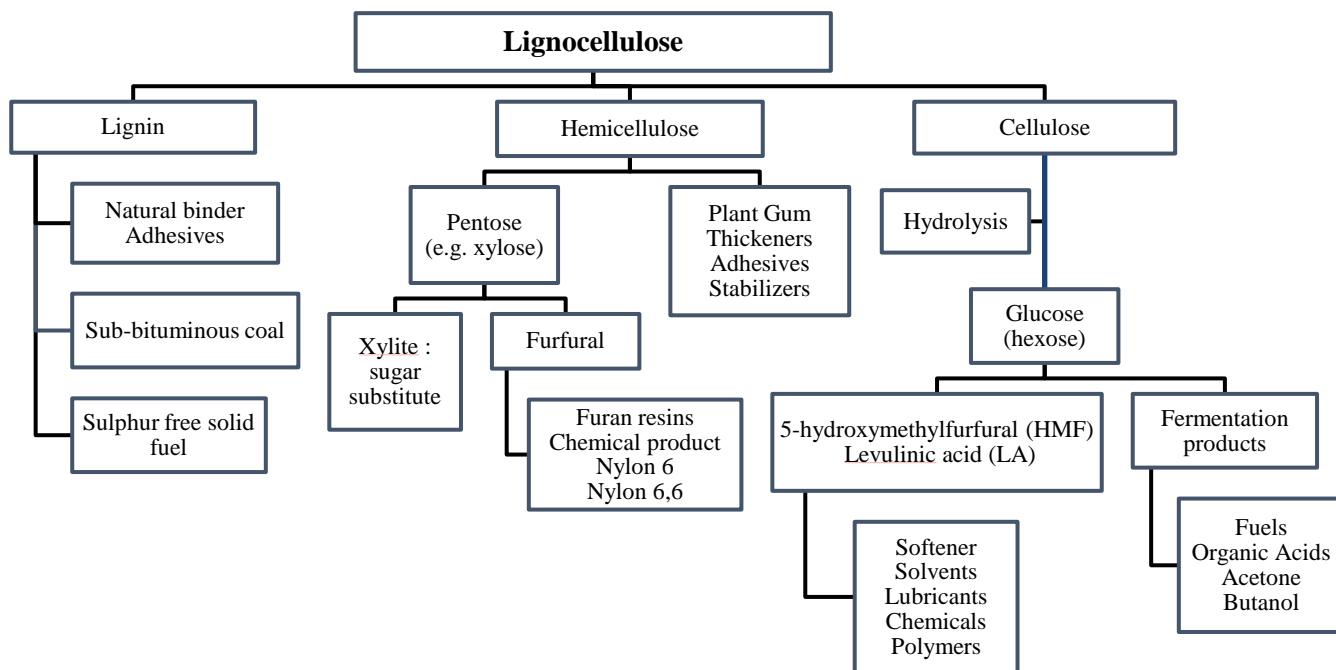
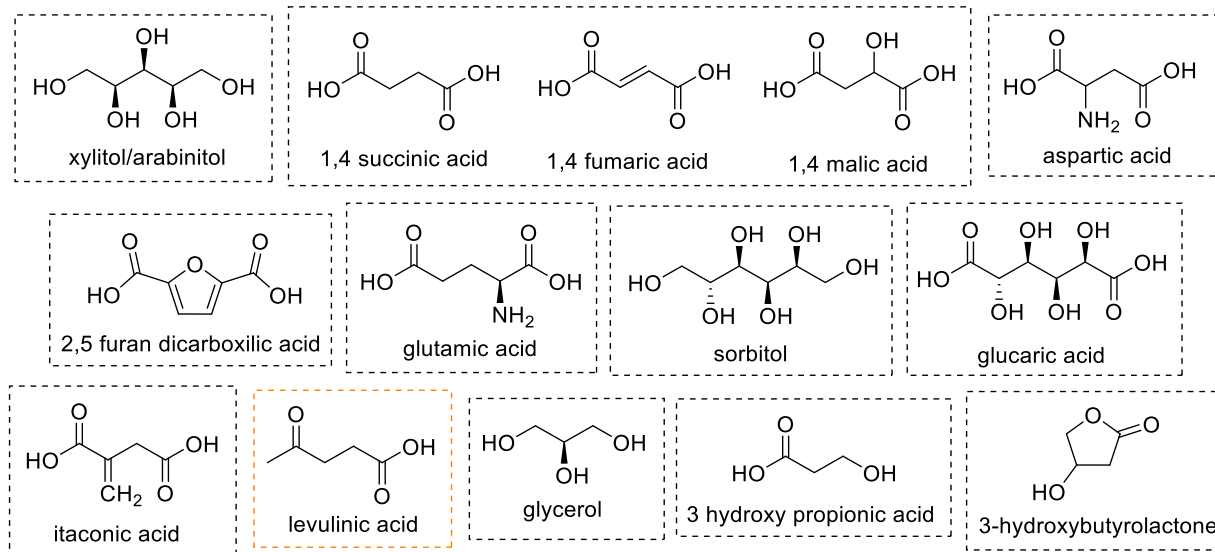**Figure 1.** Valorisation of lignocellulosic biomass[23].

**Figure 2.** Top 12 Value Added Chemicals from Biomass[24].

In order to obtain LA, firstly, lignocellulose needs to be pretreated due to its complex structure and recalcitrant nature. In the case of LA production and other bio-based molecules, the pretreatment is focused in enhancing the accessibility of the cellulose and hemicellulose. This preptreatments will allow the separation of the three main components of the lignocellulosic biomass[25]. A good pretreatment of the biomass will consist of the following[26]: fragmentation of solids, alteration of the structure, increase contact area between biomass and chemical or enzymatic reagent and reduction of the degree of crystallinity and polymerization of the cellulose.

This first step can be done through different approaches[25]:

- Physical: Fragmentation (hacking, grinding, milling, rolling), microwave radiation, sonication, pyrolysis.
- Chemical: acid hydrolysis, alkaline pretreatment, oxidation and ozonation, ionic liquids, solvents, reductive catalytic fractionation.
- Physicochemical: steam explosion, CO_2 explosion.
- Biological: bacterial treatment, enzymatic treatment, pickling.

Once cellulose is obtained, it is then broken down to low molecular weight sugars such as glucose by means of acid hydrolysis. The acid hydrolysis of cellulose takes place via protonation of the glycosidic oxygen in order to cleave the b-1,4-glycosidic bond into water-soluble cellulose oligomers and afterwards to glucose. Because of cellulose crystalline structure and its intense intra- and intermolecular hydrogen bonding, its breakdown in aqueous reaction media is a slow reaction, therefore its necessary to work at elevated temperatures and employ acid catalysis[27]. After this, by means of isomerization, glucose can yield fructose and after further dehydration (to hydroxymethylfurfural, HMF) and subsequent rehydration under the same acidic conditions, it can yield LA with formic acid as the co-product (Scheme 1)[28,29]. A model has been created in order to identify which conditions appear to be the optimal to maximize the yield of LA. This model covers a broad applicable range of conditions for this reaction, including side reactions to humins., and it has shown that high sulfuric acid concentrations and relatively low operating temperatures (423–473 K) are the optimal conditions to achieve this[30]. Nonetheless, several mineral acids have been

used to catalyse this reaction, such as HCl[31], H_2SO_4[30,32,33] and HBr[34]. In particular, the used of H_2SO_4 has been extensively studied given the introduction of the Biofine Technology[35–37]. In this technology the cellulose is firstly hydrolyse to 5-HMF in a plug-flow reactor by reacting with H_2SO_4 at 210 - 220 °C and a steam pressure of 2.5 MPa, this way minimizing side reactions. 5-HMF is then converted into LA in a second reactor at 190 - 200 °C and 1.4 MPa. With this configuration it is possible to obtain remarkable yields of LA, 0.5 kg LA per kg cellulose. However, this technology has a major drawback. The presence of H_2SO_4 represents a problem for the downstream utilization of LA, since it could have a negative effect in the catalytic activity. Moreover, the removal of H_2SO_4 depends on the usage of energy intensive processes that involve distillation and solvent extraction[33,38]. An alternative to this solution could be the utilization of heterogenous catalysts. In fact, several solid acid catalyst have been used for the production of LA, such as TiO_2[39], acid ion-exchange resins[40,41], transition metal chlorides[42], and zeolites such as MnO_x/ZSM-5[43,44]. However, the results obtained where not very promising, reaching in most of the cases low yields.
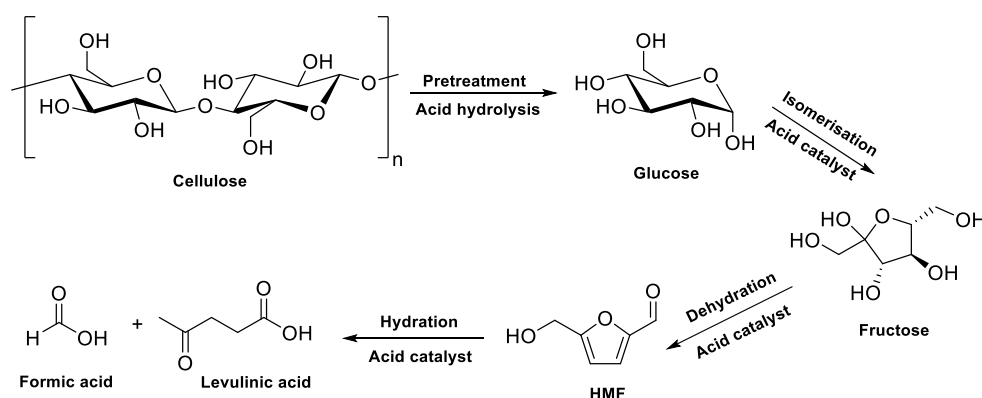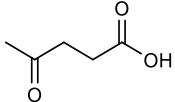

Scheme 1. Acid hydrolysis of cellulose to produce LA[29].

LA is a crystalline white solid that, as previously mentioned, contains valuable functional groups, a ketone and a carboxylic acid group (Table 1), making it a versatile building block for the synthesis of various value-added compounds in different industrial activities such as [45](Scheme 2):

7

- Solvents: tetrahydrofuran and γ-valerolactone.

- Food: LA, alkyl levulinates and angelica lactones which are used as flavouring and fragrance agents.

- Polymers: different molecules that can be used as building molecules for the production of plasticizers (1, 4-butandiol and 1,4-pentadiol), resins (acrylic acid and diphenolic acid) and polymers such as Nylon 6,6.

- Fuels: both for producing fuel additives and substrates for fuel production such as methyl tetrahydrofuran and 5-nonanone.

- Pharmaceutical: for the production of 5-bromolevulinic acid.

Table 1. Structure and physic-chemical properties of LA

Chemical Structure	Chemical Formula	CAS	Molecular Weight (g/mol)	Density ρ (g/mL)	Melting Point (°C)	Boiling Point (°C)
	$C_5H_8O_3$	123-76-2	116,112	1,134	30-33	245-246
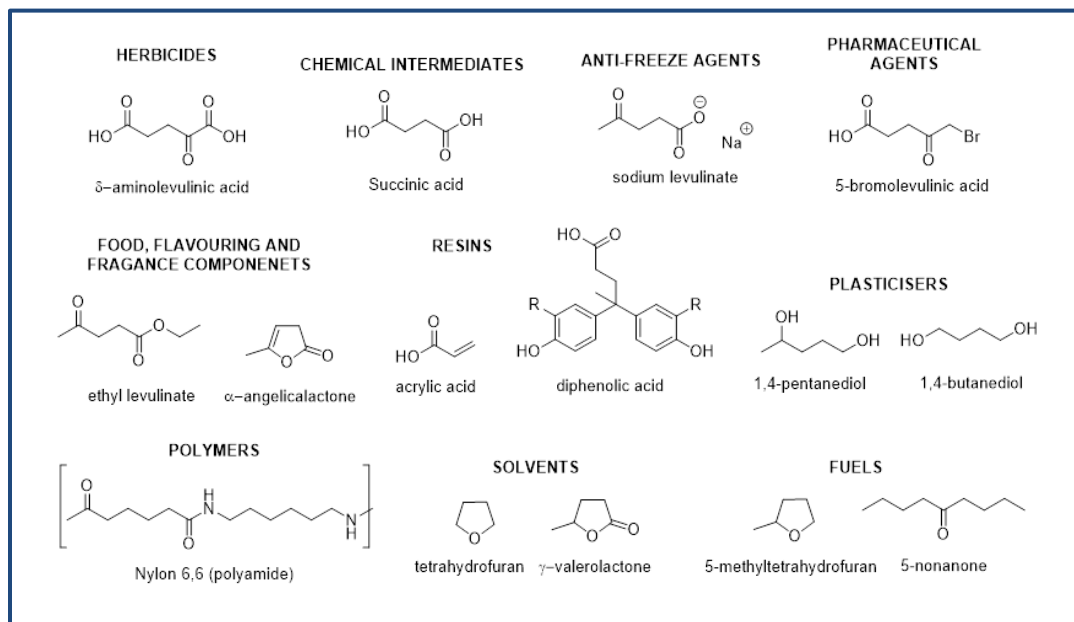
Scheme 2. Potentially interesting derivatives of LA[45].

Three main synthetic routes can be followed to obtain several of the molecules showed in Scheme 2: LA oxidation, esterification and reduction.

From the oxidation of levulinic acid it is possible to obtain compounds such as succinic acid, one of the top 12 value-added chemicals[24] and maleic anhydride (a petrochemical commodity[46]). These two molecules represent important building block for the synthesis of other added-value chemical molecules. Nowadays, succinic acid and maleic anhydride are obtained from petrochemicals. However, given recent studies, switching to a renewable feedstock has become a feasible alternative. Given that LA has a similar chemical structure to succinic acid, it could act as an adequate starting point for its production through oxidation. In fact, there are a few studies reported on the bibliography regarding the catalytic conversion of LA to succinic acid or succinic anhydride using molecular oxygen. On this line, gas phase catalysed process using V_2O_5 at high temperatures (200-400 °C) is one of the first approaches published on the literature[47]. In addition, it has also been reported the use of Ru-based magnetic nanoparticles as catalyst for the oxidation of LA to succinic acid using molecular oxygen at 150 °C and 14 bar O_2, reaching a conversion of 79.3% and a selectivity of succinic acid of 98.6%[48]. Moreover, the Baeyer-Villiger approach was successfully used for the solventless oxidation of LA to succinic acid using H_2O_2 in liquid phase, in which a LA conversion of 48% and a succinic acid yield of 75% were achieved at 90 °C after 6 h[49].

Moreover, esterification of LA yield valuable chemicals, namely the alkyl levulinates, that have potential applications in the flavouring and fragrance industries and as additives for diesel and biodiesel fuels[11,50]. In addition, ethyl levulinate (EL) and butyl levulinate have been studied for their applicability as green solvents[51]. Alkyl levulinates are obtained mainly from the esterification of LA with an alcohol. It is commonly done in liquid-phase using homogenous mineral acids as catalyst, since it offers a fast conversion and less expensive approach. The most commonly used homogenous catalysts include sulphuric acid, hydrochloric acid, phosphoric acid, p-toluenesulfonic acid, and a mixture of these acids[11]. It has been reported how both p-toluenesulfonic acid and sulphuric acid were found to be successful as catalysts for the batch conversion of LA to EL with ethanol achieving a complete conversion at 120°C during 5 hours of

reaction[52]. Nonetheless, nowadays, studies have been focused on heterogeneous catalysts. On this line, the use of sulfonated carbon catalyst in the production of EL has been reported to give high conversion of LA and ester selectivities (both values > 90%)[53]. It has been observed that the presence of Brønsted acid sites is a desired characteristic of heterogenous catalyst in order to be successfully active for the esterification of LA [54].

As previously mentioned, LA can also be valorised through its reduction. This will be thoroughly discussed in the next section, since it is one of the main focuses of this thesis.

1.4. LA dehydration and reduction

Catalytic hydrogenation of LA and its esters, is an essential pathway in the production of angelica lactones (ALs), γ-valerolactone (GVL), 2-methyltetrahydrofuran (MTHF) and 1,4-pentandiol (1,4-PDO) [55]. The reaction can occur either via the hydrogenation of LA to yield 4-hydroxyvaleric acid followed by cyclization to produce GVL or via acid-catalyzed dehydration of LA to yield α-angelica lactone (α-AL) and further hydrogenation to GVL[56]. Furthermore, GVL can undergo hydrogenation/dehydration to yield 2-MTHF or just hydrogenation to yield 1,4-PDO (scheme 3).

Table 2. LA main reduction products.

Compound	Description
ALs	• Three isomeric forms • Found in grapes, soybean, liquorice. • Sweet flavor: aromatic and dairy formulations
GVL[29,45]	• 5-carbon cyclic ester • Sweet odour: used in perfumes and food additives • Has high boiling point and low toxicity; suitable as green solvent
1,4-PDO[57]	• Obtained from GVL hydrogenation • Potential monomer for biobased plasticizers

2-MTHF[27]	• Further hydrogenation of 1,4-PDO or dehydration/hydrogenation of GVL
	• Highly flammable: fuel
	• Ability of blending up to 70% in gasoline: fuel additive

In particular, GVL has recently attracted lots of attention given its physicochemical properties and potential fuel applications[58,59]. GVL has a low melting point (−31 °C), a high boiling point (207 °C), a high flash point (96 °C) and a considerably low vapor pressure at high temperatures (3.5 kPa at 80 °C), making it easy and safe to be transported and store. Even though GVL is soluble in water, it does not react in this medium at low temperatures, making it a stable chemical[60]. Moreover, GVL is considered to be a green, non-toxic and biodegradable solvent[59–61] In fact GVL has better score than tetrahydrofuran (THF) in terms of safety in the CHEM21[62] solvent selection guide. Contrary to THF, GVL has not been reported to form peroxides for a month at 60 °C[63]. In addition, as already mentioned, GVL has potential fuel applications. GVL has a similar combustion energy to that of ethanol (29.7 MJ/kg)[64] and according to Horváth et al[59], its performance as a fuel additive is quite similar. In addition, as mentioned previously, it has a lower vapour pressure than other oxygenates which are typically used as fuel additives. Moreover, given its biodegradability and its non-toxic characteristics GVL, is a perfect chemical additive for the food industry[59].

Several scientific publications show the upgrading of both LA and its alkyl levulinates. The use of alkyl levulinate has become more widespread since the acid-catalysed alcoholysis of carbohydrates has been shown to give higher yields for alkyl levulinates[66,67]. In addition, unlike LA, alkyl levulinates have lower boiling points and acid-free characteristics, which makes them an easier alternative starting source for producing GVL. Therefore, the catalytic conversion of alkyl levulinates appears more feasible from an industrial standpoint, where, according to the literature the hydrogenation of the ketonic group is considered an important step[68].
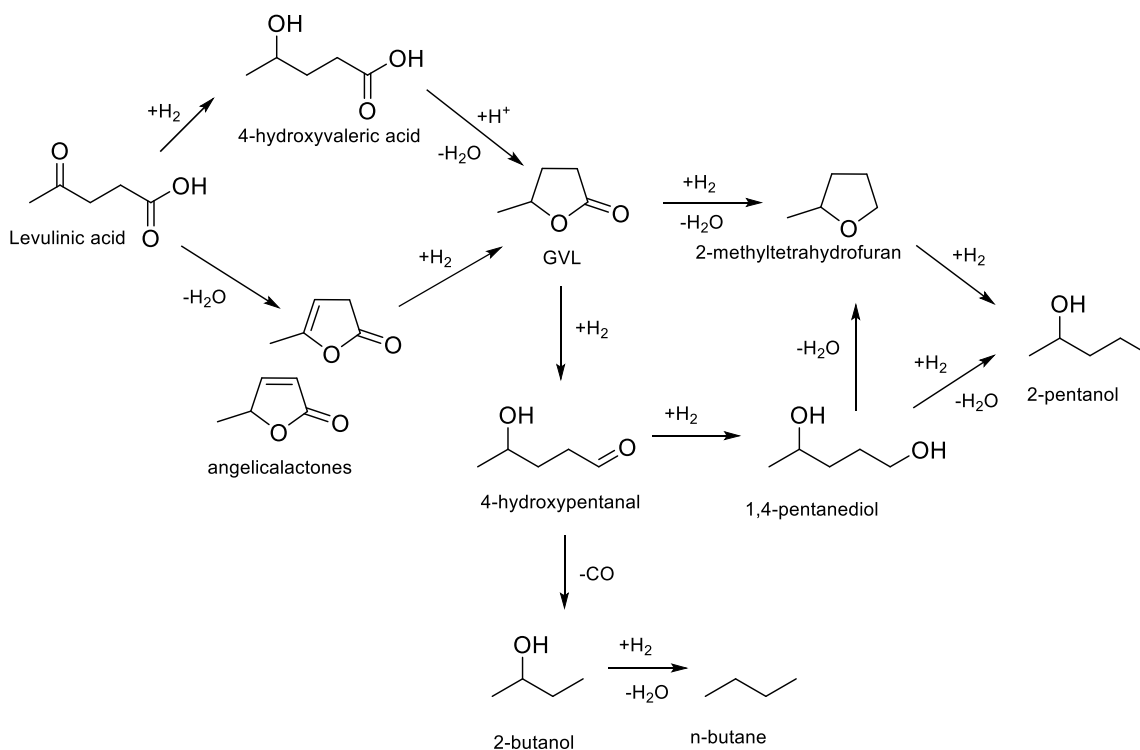
Scheme 3. Proposed pathways of LA hydrogenation[65].

Currently, catalytic hydrogenation of LA is most commonly done using molecular hydrogen. Usually, liquid phase systems are used, in which high H_2 pressures are employed (> 65 bar) and it is typically done using homogenous catalysts[56]. Homogenous catalysts are known to give high activities and good selectvities, all while working at low temperatures. In addition, homogeneous catalysts can be tuned by altering the ligand structure. Most of the catalyst used for the hydrogenation of LA to produce GVL are based on n transition-metal phosphine complexes[56]. Ru complexes have been found to be effective for the activation of the C-O in carboxylic acids. In fact, Osakada et al. tested $[RuCl_2(PPh_3)_3]$ for the reduction of LA and a GVL yield of 99% was obtained after 24 h of reaction at 180 °C and 12 bar of H_2[69]. Horvath et al. studied the in situ generation of a Ru catalyst using a combination of $Ru(acac)_3$ and phosphine $PnBu_3$ in the presence of NH_4PF_6 for LA hydrogenation to GVL at 135 °C, 100 bar of H_2 and 8 h of reaction, reaching quantitative conversion for LA and >99% yield for GVL[70]. In fact, several studies have reported the liquid phase hydrogenation of LA to GVL over homogeneous catalyst with noble metals such as Ru[56].

Even though the use of homogenous catalyst is known to yield high quantities of GVL, it possess several disadvantages: high cost of the catalyst, extreme conditions (pressure), and the complexity that arises from the separation and recovery of the catalyst and purification of the products [59]. Therefore, an alternative and more suitable approach for this transformation is offered by the development of heterogeneous catalysts, which allow enhancing the separation, recovery and purification steps[55,72]. This approach has been used at least since the 1930s, with Schuette and Thomas[73] using PtO_2 in diethyl ether, ethanol and acetic acid which enabled a maximum conversion of 87% after 48 h in a batch system. In the 1940s, Raney Ni was tested at 200°C and 50-60 bar H_2, once again in batch system. These conditions allowed to reach to GVL yield of 94% after only 3 h[74,75]. In the 1950s, Broadbent et al.[76] were able to reach a 71% yield for GVL using solvent free conditions and lower temperature (100°C) during 18h using reduced Re (termed Re "black"), however, the pressure used was considerably higher: 148 bar. However, more recently, the use of supported metal catalyst has become more attractive for the conversion of LA to GVL. On this line, supported Ru, Pt and Re catalysts are the most commonly used and generally have led to high GVL yields using liquid phase in batch systems. In fact, Manzer[77,78] screened the catalytic activity of different metals (Ni, Pd, Rh, Ru, Re, Ir nd Pt) supported on carbon, using 1,4-dioxane as solvent at 150 °C and 55 bars of H_2. In fact, Ru/C was seen to be the most active, reaching LA conversions of 80%. Upon further research, conditions were optimized, and a complete conversion was achieved with GVL selectivity of 95%. Changing the reaction condition might lead to an improvement of the catalytic activity of the catalyst, however, variations on the catalytic support might also have great influence not only on the conversion and yields of the desire products but also on the "harshness" of the reaction conditions. A summary of some of the results reported in the literature can be seen in table 3.

Noteworthy, the synthesis and study of heterogeneous catalysts have allowed to move towards continuous fixed bed systems and, moreover, to explore the possibility of working in gas-phase[57,79]. This allows to tackle some of the disadvantages present when working in liquid phase, such as the recovery of the catalyst or the high H_2 pressures.

Table 3. Summary of literature reports of different heterogeneous catalysts for GVL synthesis.

Catalyst	Temp. (°C)	H₂ Pressure (bar)	LA conversion (%)	GVL Selectivity (%)	GVL Yield (%)	Reaction setup and solvents	Ref.
PtO$_2$	25	2 - 3	-	-	87	Batch, diethyl ether	[73]
Raney Ni	220	50	-	-	94	Batch, no solvent	[75]
Re "black"	106	148	100	71	71	Batch, no solvent	[76]
5 wt% Ir/C			49	97	47		
5 wt% Ni/C			2	20	0.4		
5 wt% Pd/C			30	90	27		
5 wt% Pt/C	150	55	13	80	10	Batch, 1,4-dioxane	[77]
5 wt% Rh/C			30	95	28		
5 wt% Ru/C			80	90	72		
5 wt% Re/C			7	80	10		
Raney Ni			18	20	5		
5 wt% Pd/C	130	12	17	38	6	Batch, methanol	[72]
5 wt% Ru/C			90	95	86		
Urushibara Ni			45	5	2		
5 wt% Ru/SiO$_2$			98	76	75		
5 wt% Ru/TiO$_2$ (Degussa P25)	130	12	81	87	71	Batch ethanol/water	[80]
5 wt% Ru/TiO$_2$ (Tronox)			0	0	0		

Catalyst						Conditions	Ref
5 wt% Ru/Al$_2$O$_3$			94	80	76		
5 wt% Ru/C			99	89	89		
5 wt% Ru/Al$_2$O$_3$	150	145	99	99	99	Batch, 105 bar of scCO2	[81]
Ru/C	25	12	100	97.5	97.5	Batch, no solvent, 50h	[80]
Ru/C	190	12	100	100	100	Batch, no solvent, 45 min	
5 wt% Ru/C and Ambertlyst-70	70	30	100	100	100	Batch, acid co-catalyst, H2O	[82]
ZrO$_2$	150	-	99.9	84	84	Batch, 5 wt% butyl levulinate in 2-butanol inert gas (He, 20.6 bar)	[83]
5 wt% Cu/SiO$_2$	265	10	100	99.9	99.9	Gas phase	[57]
10 wt% Pd/C and 5 wt% Ru/C	170	-	-	-	95	Dual bed reactor alongside a reaction feed of 1-butanol, butyl levulinate and butyl formate	[84]
1 mol % Au/ZrO$_2$	150	-	>99	>99	99	Aqueous reaction mixture containing	[85]

						equimolar amounts of LA and FA	
1 mol % Au/ZrO$_2$	170	-	98	96	95	1:1 molar mixtures of butyl levulinate and butyl-formate in H$_2$O	[86]
CuO/Cr$_2$O$_3$	200	-	100	100	100	Gas phase	[79]
5 wt% Pd/C			100	90	90		
5 wt% Ru/C	265	1	100	98.6	98.6	Gas phase	[57]
5 wt% Pt/C			100	30	30		

The gas phase conversion of LA has recently been reported at atmospheric pressure over Ru/C catalyst using H$_2$, reaching a complete conversion of LA and a GVL selectivity of 98-99%[57]. On the same line, hydroxyapatite supported Ru catalysts have been tested in the gas phase using H$_2$ at atmospheric pressure, achieving a conversion of LA of 92% and a GVL selectivity of 99.8%[87]. Even though the use of noble metal catalyst has presented satisfactory results[71,72], it presents an important disadvantage because of the high cost of the catalyst. Therefore, other non-noble metal catalysts such as Cu have been studied. The gas phase hydrogenation of LA over Al$_2$O$_3$ and ZrO$_2$ supported Cu at atmospheric pressure using H$_2$ has been reported. Both catalysts gave promising results, reaching a conversion of LA of 98% and 81%, and a GVL selectivity of 87% and 82%, respectively[88]. Nonetheless, most of the published studies in the gas phase configuration still depend on molecular hydrogen as the reductant source, which makes the process less sustainable[89] since H$_2$ is still obtained from the steam reforming of fossil carbon, an energetically intensive procedure[90], even though there is also the possibility of obtaining renewable H$_2$ from water splitting. In addition, in these configurations, high pressures are needed given the low solubility of H$_2$ in several organic solvents, making the scale up more difficult and a more expensive and riskier process[65].

1.4.1. Catalytic Transfer Hydrogenation

Given the several drawbacks previously mentioned, a different approach called the "catalytic transfer hydrogenation" (CTH) using the Meerwein-Ponndorf-Verley (MPV) mechanism, has been recently investigated. This approach uses organic molecules, mainly alcohols, which may act as hydrogen donor in presence of an adequate catalyst containing Lewis acid/base properties. [65,68,91] These systems represent a more sustainable alternative to the usage of molecular hydrogen given the "friendlier" operating parameters, eliminating the need of working at high pressures and in the same way avoiding the use of robust reactors. In addition, it allows to perform partial hydrogenations by just changing the type and strength of the hydrogen donor. Moreover, since the "role" of hydrogen donor is played by organic molecules such as alcohols, it introduces the possibility of using bio-alcohols. In this way, the system becomes "greener", having both reagents obtained from biomass.

In the MPV mechanism, a six-membered intermediate is formed on the surface of the catalyst and both the hydroxyl hydrogen and the α-H from the α-C of the alcohol are transferred to the carbonyl group of the substrate, yielding a new alcohol[65]. In particular, secondary alcohols, such as isopropanol, have shown to be more suited for this mechanism because of the stabilizing effect of the two alkyl groups via inductive electron donation to the α-C. [65,83,92,93]
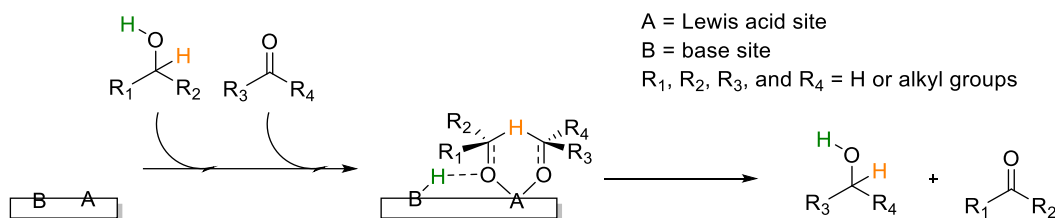
Scheme 4. Generally accepted mechanism for heterogeneous CTH reaction[65].

Noble metal catalysts have been studied for the transformation of LA to GVL through CTH. Kuwahara et al. studied $Ru(OH)x/TiO_2$ for the CTH of ML in the liquid phase using isopropanol as the H-donor. They were able to achieve an almost complete conversion of ML and a GVL yield of 80% [94]. On a similar line, Yang et al. studied the CTH of EL using isopropanol over carbon

supported Ru catalysts, achieving a GVL yield of 93%. GVL yield was further improved to 99% by using Raney Ni as catalyst in a batch reactor under very mild reaction conditions (rt to 80°C), however using a great excess of isopropanol.[93] Along a similar line, Ru/C was used for the CTH of LA using again isopropanol as reducing agent, however in this case microwave irradiation was used as a heat source in order to shorten the reaction times. In this case, after 30 minutes of reaction at 160 °C they were able to obtain a complete conversion of LA a GVL yield of 95%, in contrast to a 30% GVL yield obtained while using conventional heating technologies. Ethanol was also tested as H-donor, however even though a high conversion for LA was achieved, no detectable amount of GVL was observed[95]. It has been already discussed that using noble metals rends the system more expensive, and therefore, different metal oxides have been tested as an alternative. Along this line, CuNiO was tested for the CTH of ML using isopropanol as reducing agent, obtaining optimal results at 200 °C after just 3 h of reaction (X=98.6, GVL Y=95.8%)[96]. In another study[97], given the increased Lewis acidity that $CePO_4$ had given to Ni_3P[98], Ni_3P-$CePO_4$ catalysts were tested for the CTH of LA using isopropanol, ethanol and methanol as H-donor. As observed in other studies, isopropanol appears to be a more efficient H-donor, allowing to reach a LA conversion of 99.3% and GVL yield of 90.8% when operating at 200 °C for 1 h of reaction.

It has been reported that efficient MPV reduction can be achieved using catalysts characterised by both Lewis acid and basic sites. This characteristic allows the simultaneous activation of both the carbonyl group and the alcohol [99]. Therefore, several studies have focused on the use of ZrO_2 and ZrO_2 supported catalysts for the CTH of LA and alkyl levulinates[99]. On this line, studies have been conducted for the CTH of EL over ZrO_2 supported aluminium using different alcohols as hydrogen donors. As expected, isopropanol gave the best results reaching a EL conversion of 95.5% and a GVL yield of 83-84%[68]. $Zr(OH)_4$ was also analysed as catalyst for the CTH with several alcohols, and once again isopropanol proved to give the best results: EL conversion of 93.6% and a GVL selectivity of 94-95%[100]. Kuwahara et al.[91] tested ZrO_2/SBA-15 silica catalyst for the CTH of ML with ethanol, methanol and isopropanol as H-donor. Results once again confirm the higher efficiency of isopropanol to act as reducing agent, reaching a ML conversion of 99.5% and a yield for GVL of 91% in contrast with a ML conversion of 98% and a GVL yield of 41% when using

ethanol. Table 4 shows different results reported in the literature in which ZrO_2 based catalysts where tested for CTH of either LA or its esters. In fact, it can be seen that when using primary alcohols such as ethanol and methanol, the yield obtained for GVL is quite low. Recently, Len et al.[101] proposed a less expensive and easier to synthesize ZrO_2 based catalyst which could represent a cost-effective, sustainable, and more efficient material for MPV reduction reactions. They propose the use of renewable natural sources, such as polyphenols, lignins, porphyrins, phytic acid, and furan derivatives in order to synthesize these materials. They synthesized a ZrO_2-tannin catalyst for the CTH of EL with isopropanol, and after 14h of reaction at 150 °C, they were able to obtain a EL conversion of 93% a selectivity for GVL of 96%. Along the same line, Song et al.[102] synthesized a ZrO_2 based catalyst containing a phenate group. It has been reported that the presence of phenate increases the basicity of the catalyst[103], which according to Chia et al.[83] could enhance the activity of the CTH reaction.

Even though the publications shown so far have achieved outstanding results in terms of LA/alkyl levulinate conversion and GVL yield, most of them have been conducted in a batch system. These type of systems have several drawbacks, such as the high autogenic pressure due to high temperature and the extra step of recovery of the catalyst after reaction. Therefore, a gas-phase configuration would provide a friendlier approach. In addition, most published studies still employ isopropanol as H-donor, which is known to lead to the formation of the corresponding ketones, favoring unwanted reactions such as aldol condensations and the formation of heavier molecules[65,83,93]. Therefore, the use of simpler alcohols such a methanol and ethanol becomes highly interesting. When working in the gas-phase, methanol and ethanol's by-products from H-transfer are formaldehyde and acetaldehyde, respectively, which are known to be toxic and carcinogenic. However, formaldehyde easily decomposes to CO_x and H_2, and the latter can aid in the reduction of the substrate. In the case of acetaldehyde, it also decomposes, and in addition, it can be easily separated from the product mixture.

Table 4. Zirconium based catalysts used for LA/levulinate CTH. (*GVL selectivity)

Catalyst	Substrate	Alcohol	Temperature (°C)	Reaction Time (h)	Conversion (%)	GVL Yield (%)
ZrPO[106]	LA	2-PrOH	170	2	99.8	96.9
Zr-MOFs[107]	EL	2-PrOH	200	2	99	92.7
ZrO$_2$/SBA-15 silica[91]	ML	2-PrOH	150	3	99.5	91
		EtOH	150	3	98	41
		MeOH	90	3	4.7	1.4
Al–Zr mixed oxides[68]	EL	2-PrOH	220	4	95.5	83.2
		MeOH	220	4	68	3,4
		EtOH	220	4	63	50
Zr(OH)$_4$[100]	EL	2-PrOH	200	1	93.6	94.5*
		MeOH	200	1	50.1	12.8*
		EtOH	200	1	50.9	84.6*
Zr-Beta[108]	LA	2-PrOH	250	10	100	>99
ZrO$_2$-graphene oxide[109]	EL	2-PrOH	180	3	63.2	58.6
		EtOH	180	3	28.3	16.8
Ni/ZrO$_2$[110]	ML	2-PrOH	120	20	100	92
Zr-hydroxybenzoic acid[102]	EL	2-PrOH	150	4	100	94.4
ZrO2 - tannin[101]	EL	2-PrOH	150	14	93	96*
Zr - lignosulfonate polyphenolic polymer[111]	EL	2-PrOH	150	8	90	91*

Nonetheless, based on mechanistic studies, it has been reported that a primary alcohol is less susceptible to undergo hydride shift[104], given that the carbocationic intermediate formed is highly unstable. However, CTH has been successfully applied on the conversion of biomass-derived furfural into furfuryl alcohol and 2-methylfuran using methanol as the H-transfer agent and MgO-based catalysts, both in liquid and gas-phase reactors[105]. Pure MgO was shown to reduce furfural into its corresponding unsaturated alcohol at relatively low reaction temperatures (lower than 350 °C), thus allowing selective H-transfer from methanol to the substrate. For Mg/Fe/O catalyst the distribution of compounds obtained was different, with 2-methylfuran formation prevailing when the reaction was carried out between 300 and 400 °C. Both catalysts have proven able of chemisorbing both methanol and furfural activating the CTH processes. However, the presence of Fe^{3+} on Mg/Fe/O facilitates the oxidation of methanol to formaldehyde since Fe^{3+} can be easily reduced to Fe^{2+}.

Moreover, ethanol is an attractive H-donor because of its abundance, sustainability, non-toxicity, and environmentally benign nature, and there are just a few studies were it has been applied to CTH.[83,93,100] Along this line, supercritical ethanol has been proven to work for the gas-phase CTH of EL in the presence of amorphous ZrO_2, achieving an EL conversion of 95.5% and a GVL yield of 81.5%. However, this results were achieved under harsh reaction conditions, 250°C and 70 bar of autogenic pressure.[112]

Most of the published studies for the CTH of LA and its esters using ZrO_2 based catalyst, including those reported on table 4, have been performed in the liquid phase using batch reactors. However, recently, there have been many reports of successful CTH of bio-based building blocks in gas-phase employing continuous fixed-bed systems [105,113–115]. These types of systems offer the possibility of working in a wider range of reaction temperatures at atmospheric pressure, in this way increasing the reactivity and productivity.

1.5. Bio-ethanol production.

As mentioned previously, there has been a continuously growing attention towards the production and valorisation of bio-sugars and bio-alcohols that can be obtained from biomasses such as lignocellulose[116,117]. As mentioned in the previous sections, lignocellulose can also be valorized following a biochemical process; e.g. fermentation of sugarcane for the production of bioethanol which can be used as bio-fuel as well as feed-stock to produce building block chemicals[12,23].

The most established technologies for ethanol production use crops as a starting material. They utilize substrates such as sugar cane juices and corn-starch (Figure 3 A and B) which can be converted through hydrolysis into glucose. In addition, lignocellulose can also be used as a substrate for the production of ethanol; however, it poses a bigger challenge given its complex structure. Before being capable of undergoing fermentation, lignocellulose needs to be firstly treated in order for its monomeric components to be released. Firstly, it undergoes either a physical or chemical pre-treatment in which hexoses and pentoses are released from hemicellulose, and secondly an enzymatic treatment. Alternatively, it could also undergo acid hydrolysis by chemical procedures in order to release glucose from cellulose[118].

Nonetheless, there are still no microorganisms available that can use lignin monomers for ethanol production, and this is one of the main factors that has prevented the use of lignocellulose for this purpose. Therefore, currently available technology focuses on the production of ethanol from crops making it not only food-dependent, but also a slow process due to the relatively slower rate of biological reactions[119]. Moreover, one the main drawbacks related to the use of enzymes is the limitation of the yield of ethanol due to the biological process. The process usually follows a reaction mechanism involving the formation of a pyruvate (a C3 sugar) intermediate and its subsequent decarboxylation. Therefore, the conversion of one mole of pyruvate to ethanol would release one mole of CO_2, in this way reducing the carbon atom efficiency[119,120]. Because of this, a non-enzymatic breakdown of large biomass molecules to fuels and small molecules, such as ethanol, over inorganic-based catalyst materials with enhanced kinetics and productivity is commercially and industrially attractive [121–124].
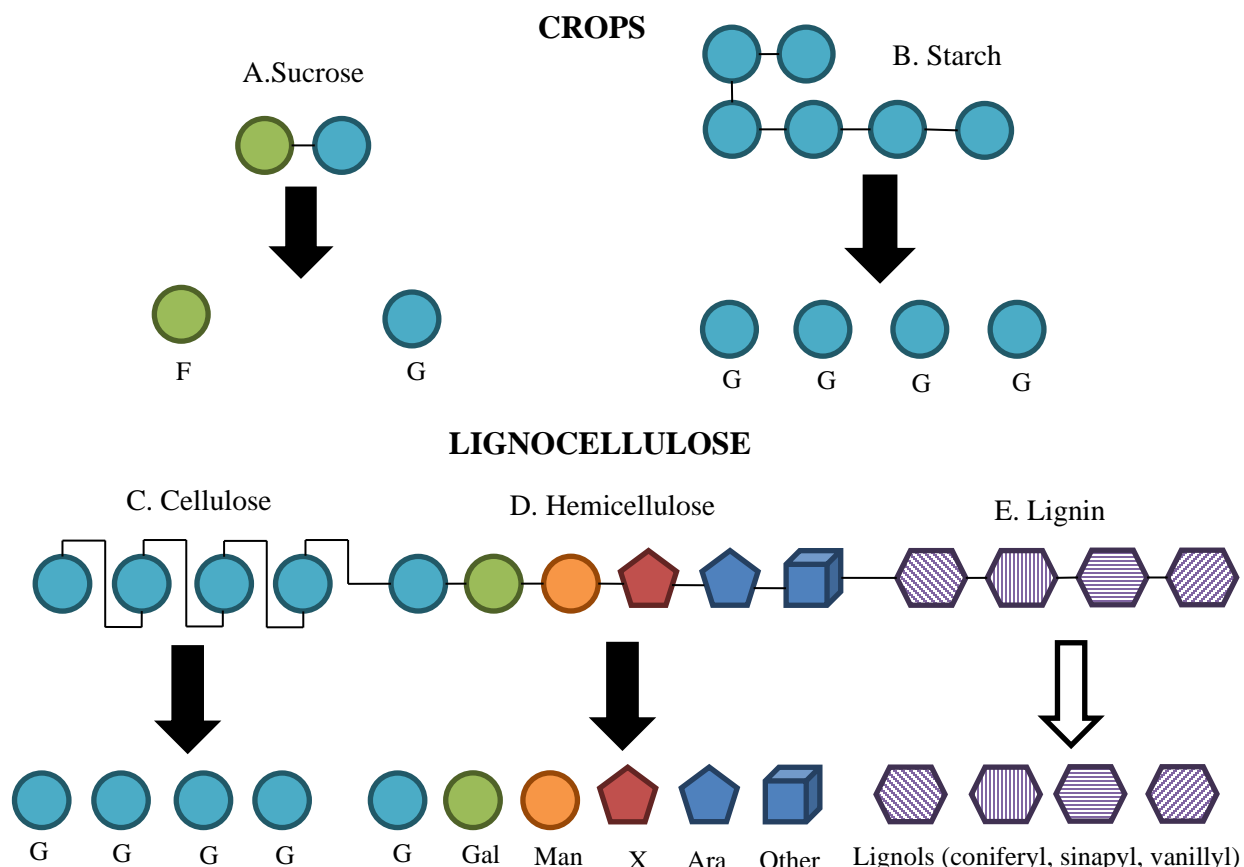
Figure 3. Origin of sugars for ethanol production. Arrows represent hydrolysis (only monomers generated from hydrolysis, represented by dark arrows, can be fermented). G: Glucose, Gal: galactose, F: fructose, Man: mannose, X: xylose, Ara: arabinose, Other: L-rhamnose, L-fucose, uronic acids[118].

As mentioned previously, the United States Department of Energy created a list of the top 12 most promising bio-based building block chemicals, which represent key renewable resources for modern bio-refineries; these compounds can be subsequently converted to a number of high-value bio-based chemicals or materials. To this regard, cellulose, hemicellulose and vegetable oils and fats derived polyols, namely sorbitol (C6 polyol), xylitol (C5polyol) and glycerol (C3 polyol) have been inserted in the list, and this polyols represent an alternative substrate for the production of bioethanol[24,125].

In comparison to fossil feedstocks, polyols obtained from biomass have the particularity of having a much higher O/C ratio, and most of the carbons present in the molecules are bonded to a hydroxyl group. Because of this, a deoxygenative approach could represent a path for the reduction of the oxygen content, and in this way leading to the production of high added value bio-based molecules[122,125–129].

A common and typical approach for the valorization of polyols is the catalytic hydrogenolysis in which cleavage of a C-C, C-O, C-H or C-OH bond takes places by the addition of H_2[130,131]. The main paths followed during the catalytic hydrogenolysis of polyols are dehydration, decarbonylation, retro-aldol condensations and/or hydrogenation. The catalytic hydrogenolysis of polyols usually takes place in the presence inorganic hydroxide bases in order to drive the selectivity toward the desired products. The main products obtained from this are alcohols which have a shorter chain than the substrate used and molecules of the same chain length, but with a lower number of OH groups such as hexanediols and pentanediols. In the case of sorbitol, it has been seen to lead to the production of glycerol, 1,2-propanediol, ethylene glycol, ethanol, isopropanol, 1-propanol. However, the selectivity will strongly depend on the nature of the catalyst and the conditions of the reaction [131,132].

In the case of the hydrogenolysis of sorbitol, most of the research has been focused on the activity of Ni, Ru, Cu, Pt and Pd based catalysts[122,127,128,131–143]. Moreover, Ru has been extensively studied for the hydrogenolysis of glycerol and it showed considerable activity in terms of conversion [133,144–146]. Moreover, copper catalysts represent an interesting alternative for the conversion of polyols such as sorbitol. This type of catalyst favor C-O cleavage leading to the production of C4-C6 products[141,143,147–150]. Besides, also platinum was found very active in hydrogenolysis and hydro-deoxygenation of sorbitol[141,144,151,152].

As far as it goes, the production of bioethanol through catalytic hydrogenolysis of polyols still represents a big challenge. There are few published studies in which considerable selectivities towards ethanol are obtained, this using different substrates. Li et al.[153] recently investigated the one-pot direct transformation of cellulose to ethanol over Ru-WO$_x$/HZSM-5. After 20 h, they

managed to obtain a full conversion and an ethanol yield of 76.8% while working in batch system, at 235 °C and 30 bar of H_2. The catalyst exhibited a synergistic catalysis: the acid sites in HZSM-5 aid cellulose hydrolysis, glucose retro-aldol condensation and ethylene glycol dehydration, and Ru-WO_x is active in the hydrogenation step. Previous publication had already showed how tungsten carbide, W, WO_3 and H_2WO_4, combined with noble metals (Pd, Pt, Rh, Ru and Ir) or nickel, were effective for the production of EG[154–156]. In addition, Song et al.[120] tried a series of Pt supported catalyst with addition of H_2WO_4 and after 5 h were able to obtain a complete conversion of cellulose with an ethanol yield of 32% while working in batch system, at 250 °C and 40 bar of H_2. H_2WO_4 was found to be responsible for the cleavage of the C-C bond, particularly the C2-C3 bond in the glucose unit, via retro-aldol fragmentation[154,157–160]. In addition, sorbitol, glucose, 1,2-pentanediol, ethylene glycol and glycerol were used as substrates, however results were not remarkable. On a different line, Liu et al.[161] tested Ni@C combined with phosphoric acid catalysts for the hydrogenolysis of cellulose. After 3 h of reaction at 200 °C and 55 bar of H_2 they managed to reach a conversion of 98% and an ethanol yield of 69.4%. In this case, H_3PO_4 plays a dual role, firstly hydrolyzing cellulose to glucose and subsequently coordinating with glucose to form a cyclic di-ester complex through dehydration of the hydroxy groups in glucose and H_3PO_4. In this case, the electronic negative surface of Ni@C originating from electron penetration from Ni to the graphene shells effectively splits the target C-O and C-C bonds for highly selective ethanol formation under synergistic hydrogenation[162,163]. However, ethanol was not detected by using sorbitol, 1,2-PDO and EG as substrate.

Moreover, several studies have focused on the usage of Pd/Fe_3O_4 for the hydrogenolysis of different polyols and also cellulose, reaching remarkable results[121,122,127,128,136,138,164–167]. These results are summarized in table 5.

As it can be seen, Pd/Fe_3O_4 gives, in almost all of the cases, high selectivities towards ethanol, even as the substrate changes. Most relevant is the study from Gumina et al.[127] in which sorbitol was fully converted giving a selectivity towards ethanol of 63.5%. In this study, different temperatures were tested for the hydrogenolysis of sorbitol. However, it was seen that high temperatures were needed in order to push the reaction towards the formation of ethanol. When

using lower temperatures, the reaction was selective towards the formation of glycerol, 1,2-PDO and EG. In addition, from tests performed under inert atmosphere the production of H_2 was detected, this way indicating the presence of aqueous phase reforming (APR). In addition, no CO was detected in the gas phase, only H_2 and CO_2, this way confirming also the presence of water gas shift reaction (WGS). The presence of hydrogenolysis products implies that the *in situ* produced H_2 directly participates in the hydrogenation of the intermediates produced from the dehydration route[166]. Scheme 5 shows the different reactions that take place in the hydrogenolysis of sorbitol on Pd/Fe_3O_4 catalyst in a batch configuration.

The presence of partially positively charged palladium nanoparticles (average particle size ranging from 1 to 2 nm) was confirmed[121,166] indicating an intimate and well dispersed interaction between the Pd nanoparticles and the support. Furthermore, through extended X-ray absorption, the existence of Pd-Fe bimetallic clusters on the catalyst surface was confirmed (characterized by a shorter scattering Pd-Fe path of 2.51 Å with respect to the Pd-Pd distance of about 2.70 Å)[121,124]. In addition, it has been previously reported that the selective cleavage of C-C or C-O of ethylene glycol in hydrogen to form ethanol might be achieved through adjusting the electronic properties of Pd nanoparticles while varying the support[121,124,164].

Table 5. Reported studies on hydrogenolysis of polyols towards ethanol production using PdFe catalysts. (*includes gas-phase products, **liquid phase selectivity)

Substrate	Catalyst	H_2 Pressure (bar)	Temperature (°C)	Reaction Time (h)	Conversion (%)	Selectivity (%)**					ref
						1,2-PDO	EG	EtOH	MeOH	n-PrOH	
EG	5%Pd/Fe$_3$O$_4$	20	195	24	9.7	-	-	12*	25*		[121]
Cellulose		5	240		100	10	0	58	-		[128]
Glycerol	13.5%Zn/PdFe	50	250	120	100	32.5	<5	31.5	5	7	[164]
EG				24	23			4.4	52.4		
1,2-PDO					25.7			50	4	22	
Glycerol	5% Pd/Fe$_3$O$_4$	5	240	24	100	9.3	0.5	70.5	9.6		[166]
1,2-PDO					78.7			90	1.4	8.6	
EG					72.1	-	-	28.2	71.8		
Glycerol		5 (He)	240	24	100	9.4	0.2	73	8.1	8.7	
EG					66.2			23.4	76.6	24	
Sorbitol	5% Pd/Fe$_3$O$_4$	5	240	24	100	5.9	-	63.5	-		[127]
Sorbitol	Pd/C				60	20.4	12.4	45.4	-		
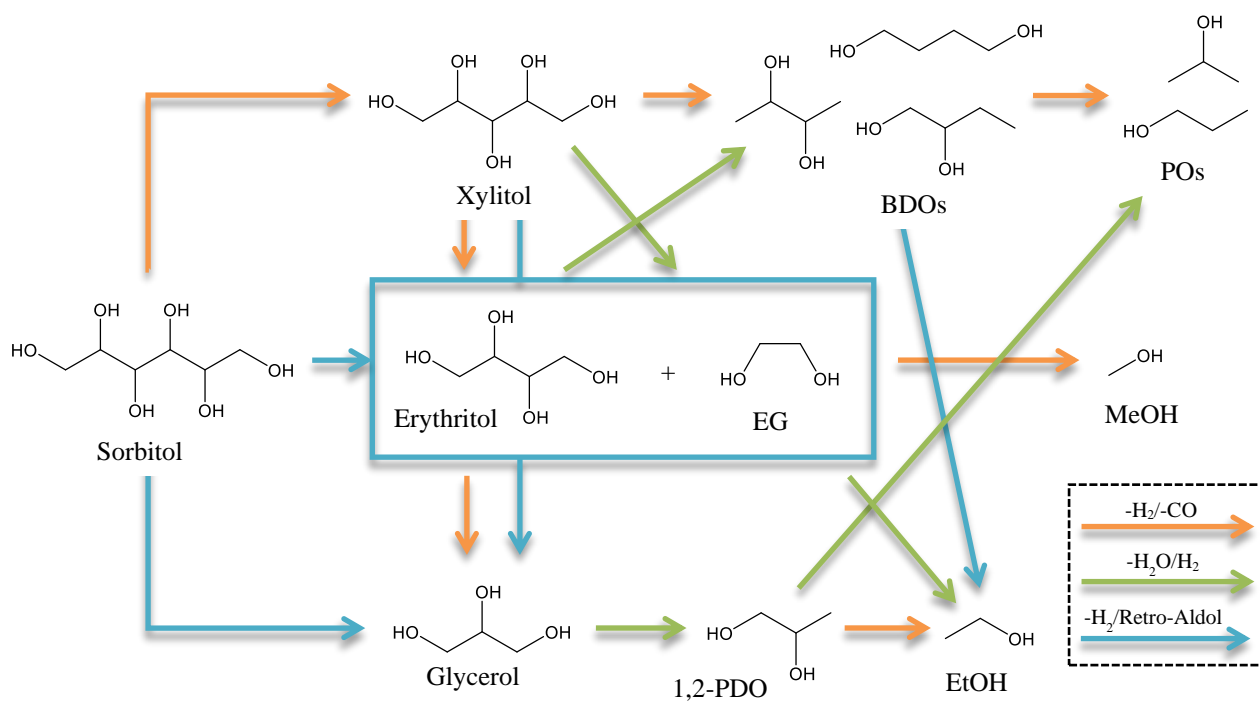
Scheme 5. Cascade reactions involved in the sorbitol hydrogenolysis over Pd/Fe$_3$O$_4$ catalyst[127].

2. Experimental

2.1. Materials

Reagents and standards used during the following experiments were analytical grade: acetonitrile ≥99.9%, octane 98%, methyl levulinate ≥98%, γ-valerolactone 99%, α-angelica lactone 98%, ethanol ≥99.8%, zirconium(IV) oxynitrate hydrate 99%, Zirconyl chloride octahydrate 98%, titanium(IV) oxysulfate solution 15%, ammonium carbonate ≥30% (NH_3 basis), ammonium hydroxide solution 28−30% (NH_3 basis), methyl pentanoate 99%, ethyl levulinate 99%, palladium(II) nitrate dihydrate 40%, ruthenium(III) chloride hydrate 30-40%, cobalt(II) nitrate hexahydrate 98%, tetraamine platinum(II) nitrate 98%, iron(III) nitrate nonahydrate 98%, pyridine 99.9%, lutidine 99%, glycerol 99.5%, 1,2-propanediol 99.5%, ethylene glycol ≥ 99%, all obtained from Sigma-Aldrich and used as received. Commercial, monoclinic ZrO2 was purchased from Sigma-Aldrich (CAS: 1314-23-4; Aldrich code: 204994). Biomass-derived ethanol was provided by Caviro, a leading wine Italian producer group. This bioethanol was a real mixture derived from agricultural waste (namely from molasses and cereals fermentation) with the following rough volumetric composition: ethanol 95%, acetic acid 1.3%, ethyl acetate 1.2%, methanol 1.8%, aldehydes and acetals 0.7%.

2.2. Catalyst Preparation

2.2.1. *Levulinic acid upgrading*

- Tetragonal ZrO_2: catalyst was prepared by the precipitation methodology proposed by Chuah[168]. A solution of $ZrO(NO_3)_2·2H_2O$ (Sigma Aldrich) 0.3 M was added dropwise to a stirred solution of NH_4OH 5M at room temperature. Afterwards, the solution was digested at 100 °C for 20 h under reflux system. The pH of the solution was adjusted to 9 during the digestion by the addition of NH_4OH. The precipitate was separated by filtration and washed with NH_4OH 5 M. Lastly, the filtered sample was dried at 100 °C overnight and then calcined in air at 500 °C for 12 h with a heating rate of 2.5 °C/min.

- Monoclinic ZrO_2: catalyst was prepared by hydrothermal synthesis. A solution was prepared by adding 3.38 g of $ZrO(NO_3)_2·2H_2O$ (Sigma Aldrich) to 20 mL of distilled water.

Afterwards, 6.06 g of urea were added, and the solution was then transferred to an autoclave with a Teflon inlet. The autoclave was placed inside a furnace with a temperature of 140 °C for 12 h. Afterwards, the precipitate was firstly centrifuged with ethanol, and then with distilled water. The sample was then dried at 100 °C overnight and then calcined in air at 450 °C for 3 h with a heating rate of 5 °C/min.

- Zr/Ti/O mixed oxide: catalyst was prepared following the methodology proposed by Afanasiev[169]. 50 mL of an aqueous solution of $ZrOCl_2 \cdot 8H_2O$ 0.2 M was slowly added dropwise to a stirred solution of $(NH_4)_2CO_3$ 0.4M (100 mL). Afterwards, 0.01 mol $TiOSO4$ dissolved in 100 mL distilled water were rapidly added. The solution was then taken to a pH of 7 using NH_4OH and immediately a precipitate was formed. This was then filtered and washed until the presence of chloride was no longer detected. The filtered sample was dried overnight at 100 °C and then calcined at 550 °C for 4 h.

2.2.2. *Ethanol through chemo-catalytic approach*

All Pd catalyst where prepared by co-precipitation and designed with a nominal Pd loading of 5 wt%.

- X/ZrO_2 (X=Pd, Ru): An aqueous solution of the corresponding precursor ($Pd(NO_3)_2 \cdot 2H_2O$ or $RuCl3_2 \cdot xH_2O$) and $ZrO(NO_3)_2 \cdot 2H_2O$ was added dropwise to a stirred solution of NH_4OH 5M at room temperature. Afterwards, the solution was digested at 100 °C for 20 h under reflux system. The pH of the solution was adjusted to 9 during the digestion by the addition of NH_4OH. The precipitate was separated by filtration and washed with NH_4OH 5 M. Lastly, the filtered sample was dried at 60 °C in a vacuum oven overnight, then calcined in air at 500 °C for 12 h with a heating rate of 2.5 °C/min and lastly reduced under H_2 flow at 200∘C for 2 h.

- $5\%X/Fe_3O_4$ (X=Pd, Ru. Pt, Co): An aqueous solution of the corresponding precursor ($Pd(NO_3)_2 \cdot 2H_2O$, $RuCl3_2 \cdot xH_2O$, $Co(NO_3)_2 \cdot 6H_2O$, $[Pt(NH_3)_4](NO_3)_2$) and $Fe(NO_3)_3 \cdot 9H_2O$ was added dropwise to a stirred solution of NH_4OH 5M at room temperature. Afterwards,

the solution was digested for 3 hours at 80 °C for 3 h under reflux system (room temperature for Pd). The precipitate was separated by filtration and washed with NH_4OH 5 M. Lastly, the filtered sample was dried at 60 °C in a vacuum oven overnight, then calcined in air at 450 °C for 4 h with a heating rate of 5 °C/min and lastly reduced under H_2 flow at 450°C for 2 h.

- 5%X/Fe_3O_4-AC (X=Pd, Ru): A solution of the corresponding precursor ($Pd(NO_3)_2 \cdot 2H_2O$, $RuCl3_2 \cdot xH_2O$) and $Fe(NO_3)_3 \cdot 9H_2O$ was added to CW20 activated carbon from the company Silcarbon. Impregnation was performed with a slight excess of solution and 20 min of stirring. Afterwards, samples were dried overnight at 100 °C and then calcined in air at 450 °C for 4 h with a heating rate of 5 °C/min. Finally, they were reduced under H_2 flow at 450°C for 2 h.

2.3. Catalyst Characterization

BET specific surface area: surface area of the catalysts was determined by N_2 absorption–desorption at liquid N_2 temperature using a Sorpty 1750 Fison instrument. 0.25 g of the sample was used for the measurement, and the sample was outgassed at 150 °C before N_2 absorption.

X-ray diffraction analyses (XRD): XRD powder patterns of the catalysts were recorded with Ni-filtered Cu Kα radiation (λ = 1.54178 Å) on a Philips X'Pert vertical diffractometer equipped with a pulse height analyzer and a secondary curved graphite-crystal monochromator.

Thermogravimetric/differential thermal analyses (TGA/DTA): Using a SDT Q 600 instrument, TG/DT analyses were performed over fresh and spent catalysts. Typically, 10 mg of the sample were used for the measurement at temperatures from room temperature up to 700 °C, with a heating rate of 10 °C/min in air.

NH₃-CO₂-temperature-programmed desorption (TPD): NH_3 and CO_2 TPD measurements were performed with a POROTEC Chemisorption TPD/R/O 1100 automated system for analysing the acid/base properties of catalysts. Fresh catalyst was pre-treated in 10 vol.% O_2 in He

(30mL/min of flow rate) at 500 °C for 1 hour following a heating ramp of 10°C/min, this in order to remove adsorbed H_2O and CO_2. For the post reaction catalyst characterisation, the pre-treatment was not performed. The samples where then cooled at 40 and 100°C for CO_2 and NH_3 desorptipon analysis, respectively. The catalyst was then exposed, during 1 h, to the probe molecule with a flow of 30 mL/min of 10 vol.0% of NH_3 or CO_2 in He. Physisorbed molecules were removed by flushing with He (30mL/min of He) for 10 min before starting recording of the analysis. Lastly, the temperature-programmed desorption was performed following the desorption with both TCD and MS, increasing the temperature with a heating rate of 10°C/min from 40/100°C to 500°C in He (30 mL/min).

Raman Spectroscopy: Raman analyses were carried out using a Renishaw Raman System RM1000 instrument, equipped with a Leica DLML confocal microscope, with 5x, 20x, and 50x objectives, video camera, CCD detector, and laser source Argon ion (514 nm) with power 25 mW. The maximum spatial resolution is 0.5 µm, and the spectral resolution is 1 cm^{-1}. For each sample, ten spectra were collected changing the surface position of the laser. The parameters of spectrum acquisition were generally selected as follows: 8 accumulations, 10 s, 25% of laser power to prevent sample damage, and 50x objective.

In Situ Diffuse Reflectance Infrared Fourier Transform (DRIFT) Spectroscopy: Spectra were taken in situ with a Bruker Vertex 70 instrument equipped with a Pike DiffusIR cell attachment. They were recorded using an MCT detector after 128 scans and with a 4 cm^{-1} resolution in the region 4000-450 cm^{-1}. The equipment was coupled with a mass spectrometer EcoSys-P from European Spectrometry Systems. As a general procedure for the determination of the acid sites of a catalyst, a sample of ZrO_2 was loaded and pre-treated at 400 °C under a flow of He (8 mL/min) for 40 min in order to remove any molecules adsorbed onto it. Afterwards, using KBr as background, spectra were acquired at different temperatures (400-300-200-100-50 °C) while cooling the sample down to 50 °C. Then, a pulse (2 µL) of the basic probe molecule (pyridine or dimethyl pyridine) was introduced. IR spectra were acquired at 1 min time intervals in order to follow the adsorption process. Lastly, the sample was heated until 400 °C (heating rate of 5 °C/min) and spectra were acquired at different temperatures (100-200-300-400 °C).

Temperature Programmed Reduction: For TPR analysis 50 mg of dry sample were placed into a quartz U-tube, which functions as a fixed bed reactor. This was then placed in a ChemBET PULSAR TPX - Quantachrome Instruments. In order to ensure a completely dry sample, the U-tube was heated to 120 °C and kept there for 30 minutes under He-flow. For the TPR measurement a flow of 5 % H_2 in Argon was applied and the Utube was heated from room temperature to 600 °C at a rate of 5 K/min. Hydrogen consumption was detected with a thermal conductivity detector (TCD).

Transmission electron microscope (TEM) images: images were obtained on a FEI Tecnai F20 TEM operated at a voltage of 200 keV equipped with ahigh-angle annular dark-field detector (HAADF). Elemental analyses were also performed using an energy-dispersive X-ray spectrometer from Oxford Instruments equipped with an SEM/STEM.

2.4.CTH Tests

2.4.1. Gas-phase CTH Tests

CTH tests were carried out by the vaporisation of an alcohol/levulinate ester or levulinic acid liquid mixture (molar ratio 10:1); liquid flow was 0.5 mL/h in a N_2 stream. The liquid mixture was fed by means of a syringe pump (KDScientific Legacy Syringe-infusion Pump) into a stainless-steel heated line in order to obtain an instant vaporisation. An inlet with the carrier gas (N_2) arrives to this line, and then this line is connected with a tubular glass reactor (length 450 mm, inner diameter 19 mm) containing 1 cm^3 of catalyst. Catalyst particles were prepared by pressing the calcined powder at 10 bar to obtain a pellet, which was then crushed and passed through sieves to obtain the desired particle size (pellets of 30-60 mesh). The residence time for the catalytic tests was 1 s and the %mol of the organic mixture was fixed between 8 and 12%. In addition, the reactor was placed inside a furnace and its inlet and outlet were covered with heating tapes equipped with an electrical resistance in order to regulate the inlet and outlet temperature. Before every CTH test, the catalyst was pre-treated inside the reactor for 2 hours at 400°C using 30 mL/min air flow. Afterwards, the temperatures of both the furnace and heating tapes was set to the desired temperature (normally 250°C and 230°C, respectively). During the CTH tests, the exit stream was

condensed using a cold trap filled with 25 mL of acetonitrile in order to collect the heavier products of the reaction. The collected acetonitrile solution was taken and analysed every 50-60 min in order to monitor the reactivity during the time-on-stream process. Blank tests were performed by feeding the mixture of ethanol and ML (10:1 molar ratio) into the reactor in the absence of the catalytic bed under the studied conditions (200-400°C). Only a slight ML conversion of 6% was obtained at 400°C, due to decomposition.

2.4.2. *Liquid-phase CHT Tests*

Batch experiments were performed in a stainless steel autoclave (160 mL, 500 rpm) (Parr Instruments 4560 mini reactor system). The reactor was loaded with 0.3 g of the catalyst which was thermally previously treated at 400 °C for 2 h under an air flow and then suspended in a 10 wt % alcoholic solution (MeOH, EtOH, 2-PrOH) containing the corresponding H-donor. The autoclave was then flushed three times with N_2 in order to eliminate any trace of air present in the system. The reactor was then pressurized with 10 bar of N_2 and heated to the final reaction temperature. At the end of the reaction, the system was cooled to room temperature, the pressure was released and the organic phase was collected for analysis. For the recycling tests, the catalyst was recovered by filtration thoroughly washed with 2-PrOH and reused under the same reaction conditions.

2.4.3. *Gas-Chromatographic analysis.*

In order to quantify the obtained products, the collected acetonitrile solutions (25 mL) were spiked by adding 20 μL of octane (as external standard) and then analysed by means of a gas-chromatograph Thermo Focus GC model equipped with a non-polar capillary column Agilent HP-5 (5% phenyl - 95% methyl siloxane) having dimensions of 25 m x 320 μm x 1.05 μm and a flame ionisation detector (FID). A flow of 1.2 mL/min of N_2 was used as the carrier. In order to optimise the separation of our products, the programmed temperature applied was 2 min isotherm at 50°C, then a 10°C/min temperature increase up to 110°C (the latter maintained for 2 min), and then 20°C/min up to 280°C (the latter for 2 min).

Each compound was calibrated with respect to the external standard, octane, in order to find the corresponding response factor in the appropriate range of concentrations ($5*10-4$ to $5*10-2$ M for LA derivatives and $5*10-3$ to $2*10-1$ M for ethanol).

The alkyl levulinate (e.g. ML) conversion (equation 1) and product yield (e.g. GVL, equation 2) were calculated using the following equations:

$$X_{reactant} = \frac{mol^{in}_{reactant} - mol^{out}_{reactant}}{mol^{in}_{reactant}} * 100 \tag{1}$$

$$Y_{product} = \frac{mol^{out}_{product}}{mol^{in}_{reactant}} * 100 \tag{2}$$

In addition, carbon balance based on alkyl levulinate was considered as follows:

$$\frac{Y}{C} = \frac{\sum products\ yield}{Reactant\ conversion} \tag{3}$$

In addition, samples were also analysed by means of GC-MS equipped with a non-polar column HP-5 (95% dimethylsiloxane and 5% phenyl, 30 m X 320 μm, same temperature ramp as reported for GC-FID analysis), coupled with a mass spectrometer (Agilent Technologies 5973 inert). The structure of products was assigned by GC-MS and, whenever possible, by comparison with commercially available samples.

The light, non-condensable compounds obtained by both ethanol decomposition tests and the reaction performed at 400°C by feeding ML:ethanol (1:10 molar ratio), were analysed using the same apparatus as described above. The stream of gaseous compounds was fed and monitored on-line by an Agilent 3000A micro-GC with 3 parallel columns: (a) a PlotQ column, with He carrier, for the separation of CH_4, CO_2, ethylene, H_2O, propylene, and methanol; (b) a OV1 column, with He carrier, for the separation of CO_2, formaldehyde, diethyl ether, H_2O, and ethanol; (c) a Molecular Sieve 5A column, Ar carrier, for the separation of H_2, O_2, N_2, CH_4, and CO; in this case a Plot U backflash column was installed to avoid CO_2 and H_2O poisoning in the third column.

Yields of each product were calculated by the same method as described in detail by Trevisanut et al.[170]

2.5. Hydrogenolysis of polyols.

Hydrogenolysis reactions were carried out in a 75 mL stainless steel autoclave at a stirring speed of 500 rpm. The autoclave was loaded with 0.1 g and 15 ml of 4 wt% C6-C2 polyol aqueous solutions. The reactor was purged three times and subsequently pressurized at the desired H_2 pressure and heated at the reaction temperature (250 ⁰C), monitored using a fixed thermocouple connected to the reactor controller. After 24 h of reaction, the system was cooled down in an ice bath and the pressure was released carefully and the liquid phase was collected for analysis.

2.5.1. HPLC Analysis

The reactant and products, in the liquid phase, were analysed using an off-line Shimadzu HPLC equipped with a Phenomenex-Rezex ROA Organic Acid H+ column (eluent: 0.005 M H_2SO_4, flow: 0.6 mL/min, dimensions: 300 x 7.8 mm, T: 70 ⁰C, P: 29 bar, t: 30 min).

The conversion and product selectivity in the liquid phase were calculated on the basis of the following equations:

$$X_{reactant} = \frac{mol_{reactant}^{in} - mol_{reactant}^{out}}{mol_{reactant}^{in}} * 100 \qquad (4)$$

$$Liquid\ phase\ selectivity_{product} = \frac{mol_{product\ liquid\ phase}^{out}}{\sum mol_{product\ liquid\ phase}^{out}} * 100 \qquad (5)$$

3. Results and Discussion

3.1. Upgrading of levulinic acid and its esters

3.1.1. Catalyst characterization

In order to achieve an efficient MPV reduction, the surface of the catalyst need to contain both Lewis acid and basic sites due to a synergistic effect[99]. Accordingly, ZrO_2 catalyst with a high surface area was synthesized in order to heighten its catalytic activity for the CTH. The methodology proposed by Chuah et al.[168] was followed and high surface area tetragonal ZrO_2 was obtained with only traces of monoclinic phase
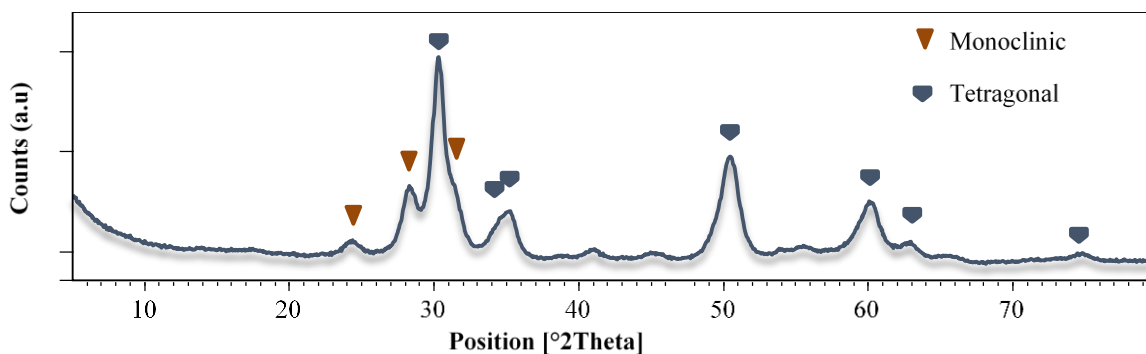
Figure 4. XRD of synthetic tetragonal ZrO_2 catalyst (ref code: 00-050-1089).

XRD patterns of the synthesized catalyst are shown in Figure 4. It can be seen that a series of sharp crystalline peaks occurred at $2\theta = 28.2°, 30.4°, 35.3°, 50.6°, 60.3°$; indicating the presence of a small amount of monoclinic phase ($2\theta = 28.2°$) and mainly tetragonal phase ($2\theta = 30.4°, 35.3°, 50.6°, 60.3°$).[168,171] In addition, Raman spectra were taken in order to confirm the presence of only tetragonal phase (143, 270, 315, 457 and 641 cm^{-1}). In fact, no bands corresponding to cubic phase (490, 579, broad bands 595-660 cm^{-1})[172–175] where seen in the spectra obtained (figure 5).

After thorough analysis of the synthesis procedure of the catalyst, factors which influence the appearance of monoclinic face were identified. When in an alkaline medium, hydrous zirconia undergoes cation exchange[176]. Its isoelectric point is around 6-7, meaning that at higher pH, the gels are negatively charged. Cations are then attracted to the sphere closest to the primary particles

and the high temperature (100°C) during digestion increases the rate of collisions between the particles so that a stabilized network is formed via condensation of hydroxyl groups. Consequently, according to Chuah[177], the adsorption of cations, such as NH_4^+, helps to stabilize the surface area. Furthermore, the presence of these cations also favours tetragonal phase formation. Chuah[177] explains that this could be due to the decreasing crystallite size with digestion that favours the tetragonal form. A summary of the characterization of the catalyst is reported in Table 6.
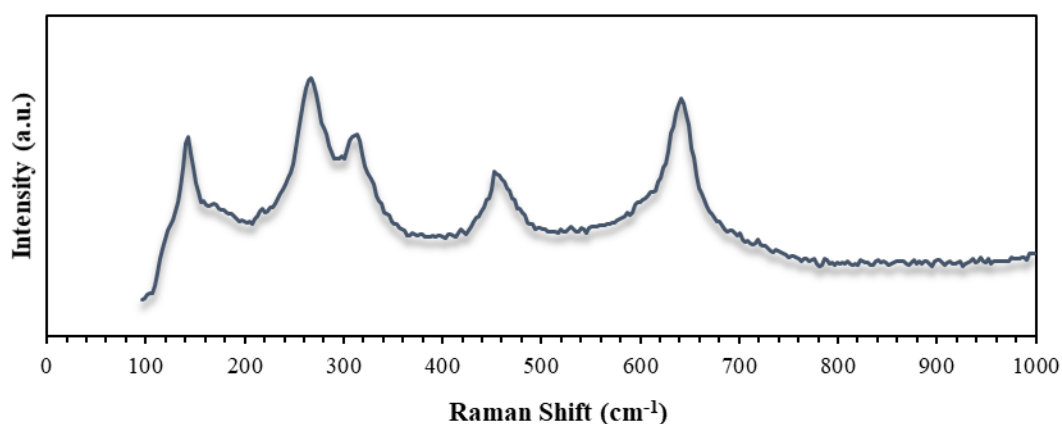
Figure 5. Raman spectra of tetragonal ZrO_2.

TPD analysis (Figure 6) of the fresh catalyst, highlights the bifunctional properties of ZrO_2. Results show the presence of basic and acidic sites. In fact, a wide peak was seen centred at around 110°C for CO_2 proving the presence of weak basic sites. Furthermore, the ammonia desorption profile shows a wide desorption peak from 180 to 450°C, indicating the coexistence of weak, moderate and strong acid sites[91,100,178].

Table 6. Nature, specific surface areas and acid and basic densities of tetragonal ZrO_2.

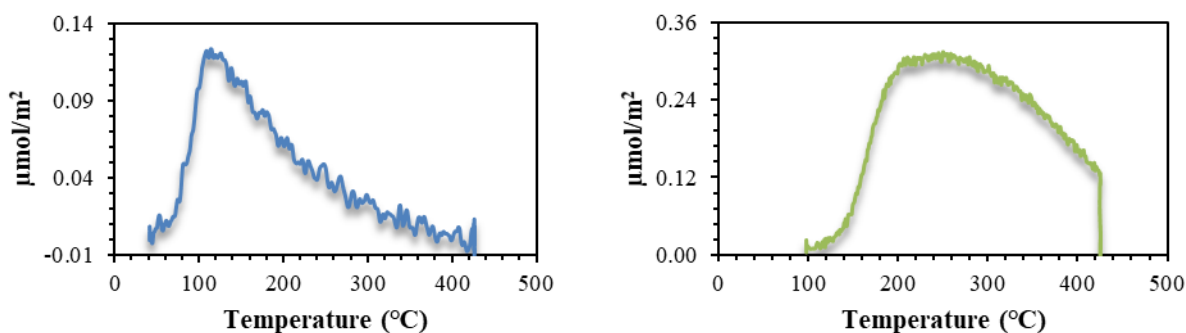| Catalyst	SSA (m²/g)	Crystalline phase (XRD)	Acid density (μmol/m²)	T max desorption (°C)	Basic density (μmol/m²)	T max desorption °C
Tetragonal ZrO_2	120	Mainly tetragonal	8.14	Wide band from 200 to 400°C	1.88	110°C

Figure 6. CO_2 -TPD (left) and NH_3 (right) profiles of synthesized tetragonal ZrO_2.

In addition, DRIFT spectroscopy tests with absorbed pyridine as probe molecule were performed at different temperatures (Figure 7-top). The spectra taken during the desorption showed three bands at 1443 cm^{-1}, 1574 cm^{-1} and 1604 cm^{-1}, which correspond to pyridine coordinated species with Lewis acid sites[179].
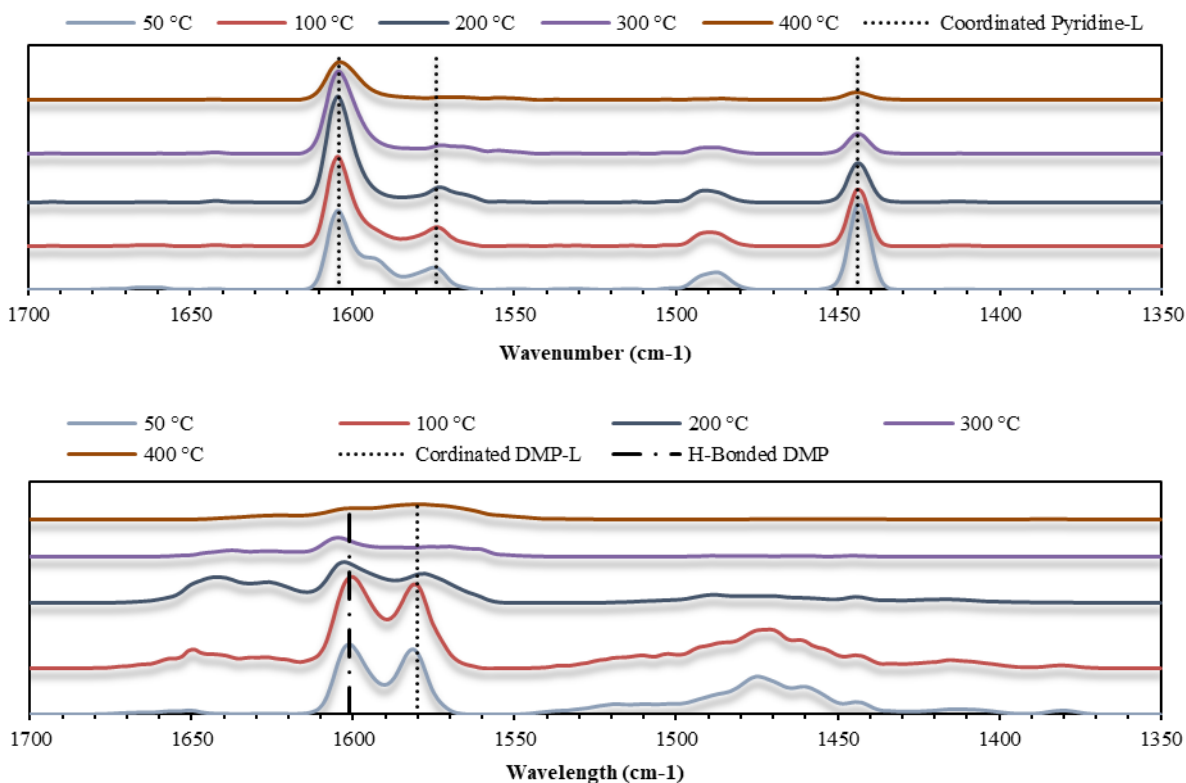

Figure 7. DRIFT spectra of absorbed pyridine (top) and DMP (bottom) on tetragonal ZrO_2.

Nonetheless, according to Busca[179], pyridine is not a strong enough base to be protonated or to form hydrogen bonds with weak Brønsted sites as the ones that might be present on ZrO_2. Hence, DRIFTs with dimethylpyridine (DMP) were performed (Figure 7-bottom). DMP's pKa is higher (6.6), and due to the steric hindrance induced by the two methyl groups, it has a weaker affinity for Lewis acid sites. Therefore it is commonly used as probe molecule to study Brønsted acidity[180]. The spectra obtained at low temperatures (50-300 °C) show the presence of a band at 1602 cm^{-1} that corresponds to H-bonded DMP (weak Brønsted sites). In addition, also at low temperatures (50−100 °C) a small band at 1473 cm^{-1} was seen, which correspond to protonated DMP. but as the temperature keeps increasing this band disappears. Nonetheless, these Brønsted acid sites have a weak strength that should not represent a drawback for CTH.

3.1.2. *Temperature screening for gas-phase CTH of ML using ethanol over tetragonal ZrO_2*

Firstly, in order to rule out the presence of internal and external diffusional limitations, few specific tests were conducted. Specifically, by doubling the inlet flow rate and diminishing the amount of catalyst, this without modifying the contact time. It is important to mention that it was not possible to increase the flow rate beyond a certain value because of the pressure drop inside the lab-scale reactor. These tests provided comparable conversions of ML, which allowed to rule out significant interparticle diffusional limitations. In addition, blank tests were performed by feeding the reactant mixtures in absence of the catalyst, in the conditions in which the study was conducted. A low conversion of 6% was detected at 400°C due to the decomposition of ML (mixture with a molar ratio of ethanol:ML equal to 10); we have also fed AL instead of ML, in this case the conversion was zero.

The catalytic activity of the tetragonal ZrO_2 was firstly tested for the gas-phase CTH of ML using ethanol as H-donor. Firstly, the temperature effect (in the range 200-400°C) was studied in order to establish the optimal conditions for the system. Tests were performed by feeding a mixture of ethanol and ML (ethanol/ML molar ratio = 10) in a stream of nitrogen (% mol organic mixture: 10%) with a 1 s residence time, for 4 h, using always a fresh sample of pre-treated pelletized catalyst. The ZrO_2 catalyst was treated in-situ inside the reactor under an air flow (30mL/min) for

1 h at 400°C in order to clean the surface from adsorbed water and CO_2. The obtained results are shown in figure 8.
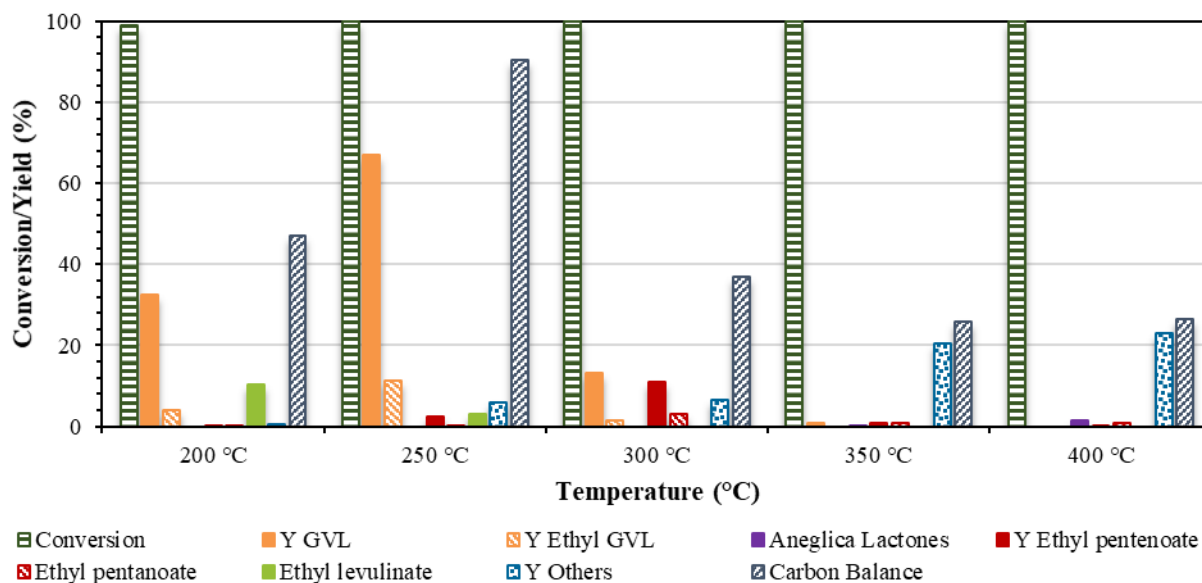

Figure 8. Catalytic results obtained in the CTH of ML with ethanol as H-donor over ZrO_2. Reaction conditions: ML:EtOH=1:10 (molar ratio), T: variable, $\tau = 1$ s, t = 4h, %mol N_2:ML:EtOH=90.1:0.9:9.

In the selected range of temperatures, the catalyst provides a complete conversion, proving to be highly active. However, even though at low temperatures such as 200 °C a GVL yield of around 33% was obtained after approximately 4 hours, high amounts of by-products such as EL and a low carbon balance (calculated as reported in the experimental section) were seen. As the temperature increases (250 °C), a higher yield of GVL is obtained (~67%). In addition, a high carbon balance of around 80% was seen; this behaviour is unexpected given the mild conditions and the use of a primary alcohol. The main by product obtained at 250 °C was ethyl-GVL, which could derive from the consecutive hydroxyethylation by acetaldehyde on the more activated α-position of the GVL ring and the consecutive dehydration and reduction of the obtained intermediate. Noteworthy, small amounts of EL were also detected at this temperature. This could indicate that ML is undergoing either transesterification reaction towards EL or the intermediate AL are undergoing alcoholysis.

Moreover, the presence ethylpentenoate was detected, but interestingly, no ALs were detected. This could be either due to their high reactivity towards the formation of GVL and/or other by-products, or to the possibility of having a different mechanism of reaction that do not undergoes intramolecular cyclisation to yield ALs but that undergoes reduction of the ketone group. However, the presence of 4-hydroxypentanoic acid derivatives was never detected under the studied reaction conditions (see Scheme 6 c).

Moreover, as the temperature was further increased, GVL yield decreased to 18% at 300 °C, and no GVL was detected at 350 and 400°C. This behaviour could be a consequence of consecutive reactions occurring on ALs and GVL, which could promote the formation of both heavier compounds and light, non-condensable compounds that could were not analysable by means of the off-line gas chromatograph.
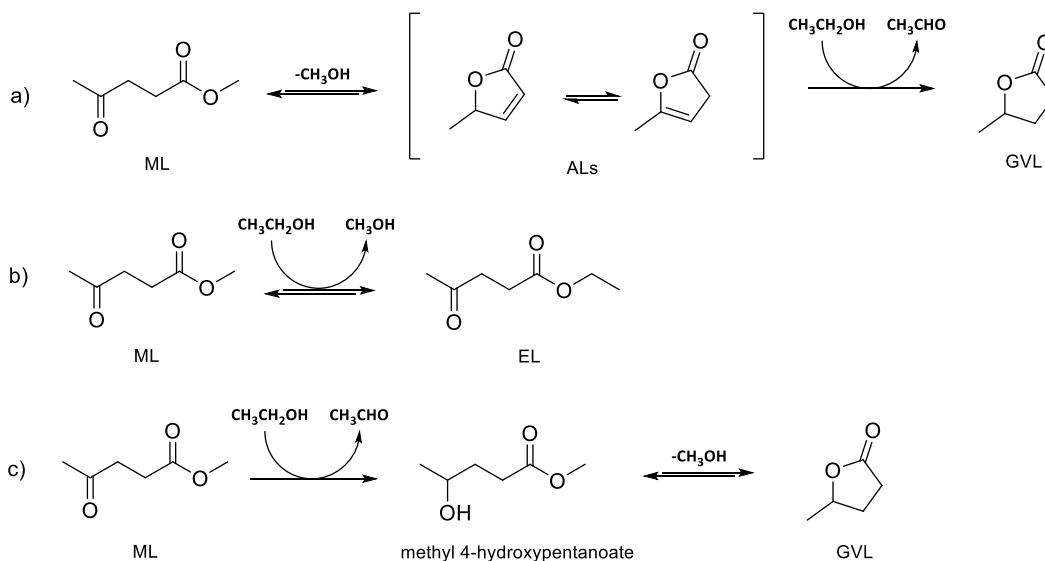
Scheme 6. GVL formation through CTH of ML with ethanol as H-donor. a) intramolecular cyclisation of ML to yield ALs and reduction to GVL; b) transesterification reaction; c) reduction of the ketone to the hydroxyacid and cyclisation.

In order to quantify the possibly formation of heavier compounds on the surface of the catalyst, thermogravimetric analyses were performed to the post-reaction catalysts. Table 7 shows that in all cases the percentage was below 4% (increasing with temperature). This means that the

formation of heavy carbonaceous material on the surface of the catalyst was not the main contributor to the low carbon balance. Instead, the light, non-condensable compounds were the ones that most probably made the main contribution to the lower carbon balance observed.

Table 7. Thermogravimetric analysis (TGA) of the spent tetragonal ZrO_2 performed under flow of air.

Reaction temperature (°C)	Reaction time (min)	Weight loss (%)	Max Desorption Temperature (°C)
250	240	2.28	323
300	240	2.51	355
350	240	3.34	352
400	240	2.79	387

In order to analyse this theory, catalytic tests were designed and performed to identify and quantify the light, non-condensable compounds. Initially, two tests were performed by feeding a solution of 10 mol% of ethanol at 250 and 400° C in order to identify the compounds that were related only to the decomposition of ethanol over the catalyst. Strangely, at 250°C (the apparent best conditions for the CHT of ML to yield GVL), ethanol decomposition was around 5% and the main products were water, diethyl ether (DEE), and 1-butene.

On the other hand, the test performed at 400°C (figure 9) (conditions in which no GVL was detected) showed rather different results. Firstly, ethanol had a complete and steady conversion during the entire time of the reaction, meaning that no important deactivation of the catalyst is occurring. In this case, DEE was detected only in traces and the main product was ethylene (yield 55%), this way proving the effectiveness of the acid sites for the promotion of ethanol dehydration. Moreover, the presence of hydrogen indicates the ability of the catalyst to produce acetaldehyde, which can rapidly undergo aldol condensation to yield C4 molecules. However, this intermediate aldol can undergo decarboxylation, this way explaining the formation of CO_2 and propylene in equimolar amounts. In addition, butadiene was also seen with an 8% yield, by means of the

Lebedev reaction. Lastly, 1-butene was detected in small quantities, which could be explained from the formation of 1-butanol (not detected) via the Guerbet pathway and its rapid dehydration.
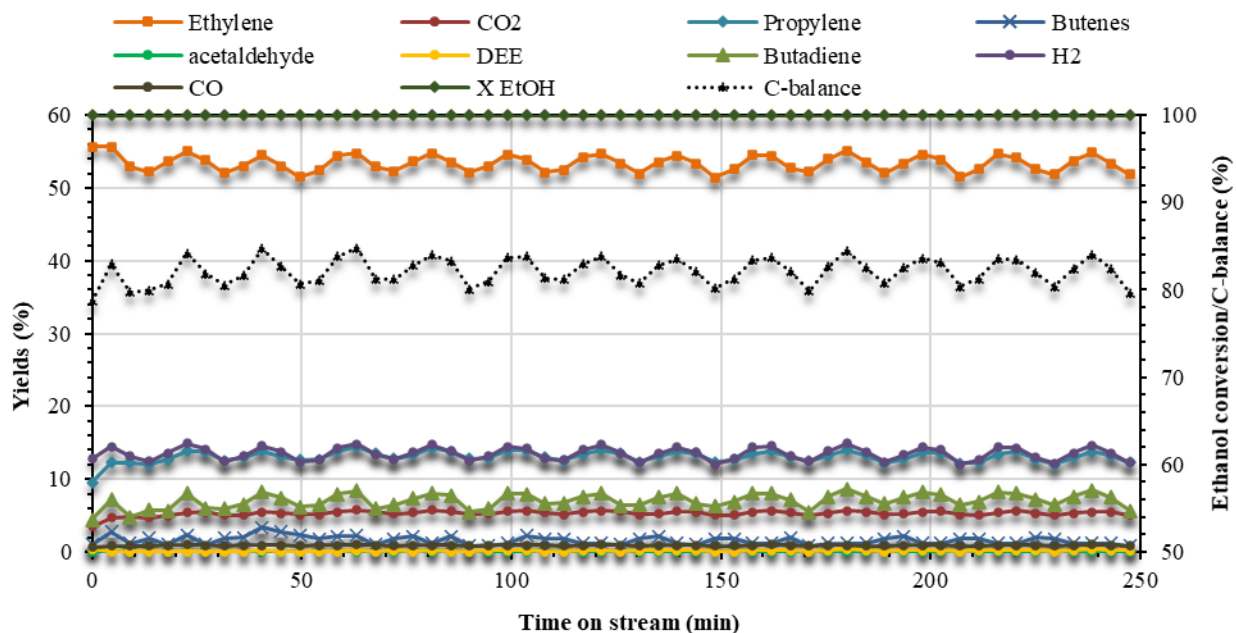

Figure 9. Ethanol decomposition over ZrO_2 at 400°C, τ = 1 s, %mol N_2:EtOH=89:11. Ethanol conversion is shown on the secondary vertical axis (right side), yields of the main products are shown on the left. Yields refer to inlet ethanol and on C atoms; H_2 yield refers to inlet ethanol and on H atoms.

In addition, a third test was performed in order to identify the light non condensable compounds obtained from the CTH of ML with ethanol. For this, a mixture of EtOH:ML (10:1) was fed to the reactor at 400°C (figure 10) and in order to avoid blockages in the columns of the micro-GC, the "heavy" compounds were condensed in acetonitrile. In this case, ethylene, propylene, and butadiene were formed with 40%, 18%, and 12% yields, respectively; other products detected were hydrogen, CO_2, and butenes. An increase in the formation of C3 and C4 unsaturated compounds can be seen. In addition, an increase in the amount of CO_2 was detected. This behaviour could be related to the decomposition of some of the reaction intermediates (such as ALs and GVL) by

decarboxylation. With these results, an overall reaction scheme of ethanol decomposition was proposed (Scheme 7).
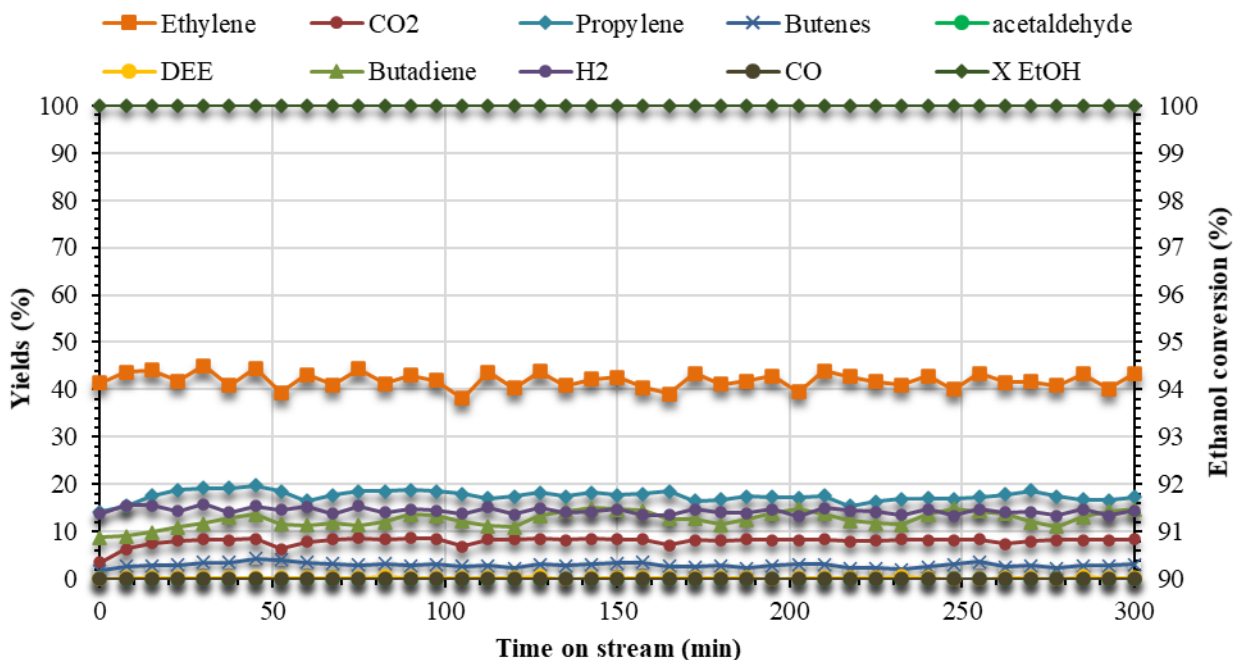

Figure 10. Light products obtained in the ML CTH with ethanol as H-donor over ZrO_2. Reaction conditions: ML:EtOH=1:10 (molar ratio), T: 400°C, τ = 1 s, %mol N_2:ML:EtOH=89:1:10. Ethanol conversion value is shown on the secondary vertical axis (right side), the yields of main products are shown on the left (yields were calculated referring to ethanol only). Considering the condensation of the heavy compounds in acetonitrile it was not possible to evaluate the carbon balance.

The results obtained so far strongly suggest that in fact high surface area tetragonal ZrO_2 has the ability of activating ethanol, a primary alcohol, to act as an H-donor in CTH reactions. Most studies published so far have shown only the activation of secondary alcohols such as isopropanol, this is due to the stability of the intermediate that is formed from isopropanol during the reaction.
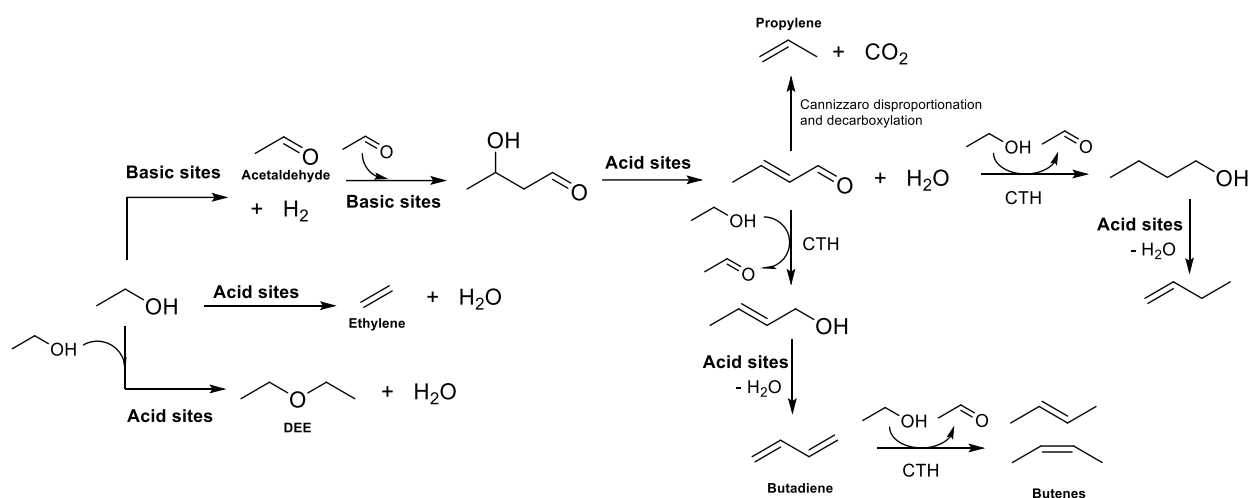
Scheme 7. Proposed reaction pathways for ethanol decomposition over ZrO₂ catalyst.

3.1.3. CTH of ML using ethanol over monoclinic ZrO₂

In order to confront the catalytic activity of the different crystalline phases in which ZrO_2 can be found, catalytic tests were performed using a commercial, monoclinic, low SSA (3 m²/g) ZrO_2 (CAS: 1314-23-4; Aldrich code: 204994). Results obtained can be seen in figure 12.
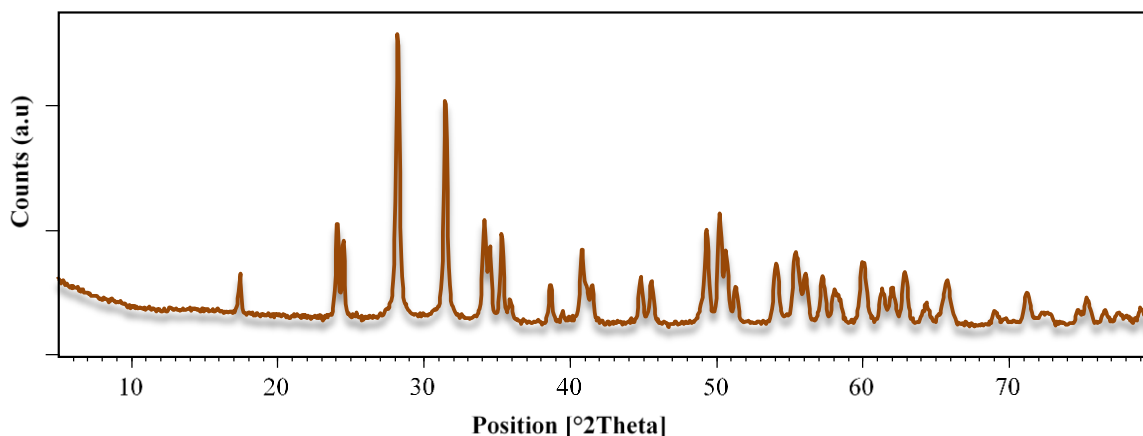

Figure 11. XRD of commercial ZrO_2 catalyst (Baddeleyite ref code. 00-007-0343).

In comparison to the tetragonal high surface area ZrO_2, the commercial monoclinic ZrO_2 shows a low activity. At 250 °C and 300 °C ML reaches a conversion of 28% and 30% and the GVL yield reaches 4% and 5%, respectively. However, it's important to mention that in both cases ALs were

detected, even if in small quantities. This confirms that in fact ALs are the main intermediates of the reaction (scheme 6 a). Moreover, EL was also detected in both tests, this time in higher amounts, once again suggesting that either ML is undergoing transesterification with ethanol or that ALs might be undergoing alcoholysis. As the temperature increase to 400 °C, the conversion of ML also increases, reaching a value of 96%. In addition, GVL yield reaches a value of 23% and ALs yield reaches a value of 6%.
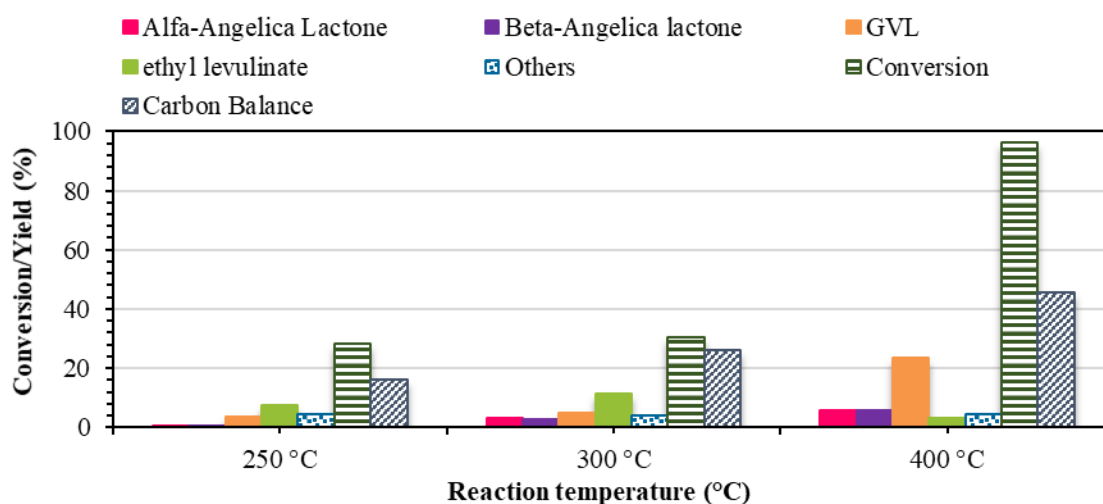
Figure 12. Catalytic results obtained in the CTH of ML with ethanol as H-donor over commercial monoclinic ZrO_2. Reaction conditions: ML:EtOH=1:10 (molar ratio), T: variable, τ = 1 s, t = 4h, %mol N_2:ML:EtOH=90.1:0.9:9.

Nonetheless, the difference in catalytic activity of this samples is mainly due to the different surface areas, and a direct influence of the crystalline phase cannot be ignored. Because of this, a high surface area monoclinic ZrO_2 was synthetized. A modified version of the procedure (hydrothermal) reported by Cheng et al. was followed[181]. The catalyst obtained had mainly monoclinic phase, but most importantly, as seen in table 8, it had a high surface area, this way allowing to make a comparative analysis between the two crystalline phases and understand its influence in the catalytic activity.
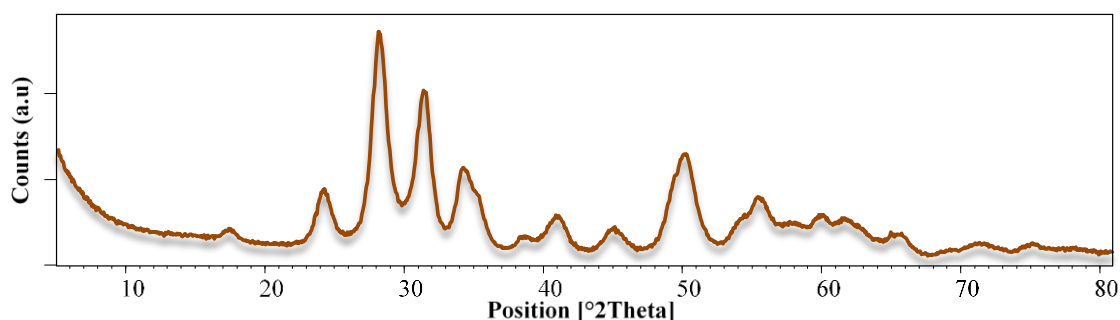
Figure 13. XRD of synthesized monoclinic ZrO_2 catalyst (Baddeleyite ref code. 00-024-1165).

In addition, TPD analysis (figure 14) where conducted on the monoclinic ZrO_2, and it was evident how this catalyst has a higher basic and acid density in accordance with the literature[182]. Indeed, monoclinic zirconia shows a lower coordination state of both Zr^{4+} and O^{2-} atoms over the surface compared to the tetragonal phase. Just like the tetragonal ZrO_2, the ammonia desorption profile showed a wide desorption peak from 180 to 450°C, indicating the coexistence of weak, moderate and strong acid sites[91,100,178]. In the case of CO_2 desorption profile, again one wide peak was observed, however this time the peak was centred around 140°C, indicating stronger basic sites. Moreover, table 8 shows how the basic density of monoclinic ZrO_2 is around 4 times higher than the one present in tetragonal ZrO_2. This big difference might promote a different catalytic activity than the one obtained with a tetragonal phase.

Table 8. Nature, specific surface areas and acid and basic densities monoclinic ZrO_2.

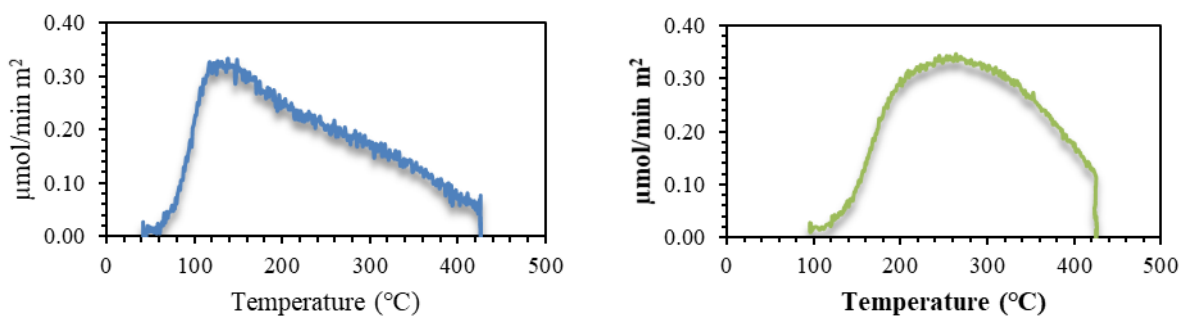| Catalyst	SSA (m^2/g)	Crystalline phase (XRD)	Acid density $(\mu mol/m^2)$	T max desorption (°C)	Basic density $(\mu mol/m^2)$	T max desorption °C
Monoclinic ZrO_2	117	Mainly monoclinic	8.47	Wide band from 200 to 400°C	7.71	Wide band from 130 to 350°C

Figure 14. CO_2-TPD (left) and NH_3 (right) profiles of synthesized monoclinic ZrO_2.
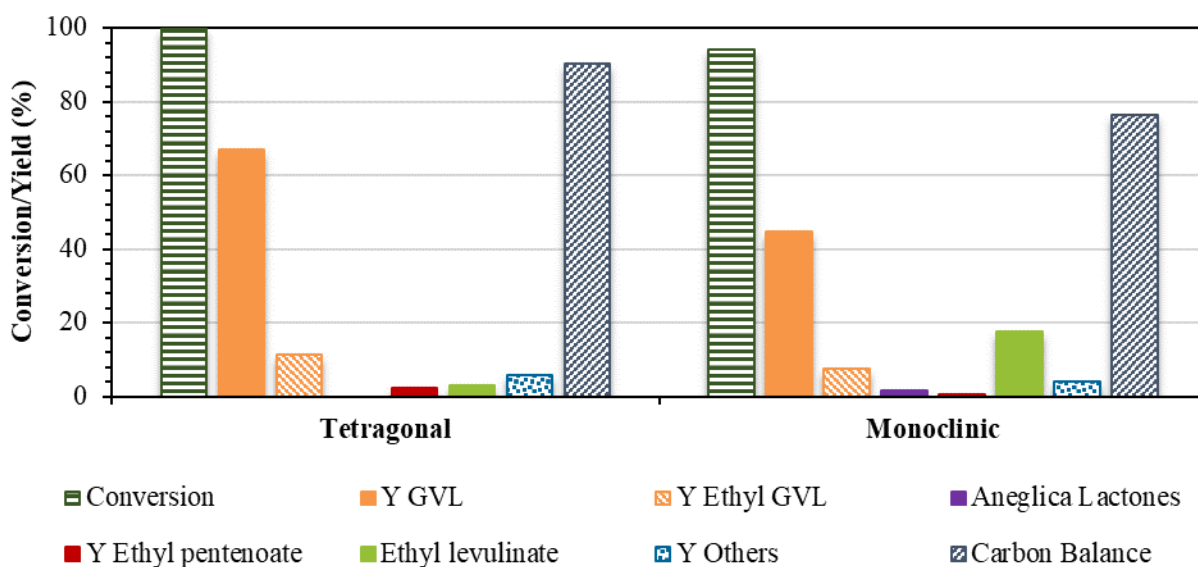

Figure 15. Catalytic results obtained in the CTH of ML with ethanol as H-donor over synthetized tetragonal and monoclinc ZrO_2. Reaction conditions: ML:EtOH=1:10 (molar ratio), T: 250 °C, τ = 1 s, t = 4h, %mol N_2:ML:EtOH=90.1:0.9:9.

Monoclinic ZrO_2 was then tested under the previously optimized conditions (250 °C) for the CTH of ML with ethanol. The results obtained were similar to those obtained while using tetragonal ZrO_2 (figure 15). However, GVL yield reached a lower value when using monoclinic ZrO_2 in comparison to that obtained when using tetragonal ZrO_2, 45% and 67% respectively. In addition, monoclinic ZrO_2 yielded higher amount of EL, once again suggesting either the transesterification of ML or the alcoholysis of ALs. Noteworthy, while using monoclinic ZrO_2, ALs were seen in

small quantities, this way hinting that the mechanism of reaction indeed follows an intramolecular cyclization of ML to form ALs that then undergo CTH to yield GVL. This way, once again, discarding the possibility of another mechanism of reaction through the reduction of the ketonic group as mentioned previously.

3.1.4. *CTH of alkyl levulinates using methanol and isopropanol as H-donor.*

In order to perform a thorough study of the tetragonal high surface area ZrO_2 and its use in CTH reactions, the catalyst was also tested for the CTH of different alkyl levulinates (EL) using both primary (methanol) and secondary alcohols (isopropanol). These tests were performed under the best conditions observed with ML and ethanol. Results can be seen in figure 16.

It can be seen that, just as with ethanol, tetragonal ZrO_2 provides a complete conversion of ML and a high yield for GVL (80%) when isopropanol is used as H-donor. The reaction follows a similar behaviour as with ethanol, GVL yield is limited by two consecutive reactions:

    i.   Alcoholysis of GVL which yields propyl pentenoate

    ii.   Consecutive reduction/dehydration of GVL to 2-methyltetrahydrofuran (2-MTHF), seen only in small quantities (yield <5%).

Nonetheless, isopropanol provides a more stable catalytic activity. This behaviour might be a consequence of either the higher steric hindrance of the secondary alcohol, which hinders the transesterification of ML and/or the alcoholysis of ALs, or the higher reactivity of isopropanol might limit parasite reactions which could promote the formation of heavy carbonaceous material on the surface of the catalyst. Just as expected and as reported in the literature, isopropanol has proven to be a more active H-donor for the CTH of ML.

When using methanol as H-donor, a completely different behaviour was seen, in which ML conversion reaches an average value of 35%, providing a very low GVL yield (4%) and a high carbon loss. These results could lead to think that an equilibrium limitation could be present during

the reaction of intramolecular cyclisation of ML to form ALs in the presence of an excess of methanol.

However, in order to further properly explain the poor reactivity of methanol, it is necessary to take into consideration the results obtained from the CTH of EL. In this case, the CTH of EL with methanol shows a higher reactivity compared to ML (90% and 35% of average conversion respectively). This behaviour might be due to an increased efficiency of ethyl as leaving group during the intramolecular cyclization of EL to form ALs (detected only in small quantities) and most probably to the transesterification of EL with methanol to form ML. It can be seen that methanol is the least active alcohol for CTH of alkyl levulinates, which can be confirmed, again, from the high quantities of ML detected from either the transesterification of EL with methanol or the alcoholysis of ALs.

Analysing the results obtained from the CTH of EL with ethanol, provides further evidence of the higher reactivity of EL, and in addition allows further confirmation of the absence of an equilibrium limitation for the intramolecular cyclization. In fact, a similar result to that obtained with ML was obtained; a complete conversion of EL, being GVL and ethyl-GVL the main products.

Lastly, Figure 16 shows that when using isopropanol as H-donor for the CTH of EL a similar behaviour to that of ML is obtained, reaching a complete conversion of the alkyl levulinate with GVL and propyl pentenoate as the main products. However, the yield for GVL was lower and there was a higher carbon loss.
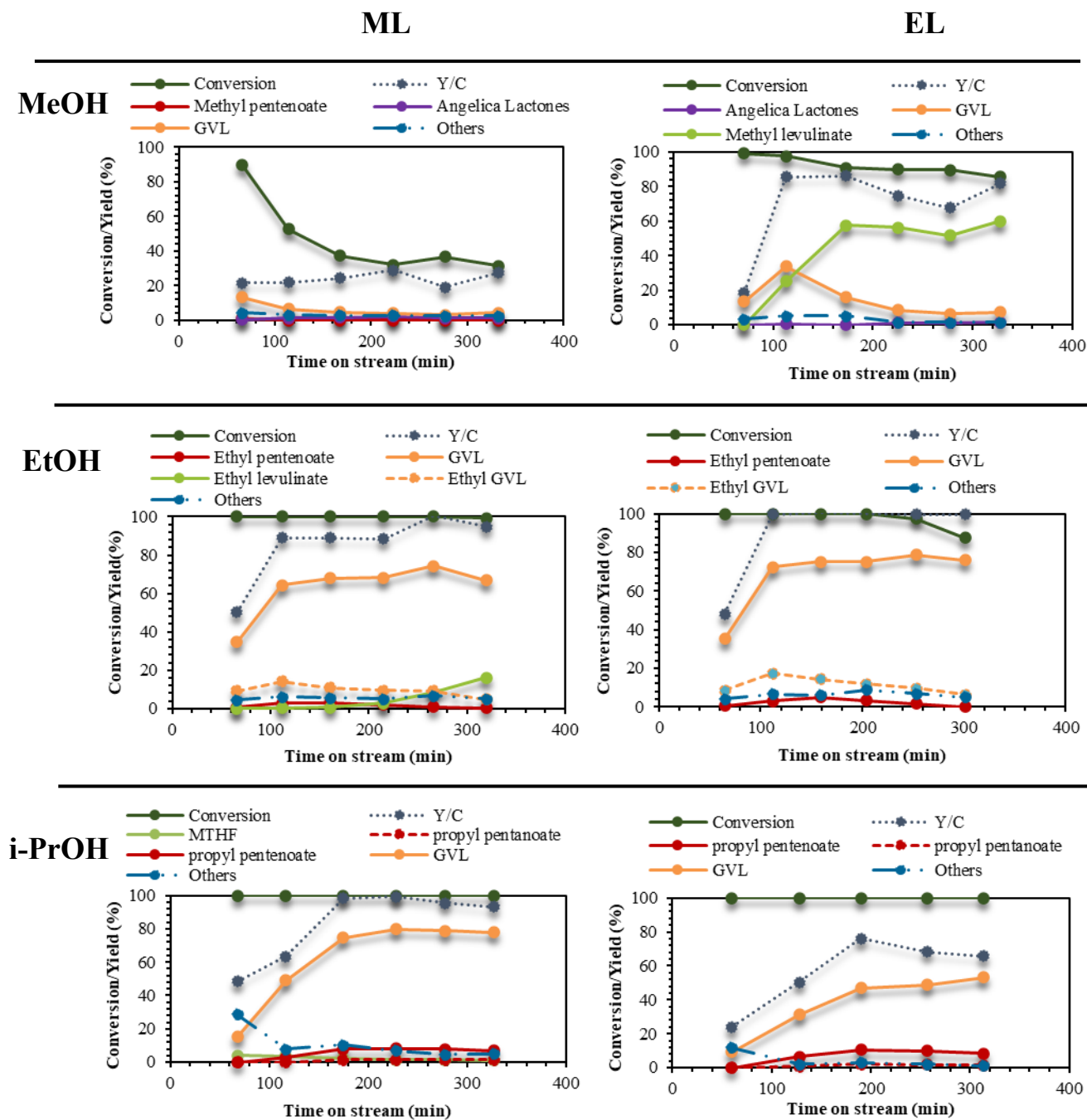
Figure 16. Catalytic results obtained in the CTH of ML and EL with different alcohols as H-donor over tetragonal ZrO_2 in the gas-phase. Reaction conditions: (EL or ML):EtOH=1:10 (molar ratio), T: 250 °C, τ = 1 s, %mol N_2: (EL or ML):(alcohol)=90.1:0.9:9.

To further understand the catalyst deactivation and the poor carbon balance obtained in some of the catalytic tests, TGA analyses were conducted the post-reaction catalysts (table 9). Results show that when using methanol as H-donor, a higher amount of carbonaceous material is deposited on the surface of the catalyst, which has a direct effect on the carbon balance. This could be a consequence of the formation of formaldehyde from the dehydrogenation of methanol, which could promote the oligomerization of ALs, leading to catalyst deactivation. On the other hand, the similar weight loss observed using isopropanol as H-donor for the reduction of both ML and EL confirm that the increased reactivity of the substrate (EL) together with the high reactivity of this secondary alcohol promote the formation of undetectable light compounds finally lowering both the C-balance and GVL yield.

Table 9. TGA of the spent tetragonal ZrO_2 performed under flow of air.

Alkyl levulinate	H-donor	Time-on-stream (min)	Weight lost (%)	Accumulation (mg/min)
EL	2-PrOH	314	3.03	0.00135
EL	EtOH	301	3.13	0.00164
EL	MeOH	328	4.00	0.00088
ML	2-PrOH	327	3.20	0.00098
ML	EtOH	320	3.05	0.00130
ML	MeOH	332	7.66	0.00246

As it was performed for ethanol, tests were conducted in order to identify and quantify the light, non-condensable compounds that might be formed due do the decomposition of methanol and isopropanol. For this reason, a dedicated test was performed by feeding only the alcohol over the catalyst and analysing the outlet stream with an on-line micro-GC. In the case of methanol, the conversion was close to 78% for the entire time of the reaction (ca. 3h). Dimethyl ether (DME) and water were the main products obtained, with yields of around 60% and 25% respectively, and small amounts of CO and H_2 were also detected, around 4% yield for both, both product of the decomposition of formaldehyde which was not detected.
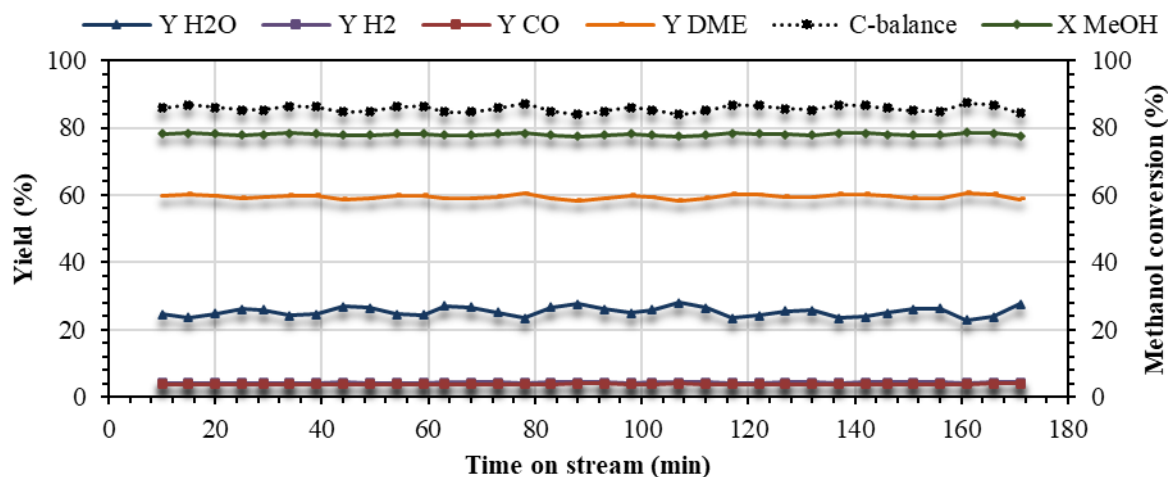
Figure 17. Methanol decomposition over ZrO_2 at 400°C, τ = 1 s, %mol N_2:MeOH=85:15. Methanol conversion (green) is shown on the secondary vertical axis (right side), yields of the main products are shown on the left. Yields refer to inlet methanol and on C atoms; H_2 and H_2O yield refers to inlet methanol and on H atoms.

The main reaction involved in the decomposition of methanol are the following:

$$2\ CH_3OH \rightarrow CH_3OCH_3 + H_2O \tag{5}$$

$$CH_3OH \rightarrow CH_2O + H_2 \tag{6}$$

$$CH_2O \rightarrow CO + H_2 \tag{7}$$
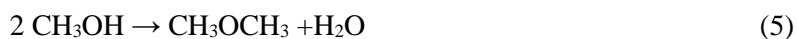
The low quantities of H_2 and CO detected allow to confirm again the poor role that ZrO_2 plays in activating methanol to act as H-donor.

In the case of isopropanol (figure 18), during the first 50 minutes on stream, the conversion is complete. However, as time passes by, the conversion slightly decreases till a constant value of 98%. This means that the catalyst slightly deactivates with time and it could be related to the deposition of heavy carbonaceous material formed due to consecutive reactions such aldol condensation of acetone[65,83,93]. In fact, small amounts of acetone were detected, and interestingly, its yield increases as the conversion of isopropanol starts to decrease. In addition, small quantities of H_2 were detected, consequence of the dehydrogenation of isopropanol to yield acetone. The

main product observed was propylene (yield 70%) this way demonstrating the effectiveness of the acid sites for the promotion of dehydration. In addition, small quantities of CH_4 and CO_2 where observe, and this might come from acetone's consecutive reactions such as aldolic condensations.
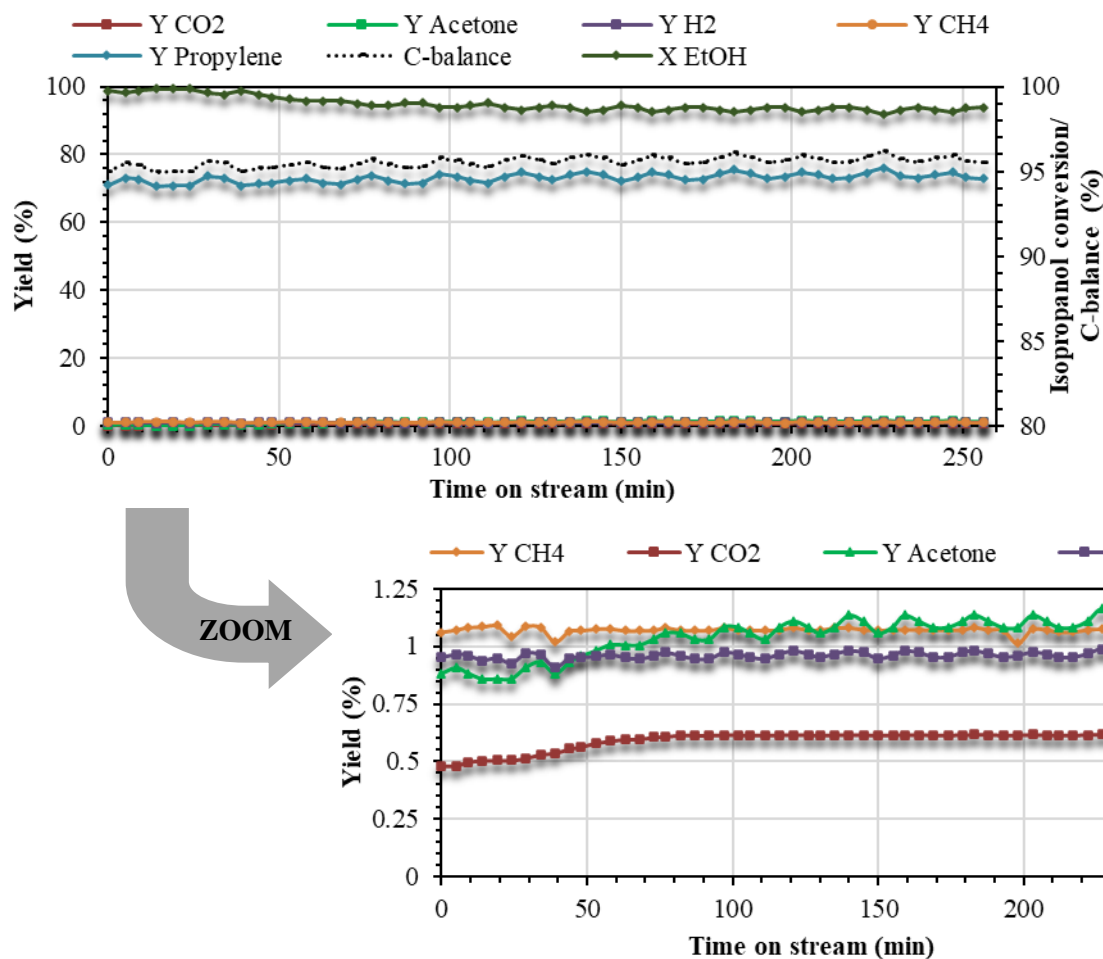

Figure 18. Isopropanol decomposition over ZrO_2 at 400°C, τ = 1 s, %mol N_2:i-PrOH=91:9. Isopropanol conversion (green) is shown on the secondary vertical axis (right side), yields of the main products are shown on the left. Yields refer to inlet isopropanol and on C atoms; H_2 yield refers to inlet isopropanol and on H atoms.

3.1.5. Catalyst stability test in the gas-phase CTH of alkyl levulinates

Even though isopropanol appeared to be the most efficient H-donor in the gas-phase CTH of alkyl levulinates, the results obtained with ethanol show, for the first time, a successful activation of ethanol, a primary alcohol, for the gas-phase CTH of alkyl levulinates. Because of this, the stability of the catalyst was studied by performing a deactivation test, increasing the time on stream. Figure 19 shows that during the first 300 minutes of reaction, a steady complete conversion was achieved, with a high carbon balance (92%) and with a high yield and selectivity towards GVL (maximum value of 71%), as it has already been observed in figure 8. However, at longer reaction times, the catalyst appears to suffer a progressive deactivation, providing a slightly lower conversion of ML (92%). Noteworthy is the fact that, as soon as the conversion starts to decrease, the yield of the intermediate ALs, which were previously not detected, starts to increase, once again providing evidence that they seem to be the intermediates of the reaction.

In addition, a shift on the chemoselectivity of the reaction starts to occur with the catalyst deactivation. In fact, a progressive increase in the selectivity towards EL was observed with a contemporaneous decrease of GVL. This phenomenon could be the effect of possible changes in the active sites of the catalyst, which could favour either the transesterification of ML with ethanol, or the alcoholysis of ALs to yield EL.

After 10 hours of reaction, the catalyst was regenerated *in-situ* by feeding a flow of 30 mL/min of air at 400°C for 2 hours, and then it was used once again for the CTH of ML with ethanol at 250°C. Figure 19 shows that an almost complete recovery of the initial behaviour was achieved, this suggests that the deactivation is probably due to the deposition of heavier carbonaceous compounds on the surface of the catalyst which might block the active sites in ZrO_2.
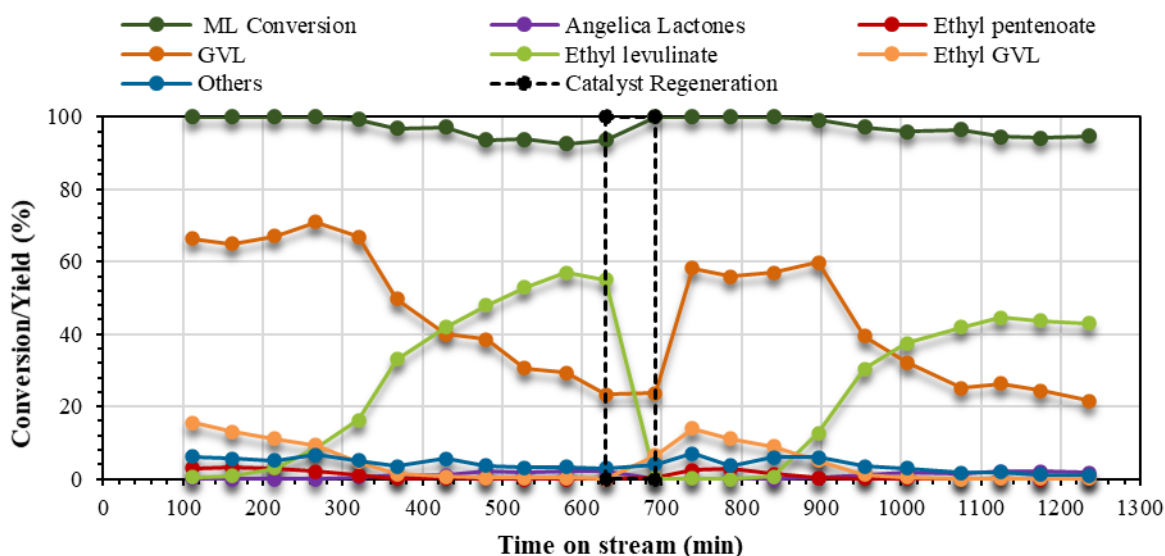
Figure 19. Catalytic results obtained in the CTH of ML using ethanol as H-donor over tetragonal ZrO_2. Reaction conditions: ML:EtOH=1:10 (molar ratio), T: 250°C, τ = 1 s, %mol N_2:ML:EtOH=90.1:0.9:9.

The stability of monoclinic ZrO_2 was also studied by increasing the time on stream, results can be seen in figure 20. The catalytic behaviour observed is quite similar to the one obtained when using tetragonal ZrO_2; it can be seen a maximum value in the yield of GVL after 200 minutes of reaction (63%), faster than with tetragonal ZrO_2. However, after this, a sudden drop in both ML conversion and GVL yield was observed. Following the same trend as seen when using tetragonal ZrO_2, as the catalyst experiences a progressive deactivation, a change in the chemo-selectivity of the reaction is observed. A continuous decrease in GVL yield is seen whit a simultaneous increase in the yield of EL. In this case, the yield of GVL and EL are equal when 250 minutes on stream have passed. While using tetragonal ZrO_2, this only occurs after 430 minutes on stream. In addition, as already seen in figure 19, as soon as the monoclinic ZrO_2 starts to deactivate, the yield in ALs increases. In this case, the yield for ALs is higher to that obtained while using tetragonal ZrO_2. This and the fact that the catalyst has a faster and higher deactivation, could be due the formation of heavy carbonaceous material in the surface of the catalyst. In fact, it has been known that when ALs lactones are in contact with catalyst with strong acidity and basicity, they tend to form

oligomers[183–185], and as previously mentioned, monoclinic ZrO_2 has a higher basic and acid density than tetragonal ZrO_2. In addition, only small amounts of ethyl pentenoate related to consecutive reactions over GVL were observed. This again probably related the deposition of heavy carbonaceous material on the surface of the catalyst that might be blocking the active sites.
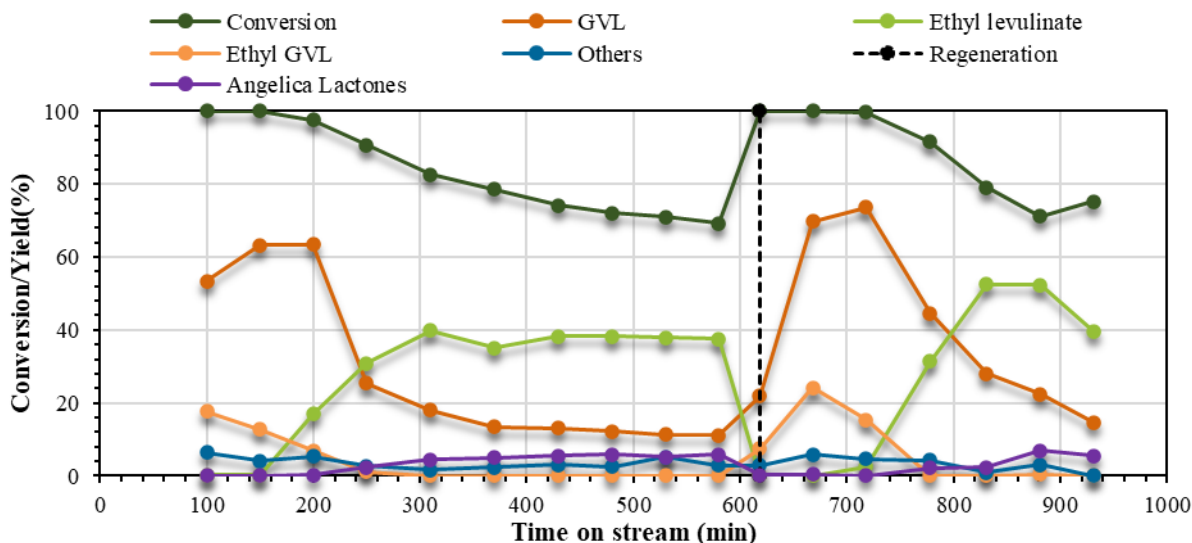

Figure 20. Catalytic results obtained in the CTH of ML using ethanol as H-donor over synthesized monoclinic ZrO_2. Reaction conditions: ML:EtOH=1:10 (molar ratio), T: 250°C, $\tau = 1$ s, %mol N_2:ML:EtOH=90.1:0.9:9.

This difference in behaviour can be explained due to a difference in acid and basic density presented in the monoclinic ZrO_2. In fact, as seen in table 8, monoclinic ZrO_2 has both a higher acid and basic density. The basic sites firstly favour the intramolecular cyclization of ML to yield ALs that then, through the acid sites, appear to be polymerizing forming heavy carbonaceous material on the surface of the catalyst, favouring a faster deactivation of monoclinic ZrO_2. For this, thermogravimetric analyses were performed on the spent catalysts. Indeed, as seen on table 10, monoclinic ZrO_2 appears to form higher amount of carbonaceous material on the surface of the catalyst.

Table 10. TGA of the spent monoclinic and tetragonal ZrO_2 performed under flow of air.

Catalyst	Time-on-stream (min)	Weight lost (%)	Accumulation (mg/min)
Tetragonal ZrO_2	630	2.3	0.098
Monoclinic ZrO_2	580	5.4	0.168

As stablished by Zhao et al., one of the main differences between monoclinic and tetragonal ZrO_2 is the coordination of the cations and anions in the structure. In fact, in monoclinic ZrO_2, Zr^{4+} cations are heptacoordinated and O^{2-} anion are either tri- or tetracoordinated. In contrast, in a tetragonal crystalline phase, Zr^{4+} cations are octacoordinated and O^{2-} anion are only tetracoordinated[186,187]. These variation in structural arrangements and coordination of the cations provides different coordinatively unsaturated surface sites which lead to diverse acidic and basic properties[182], which has already been demonstrated from CO_2 and NH_3 TPD analyses. Moreover, these differences in structure also affect the distribution of the hydroxy groups[182]. In fact, previous studies have shown the different forms of coordination of the hydroxy groups with the unsaturated centres in the surface of the catalysts; both mono- and multi-coordinated for monoclinic ZrO_2 and only multi-coordinated for tetragonal ZrO_2[187].
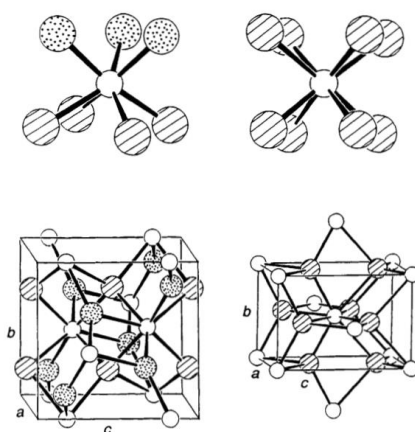

Figure 21. Coordination polyhedral for Zr^{4+} and unit cells in monoclinic (left) and tetragonal (right) ZrO_2. (Zr^{4+}: small circles, oxygen: large circles; tricoordinated O^{2-}: spotted, tetracoordinated O^{2-}: lined)[188].

According to Albuquerque et al., coordinatively unsaturated cations are responsible for Lewis acidity and because of this, the existence of different surface Zr^{4+} sites induced by the presence of different types of O^{2-} anions becomes plausible[182]. In fact, it has been reported that the tri- and tetracoordinated O^{2-} anions on monoclinic ZrO_2 produce two different surface sites of Zr^{4+}, and correspondingly only one type in tetragonal ZrO_2, this way offering a possible explanation for the slightly higher acidity in monoclinic ZrO_2[186,188].

Monoclinic ZrO_2 was also regenerated *in-situ* by feeding a flow of 30 mL/min of air at 400°C for 2 hours, and used once again for the CTH of ML with ethanol at 250°C. Once again, an almost complete recovery of the initial catalytic behaviour was obtained. These results agree with has been previously stated regarding the deposition of carbonaceous material in the surface of the catalyst.

3.1.6. *Deactivation studies*

Even though high conversion, high GVL yields and good selectivity are achieved during the first 300 min of reaction while working with ethanol as H-donor and ML as substrate, the particularity of the contemporaneous chemo-selectivity change and deactivation of the catalyst is present. In order to understand this behaviour, characterization of fresh and spent tetragonal ZrO_2 by means of both *ex-situ* and *in-situ* techniques was performed.

It has been already mentioned that ethanol is an attractive H-donor given its abundance, sustainability, and environmentally benign nature, it has been rarely applied to perform CTH[83,93,112]. In fact, this has been, in part, attributed to the catalyst deactivation caused by the alcohol dehydrogenation product. It has been reported that acetaldehyde easily suffers metal mediated decarboxylation, this way generating catalytically inactive metal carbonyl species (Scheme 8)[189].
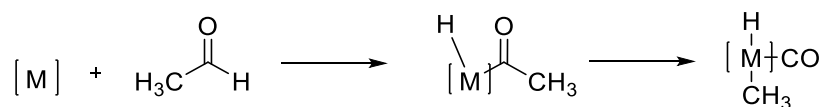
Scheme 8. Formation of carbonyl species over transition metal catalysts.

60

Considering this situation, a catalytic test feeding a lower excess of ethanol with respect to ML (ethanol:ML molar ratio of 4) was performed to identify if in fact limiting the amount of ethanol could affect the deactivation rate (Figure 22). Curiously, the results obtained showed a much faster deactivation, this way demonstrating that under the optimized conditions, ethanol and the *in-situ* formed acetaldehyde are not the main responsible for this event.
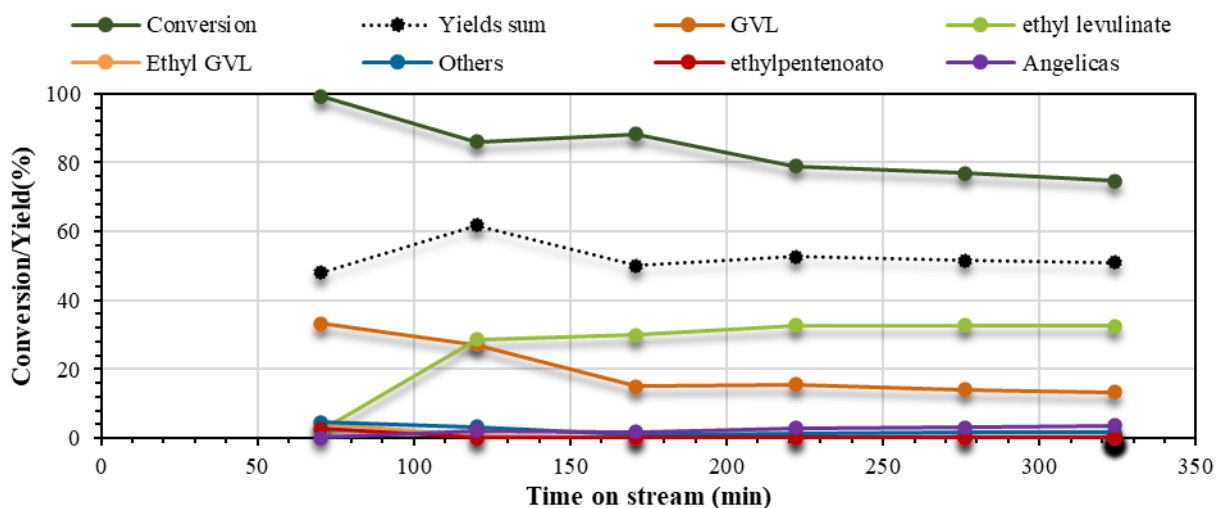

Figure 22. Catalytic results obtained in the ML reduction via H-transfer with ethanol over tetragonal ZrO_2. Reaction conditions: ML:EtOH=1:4 (molar ratio), T: 250°C, τ = 1 s, %mol N_2:ML:EtOH=91:1.8:7.2.

It could be assumed that ML attaches to the active sites and rapidly react to form ALs. However, ALs are detected only in small quantities (<5%). This might be due to the lack of reducing agent (ethanol), which hinders the reduction of the doble bond in ALs. Instead, they quickly react through condensation pathways to form oligomers that could block the active sites of the catalyst, this way explaining the faster deactivation[183,185].

In order to have a broader understanding of what happens on the surface of the tetragonal ZrO_2
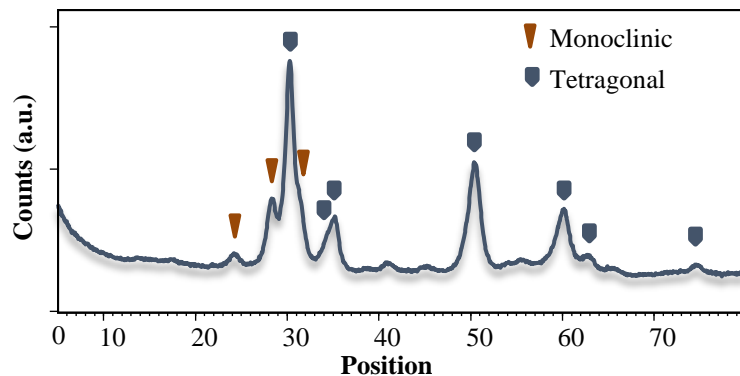

Figure 23. XRD of spent tetragonal ZrO_2 catalyst (ref code: 00-050-1089).

after reaction and after regeneration, several characterizations were performed. Firstly, XRD and BET analyses were conducted on the spent and regenerated catalyst in order to identify any changes in the crystalline phase and specific surface area that might have occurred during the reaction. In fact, after BET, it was determined that

the specific surface area of tetragonal ZrO_2 had changed from 120 to 84 m^2/g after the CTH of ML with ethanol as H-donor. This is most likely due to the deposition of heavy carbonaceous material on the surface of the catalyst which led to a decrease in the specific surface area. On the other hand, figure 23 shows X-ray diffraction patterns of the spent catalyst, and it can be clearly seen that there are no noticeable changes to the crystalline structure of the catalyst. In addition, BET measurement was performed on the regenerated catalyst, and no significant change in the specific surface area was observed in comparison to the fresh catalyst.

Moreover, the spent and regenerated tetragonal ZrO_2 were characterized by means of DRIFTs. Figure 24 (A and B) shows the DRIFT spectra obtained from the pyridine absorption of the spent and the fresh catalyst, and it can be seen that the spent catalyst has lost the bands corresponding to the coordination of pyridine with Lewis acid sites. However, figure 24 C shows that after treating the catalyst for regeneration, a partial recovery of the active sites is achieved, this way evidencing how the loss of the sites is taking place due to the deposition of heavy carbonaceous materials.
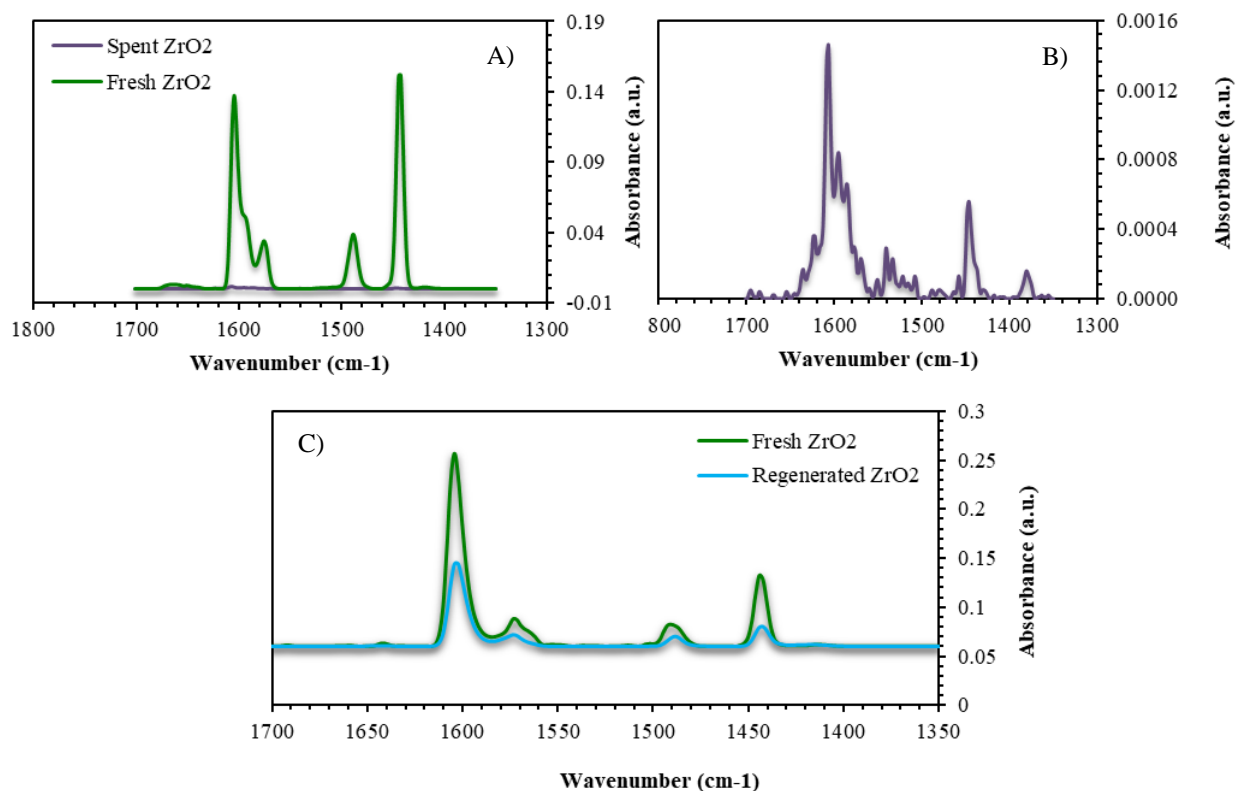
Figure 24. DRIFT spectra of adsorbed pyridine on the fresh, spent, and regenerated tetragonal ZrO_2. A) Spent and fresh ZrO_2, B) Spent ZrO_2, C) Fresh and regenerated ZrO_2.

In addition, TPD analyses were performed in order to analyse the acid and basic density of the spent and regenerated tetragonal ZrO_2. In the case of NH_3-TPD, they confirm the results already seen from DRIFT analyses. The spent catalyst showed to have a complete loss of its acid sites while the regenerated showed a partial recovery, reaching an acid density of 6.154 $\mu mol/m^2$ as seen on table 11 and figure 25. In the case of CO_2-TPD the spent catalyst was firstly treated with He at 500 °C for 1 hour. Interestingly, it can be seen in figure 27 that a non-neglectable amount of CO_2 is released while treating the spent catalyst in an inert atmosphere. This CO_2 could be formed from the decarboxylation of heavy compounds that might have been deposited in the surface of the catalyst during the reaction.

Table 11. Nature, specific surface areas and acid densities spent and regenerated tetragonal ZrO_2.

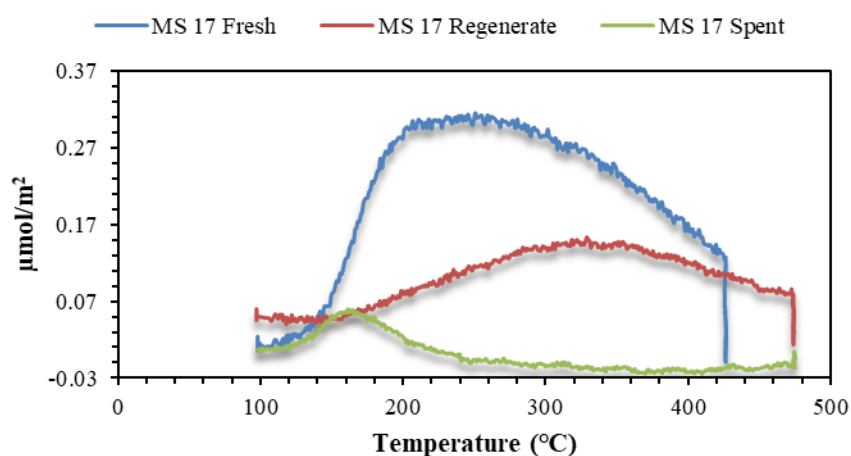| Catalyst	SSA (m²/g)	Crystalline phase (XRD)	Acid density (μmol/m²)	T max desorption (°C)
Spent ZrO_2	80	Mainly tetragonal	0.008	160 °C
Regenerated ZrO_2	120	Mainly tetragonal	6.154	Wide band from 200 to 400°C

Figure 25. NH$_3$-TPD on spent, regenerated and fresh tetragonal ZrO_2.

As mentioned previously, ALs are known to form oligomers in presence of amphoteric catalyst, but moreover, they have been seen to form polymers containing carboxylic groups[190], which could be the responsible for the release of CO_2 seen in figure 26.

This phenomenon does not allow for the basic density of the spent catalyst to be analysed by means of CO_2-TPD. In addition, besides CO_2, there was also a release of a CO, which might also come from these heavy carbonaceous compounds formed in the surface of the catalyst. After pre-treatment in He, the catalyst was exposed to a flow of CO_2 for 1 hour at 40 °C. Physiosorbed molecules were removed by flushing with He for 60 min before starting with the temperature-programmed desorption. Interestingly, during the desorption, the basic density of the catalyst was 1.39 µmol/m², quite similar to that of the fresh catalyst (1.88 µmol/m²), this way demonstrating

that a partial recovery of the basic sites can be achieved by thermally treating the spent catalyst also in an inert atmosphere.
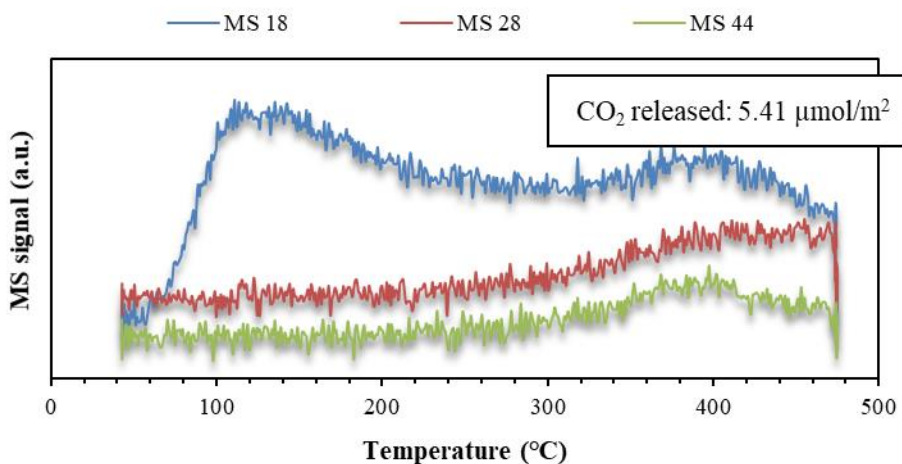

Figure26. He pre-treatment for CO_2-TPD on spent tetragonal ZrO_2.

In order to further improve the performance of tetragonal ZrO_2 or limit its deactivation rate, a test was conducted in which water was co-fed with ML and ethanol. Surprisingly, the obtained results (Figure 27) showed that water actually has a detrimental effect on the desired CTH reaction, both decreasing GVL yield, favoring the formation of EL and promoting a faster deactivation of the catalyst.

A probable explanation could be that water might promote the formation of Brønsted acid sites and according to Kon et al.[191], the products of levulinic acid hydrogenation depend on the type of acid sites on the surface of the catalyst. When the catalyst contains mainly Brønsted acid sites, the formation of pentanoate from the GVL alcoholisys and the formation of levulinates from the alcoholysis of ALs are the most favored reactions. In the case the catalyst contains mainly Lewis sites, the formation of GVL through the CTH mechanism is the most favored reaction. Nonetheless, another possible explanation could be that water might also be promoting the hydrolysis of the levulinate ester, forming LA, which tends to adsorb strongly to the surface of the catalysts.
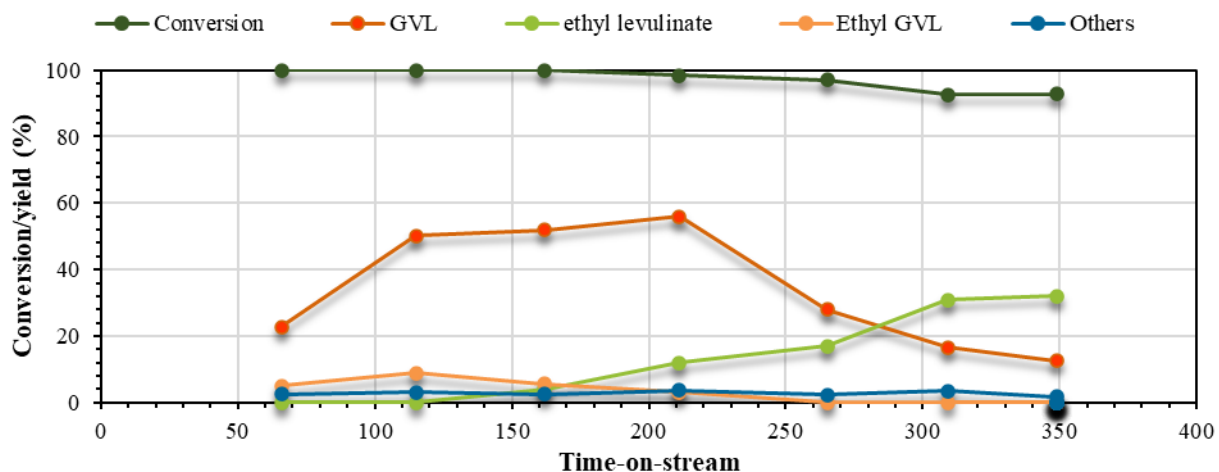
Figure 27. Catalytic results obtained in the CTH of ML with ethanol as H-donor over tetragonal ZrO$_2$. Reaction conditions: ML:EtOH:H$_2$O=1:10:5 (molar ratio), T: 250°C, τ = 1 s, %mol N$_2$:ML:EtOH:H$_2$O=87.8:0.8:7.6:3.8.

As mentioned previously, tetragonal ZrO$_2$ is characterized by the presence of mainly Lewis acid sites, which, according to the literature should favor the formation of GVL. However, the results obtained while co-feeding water suggest that the formation of Brønsted acid sites could occur during reaction due to the dissociative adsorption of water as one of the reaction co-products[192], making water partly responsible of the change in chemo-selectivity and the deactivation of the catalyst. In order to study this hypothesis, a sample of the fresh catalyst was exposed to a stream of water vapor for 3 hours at 250°C, and then it was analyzed by means of DRIFT spectroscopy with absorbed pyridine (Figure 28). A noticeable decrease in the intensity of one of the two main bands corresponding to Lewis acid sites (1604 cm^{-1}) was clearly seen. In addition, a small band at 1540 cm^{-1} (attributable to Brønsted sites) appeared when the catalyst was exposed to the stream of water vapour. Nonetheless, as mentioned previously, Brønsted sites that might be present on ZrO$_2$ are quite weak which makes them difficult to be detected by the adsorption of pyridine[179]. Because of this, it is necessary to perform the analysis using DMP as probe molecule. However, weak Brønsted acid sites were already detected in the fresh tetragonal ZrO$_2$. Therefore, it was not possible to identify the formation of new sites.
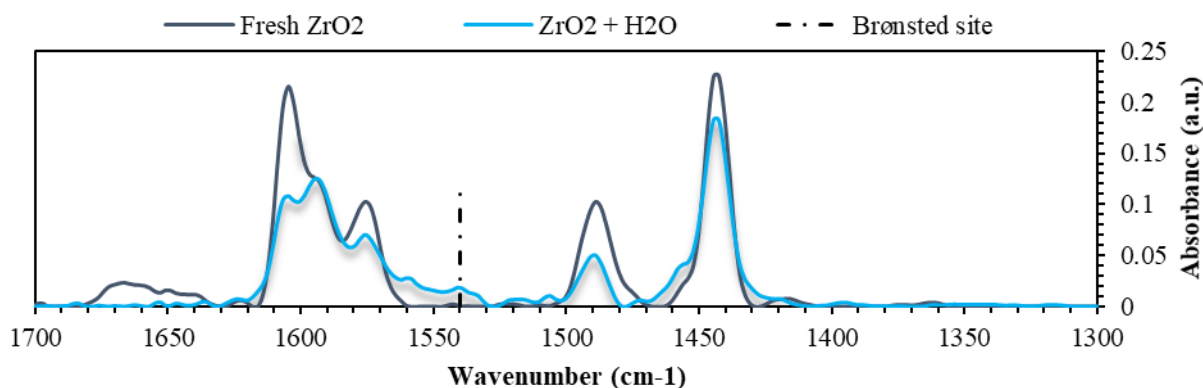
Figure 28. DRIFT spectra of absorbed pyridine on the fresh and water-exposed tetragonal ZrO_2 catalyst.

3.1.7. *Liquid-phase CTH tests*

In order to do a comparative analysis and understand the advantages in terms of conversion and selectivity of the gas-phase CTH of alkyl levulinates with alcohols, the reactions previously performed in the gas-phase were reproduce using a batch liquid phase system. Results can be seen in Figure 29. In this case, it can be seen how the results using methanol as H-donor in the liquid-phase are in agreement with the ones from gas-phase tests. Methanol is once again not active as H-donor for CTH of ML for yielding GVL, reaching a conversion of less than 5% and a yield for GVL of approximately 1%. In the case of the CTH of EL with methanol, a higher conversion is achieved (25%) providing a high selectivity (79%) towards the transesterification of EL to yield ML. In this case, only traces of GVL were seen.

When using ethanol as H-donor in the liquid-phase, the results obtained are not as remarkable as those obtained on the gas-phase. ML shows a conversion of 22%, being selectivity once again towards the transesterification reaction of ML into EL and showing a low selectivity towards GVL. On the other hand, EL conversion was 12% with a good selectivity towards GVL.
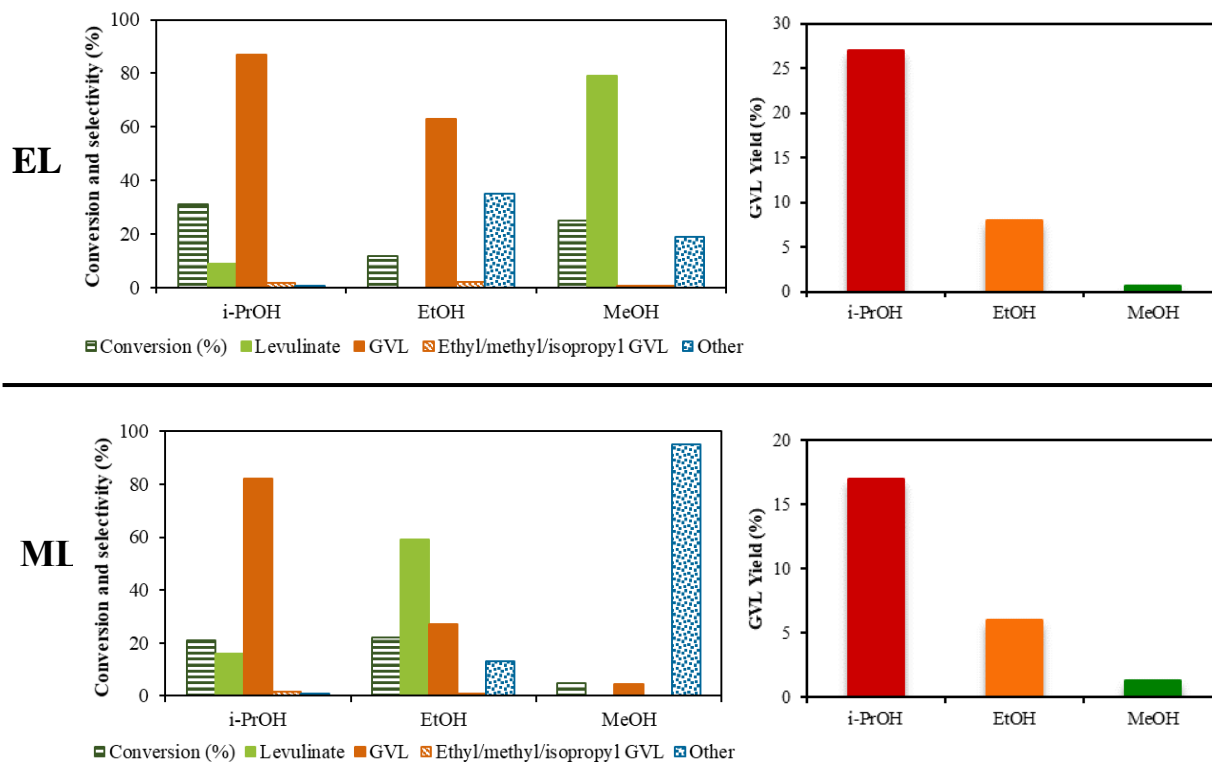
Figure 29. Catalytic results obtained in the CTH of ML and EL with different alcohols as H-donor over ZrO_2 under batch conditions. Reaction conditions: 40 mL solution of ML or EL (10 wt %), T: 250 °C, 0.30 g of ZrO_2 catalyst, reaction time 8 h, N_2 pressure 10 bar, stirring 500 rpm.

As expected, and in agreement with the CTH test in the gas-phase, isopropanol is the most active as H-donor for the CTH, reaching higher conversions and providing a higher selectivity towards GVL. In this case ML and EL were converted (21% and 31%, respectively) quite selectively into GVL with a higher yield (17% and 27%, respectively) after 8 h at 250 °C. In this case, the higher reactivity of EL maybe attributed to an increased efficiency of ethyl as leaving group[91].

In this case, while using isopropanol as H-donor, traces of propyl-GVL were also detected, indicating that also in this case tetragonal ZrO_2 can promote the alkylation of ALs. In addition, a significant amount of isopropyl levulinate was observed, which was not detected on the gas-phase CTH tests. This might be occurring via two different reaction pathways:

i.   Transesterification of ML and EL with isopropanol.

ii.   As previously discussed, the alcoholysis of ALs.

However, due to the higher steric hindrance of the isopropyl group, there is lower probability for the transesterification reaction to take place.

In addition, the effect of reaction time on the liquid-phase CTH of EL with isopropanol as H-donor was also analysed. Figure 30 shows the progressive increase of GVL yield at higher reaction time, reaching the highest value of 70% after 24 h.
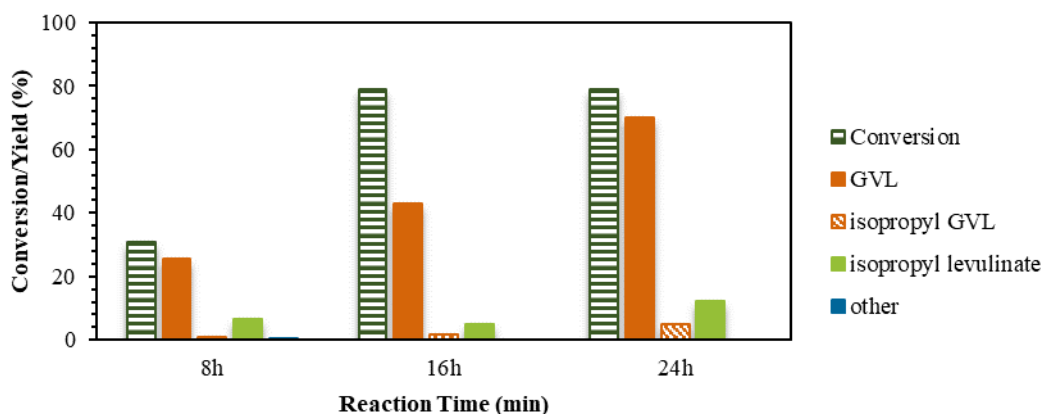

Figure 30. Reaction time effect in the liquid-phase CTH of EL with isopropanol as H-donor under batch conditions. Reaction conditions: 40 mL solution of EL (10 wt %), T: 250 °C, 0.30 g of ZrO_2 catalyst, N_2 pressure 10 bar, stirring 500 rpm.

In addition, the reusability and stability of catalysts under liquid phase and batch conditions was also studied. For this, five consecutive recycling tests at 250 °C for 24 h were performed. As shown in figure 31 the selectivity of the reaction does not suffer any changes when recycling the catalyst. However, a significant reduction of the activity was seen, reaching a conversion of EL of 31%. The spent catalyst was regenerate by being exposed to an air flow at 400 °C for 2 h and was afterwards reused for another test. The initial catalytic activity was recovered, reaching an EL conversion of 84% and a GVL yield of 60%. These results suggest that the decrease in activity could be a consequence of the deposition of heavy carbonaceous material on the surface of the catalyst.
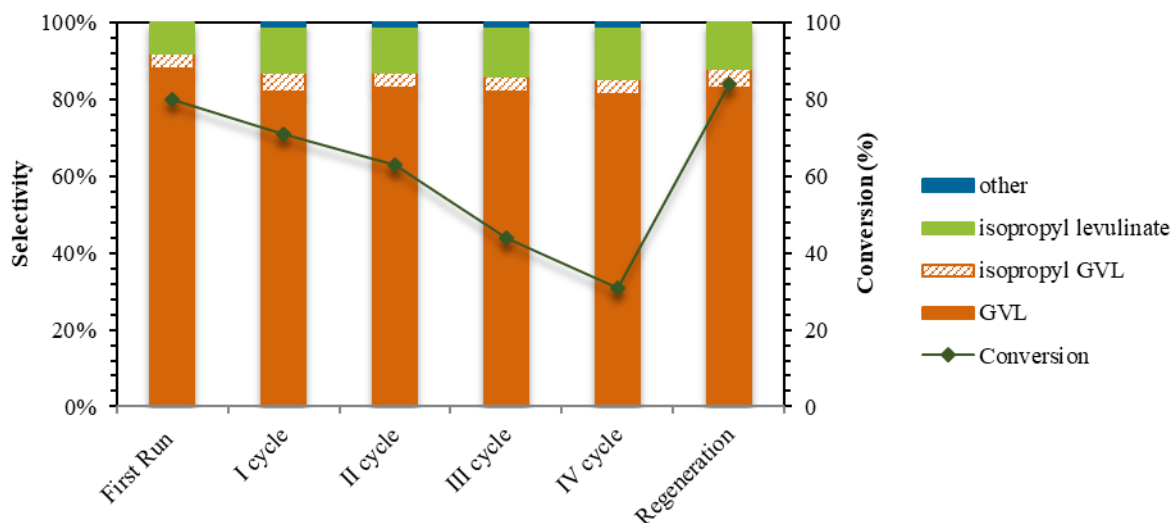
Figure 31. Reusability tests of the ZrO_2 catalyst in the liquid-phase CTH of EL with isopropanol as H-donor in batch conditions. Reaction conditions: 40 mL solution of EL (10 wt %), T: 250 °C, 0.30 g of ZrO_2 catalyst, reaction time 24 h, N_2 pressure 10 bar, stirring 500 rpm.

3.1.8. Mechanistic studies

With the aim of gaining some insight into the mechanism of the reaction and to identify the key intermediates, tests were carried out by changing the contact time (Figure 32). All the tests performed showed high conversions of ML (80-100%). Moreover, at low contact times, the presence of small quantities of ALs is detected, which disappear when increasing the contact time. These results provide more evidence that in fact ALs are the intermediate products in CTH of ML with ethanol to yield GVL. In addition, when using low contact times (0.3-0.5 s), the main product obtained is EL. As the contact time is increased, the amount of EL decreases and the selectivity toward GVL increases. This could be a consequence of a complex reaction pathway that involves the reactivity of different alkyl levulinates. The transesterification of ML and the alcoholysis of ALs yield EL which, as discussed previously, has a higher reactivity compared to ML itself.

Moreover, as previously mentioned, as the contact time increases, EL yield decreases reaching a value <5%. At the same time, there is an increase of GVL and the emergence of ethyl pentenoate, product of the alcoholysis of GVL.
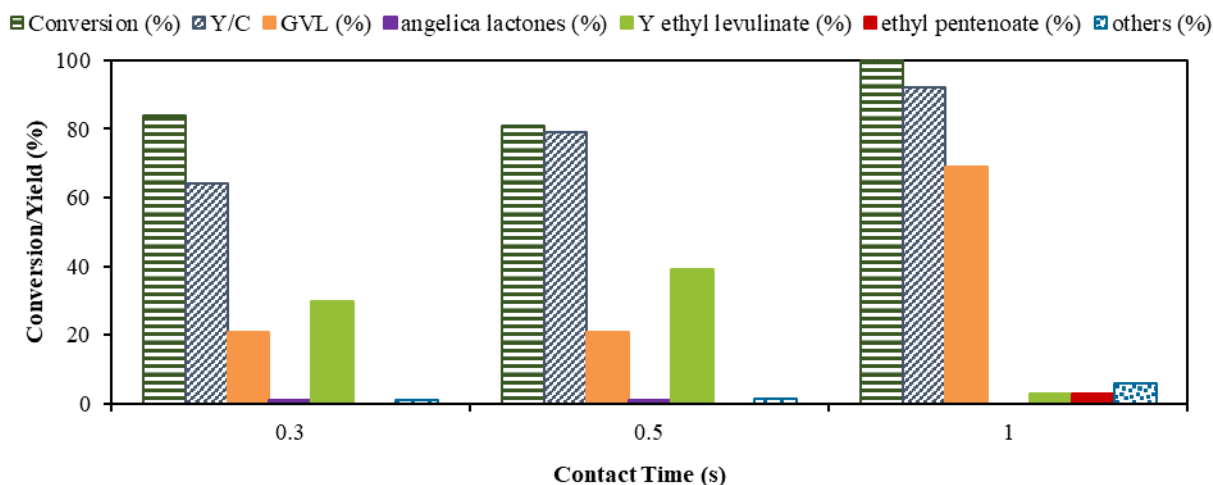
70

Figure 32. Catalytic results obtained in the CTH of ML with ethanol as H-donor over tetragonal ZrO$_2$ in the gas-phase, varying the contact time over. Reaction conditions: EL:EtOH=1:10 (molar ratio), T: 250 °C, τ = variable, t = 100 min, mol % N$_2$:EL:EtOH=90.1:0.9:9.

The reaction mechanism was also studied by feeding the reaction intermediates and products under the previously optimized conditions for the gas-phase CTH (250°C, τ = 1s, ethanol as H-donor). In particular, α-AL and GVL were fed to the reactor instead of the alkyl levulinates; the results are reported in Figure 33 and 34 respectively. The catalytic behavior obtained from the test performed with α-AL was comparable to the one observed during the experiment performed with ML. During the first 300 minutes of reaction, the α-AL conversion was complete, yielding mainly GVL and ethyl GVL. In addition, the previously mentioned change in chemo-selectivity was also observed. This phenomenon suggests that the mechanism of reaction followed for the formation of EL is that of the alcoholysis of ALs. These results strongly imply, once again, that in fact ALs are the key intermediate in the gas-phase CTH of ML with ethanol and that tetragonal ZrO$_2$ is able to promote the rapidly cyclisation of ML.

In addition, a test feeding GVL instead of the alkyl levulinate was performed in order to investigate the stability of the target product at the reaction conditions previously optimized. The results shown in figure 34 underline that GVL is not completely stable under these conditions and that it can undergo to consecutive reactions (with an average conversion of 40%) to yield ethyl

pentenoate as main detected product. This compound most probably is formed due to the ring opening of GVL to produce ethyl 4-hydroxypentanoate (not detected) that can then undergo dehydration to ethyl pentenoate. Moreover, a low carbon balance is obtained, which could indicate the formation of light, non-condensable compounds and heavy carbonaceous materials due to consecutive reactions. No formation of ethyl GVL was observed, suggesting that is not formed by the (hydroxy)alkylation of acetaldehyde on GVL but rather on the double bond of AL.
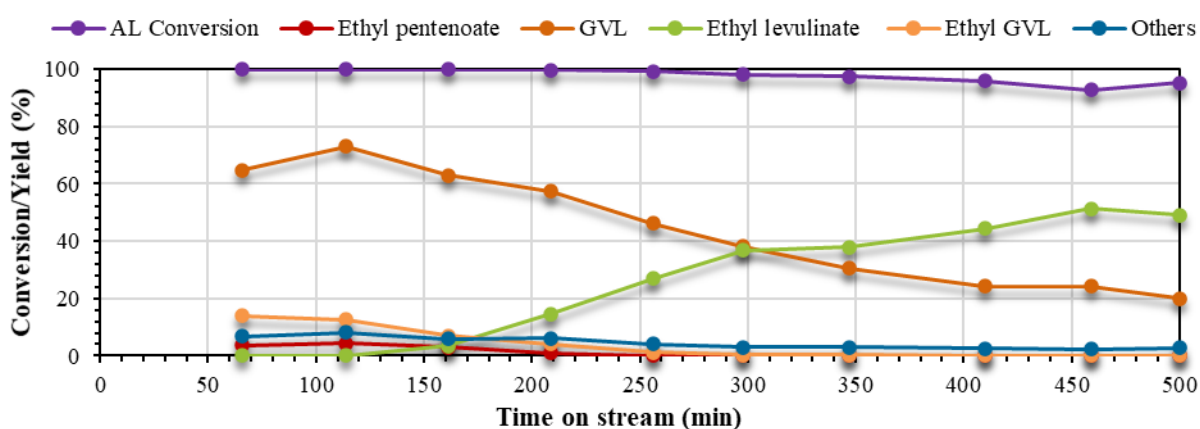
Figure 33. Catalytic results obtained in the CTH of α-AL with ethanol as H-donor over tetragonal ZrO$_2$. Reaction conditions: α-AL:EtOH=1:10 (molar ratio), T: 250°C, τ = 1 s, %mol N$_2$:α-AL:EtOH=90.1:0.9:9.0.

Collecting all the information of the previous tests, a reaction mechanism has been proposed (scheme 8). Considering the deactivation studies previously discussed and the catalytic results obtained so far, it could be plausible that the basic sites are maintained throughout the reaction, this way explaining the high ML conversion during the entire time on stream. On the other hand, the formation of heavy carbonaceous material, most probably due to the oligomerization of ALs, poison the Lewis acid sites which are necessary for the CTH to take place.
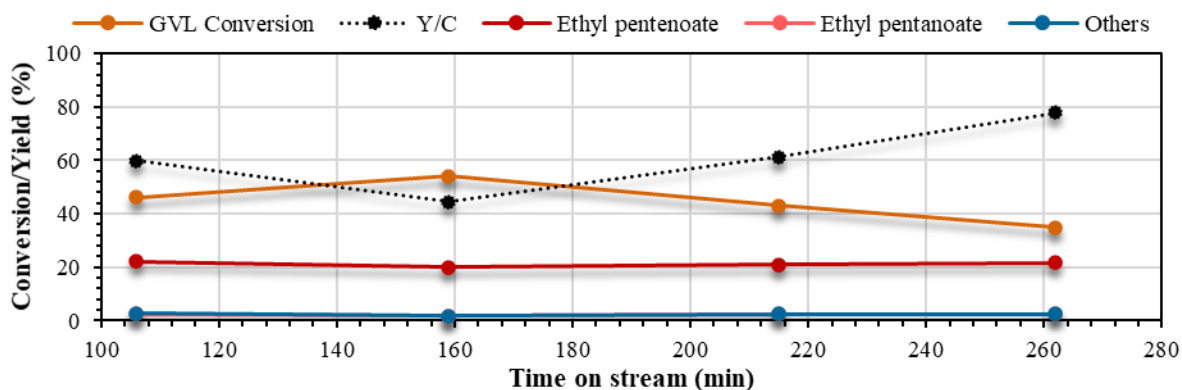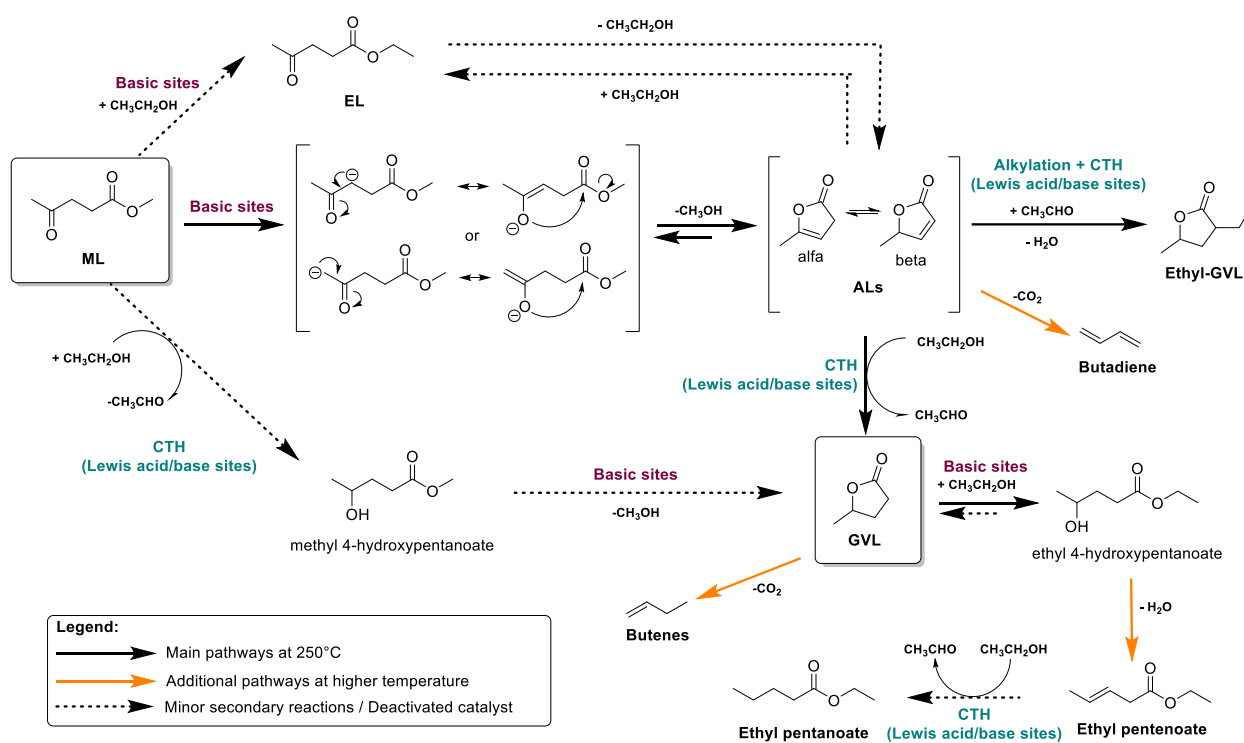
Figure 34. Catalytic results obtained by feeding GVL and ethanol over tetragonal ZrO_2. Reaction conditions: GVL:EtOH=1:10 (molar ratio), T: 250°C, τ = 1 s, %mol N_2:GVL:EtOH=90.1:0.9:9.0.

Scheme 9. Overall proposed reaction network from ML to GVL and by-products.

3.1.9. Bioethanol as H-donor.

A real bioethanol mixture (see Experimental for the composition) was tested as H-donor for the gas-phase CTH of ML over tetragonal ZrO_2 at the conditions previously studied and optimized. As it can be seen in figure 35, the use of bioethanol gave a slightly less satisfactory performance compared to that of pure ethanol. This behavior might be a consequence of the impurities present in the sample of bio-ethanol (i.e. acetic acid, aldehydes and acetals) which could have led to the formation of heavy carbonaceous materials on the surface of the catalyst, promoting a faster deactivation of the catalyst and decreasing the maximum obtained yield for GVL.
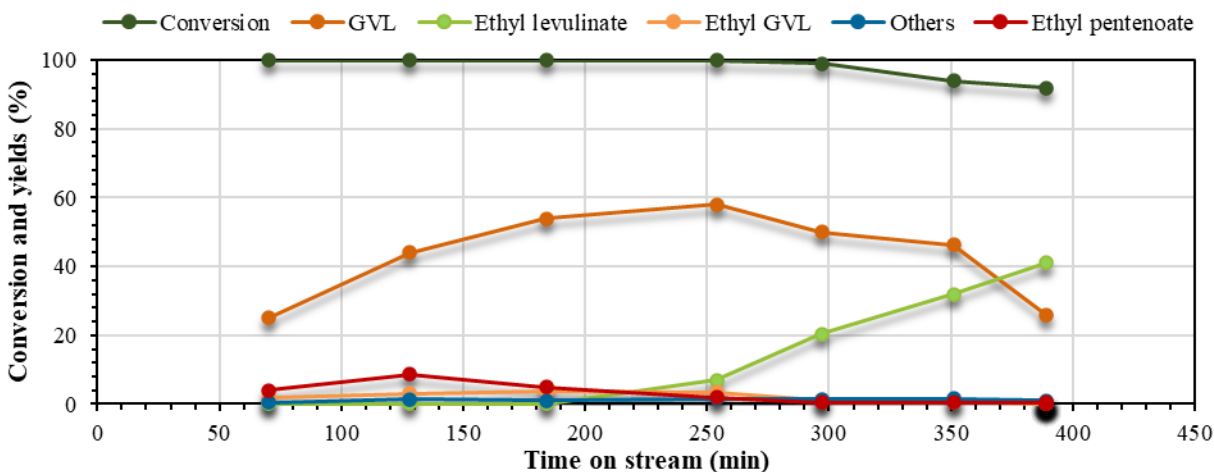
Figure 35. Catalytic results obtained in the ML reduction via H-transfer with ethanol over tetragonal ZrO_2. Reaction conditions: ML:Bio-EtOH=1:10 (molar ratio), T: 250°C, $\tau = 1$ s, %mol N_2:ML:EtOH=90.1:0.9:9.

Nonetheless, the possibility to directly use bioethanol as H-donor for the CTH of ML provides a window for the further improvement of the sustainability of the overall process, in this way having both the main reagents coming from renewable feedstock.

3.1.10. Levulinic acid gas-phase CTH

Given the satisfactory results obtained for the CTH of ML with ethanol as H-donor in the gas-phase over ZrO_2, the use of levulinic acid (LA) as substrate was tested. As previously mentioned,

the acid characteristics of LA and its high boiling point make it a challenging substrate. Moreover, because of the Teflon seals used in the inlet of the reactor, the maximum temperature at which it is possible to vaporize the reactants is limited to a value of 230 ° C, which is not adequate for LA as a substrate since its boiling point is 245-246°C. This restriction is a limiting factor for the setup of the reaction system since the effective vaporization of the reactant mixture could be limited, leading to deposition of organic residues inside the inlet line and risking their occlusion. Therefore, modifications were performed to the setup of the reagent supply. The reaction mixture was directly introduced inside the reactor by means of high precision infusion pump, through a capillary which end is placed directly inside the core of the reactor, just a few centimetre over the catalyst bed inside the oven, in this way obtaining a perfect vaporization.

Catalytic tests were performed at the previously optimized conditions (250°C) and with increasing temperature in order to study the effect of temperature on LA reactivity. In figure 36 can be seen that when working at 250 °C, a GVL yield of around 50% was achieved during the first 250 minutes of reaction. However, when working with LA at 250°C, the change in chemo-selectivity can be observed earlier than when working with ML. Moreover, ALs are seen in higher amounts. The catalytic behaviour obtained is similar to the one seen in figure 27, where ML is used as substrate and water is co-fed. This behaviour suggests that in fact water could promote the hydrolysis of ML to produce LA. On the other hand, as temperature is increased to 275°C, the change in chemo-selectivity is no longer observed. In addition, it seems that, after the first 200 min of reactions, GVL yield reaches a steady value of approximately 50% with a steady carbon balance of around 70%. In this case, no ALs were seen. When further increasing the temperature to 300°C, a continuous increase of GVL yield is seen with the time on stream, with a correspond increase in the carbon balance. In this case, a stable yield of ethyl pentenoate ethyl pentanoate of around 10% and 2% respectively.

The catalytic tests performed with LA were analysed by means of GC using a non-polar column, which is not suitable for the quantification of acids such as LA. And in fact, because of this it was not possible to adequately determine the conversion of LA in the different tests. Hence, an

adequate analytical method (most probably by means of HPLC) needs to be designed in order to properly determine the conversion of LA in the previously discussed tests.
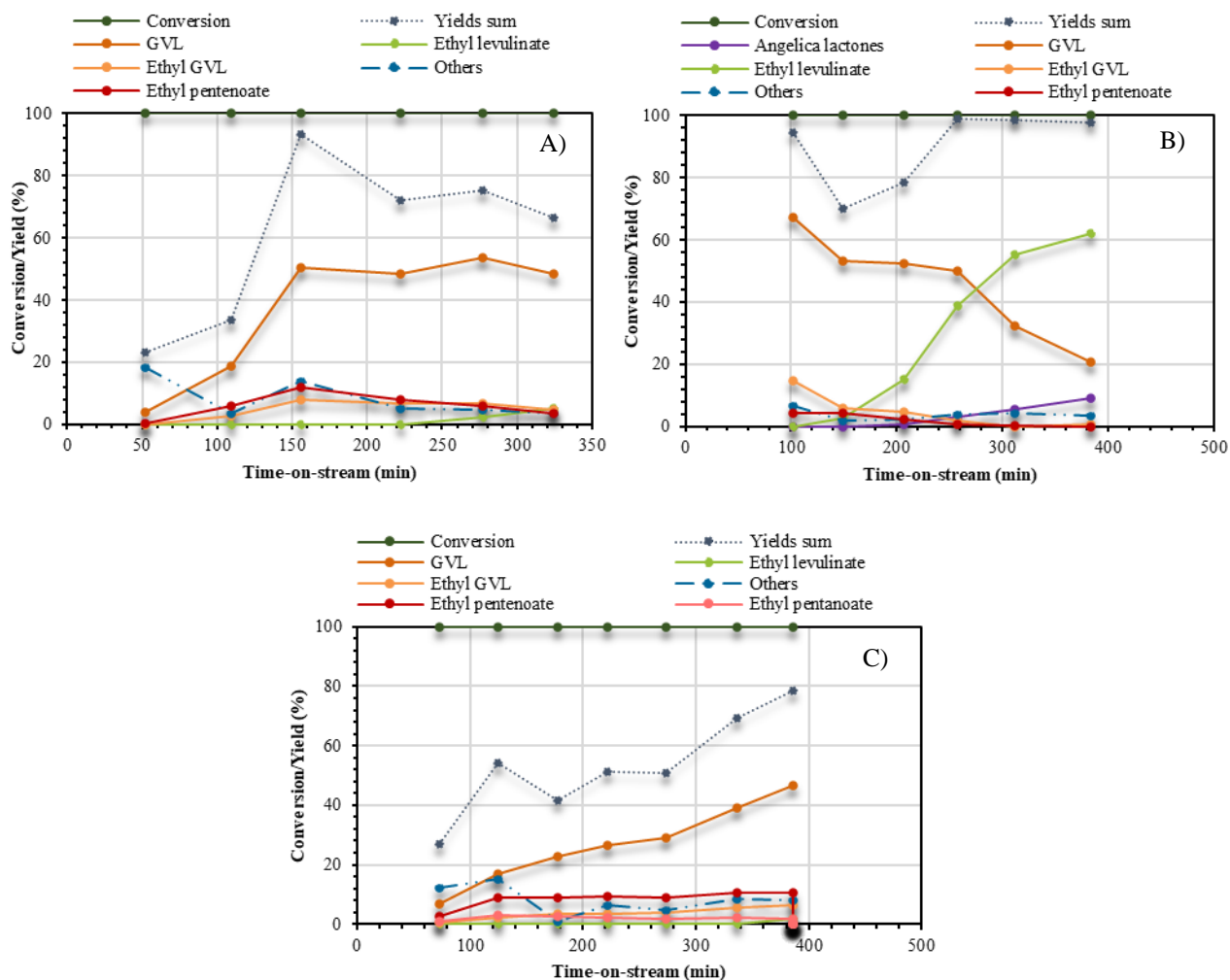
Figure 36. Catalytic results obtained in the CTH of LA using ethanol as H-donor over tetragonal ZrO$_2$. Reaction conditions: LA:EtOH=1:10 (molar ratio), τ = 1 s, %mol N$_2$:LA:EtOH=90.1:0.9:9; A) T:250°C, B) T:275°C, C) T:300°C.

3.1.11. Catalyst improvement

In order to improve the performance of the catalyst, it was decided to synthesize a mixed oxide which could have a higher Lewis acid strength, this way seeking to avoid the deactivation of the

catalyst. Therefore, TiO_2-ZrO_2 mixed oxide was synthesized following the methodology proposed by Afanasiev[169].
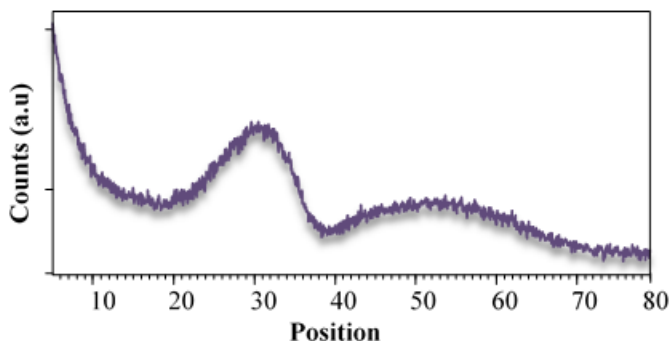
Figure 37. XRD of synthesized Ti/Zr/O catalyst.

X-ray diffraction analysis shows that the catalyst obtained after calcination at 550°C for 4 h gave an amorphous solid. Therefore, further characterization such as SEM-EDX still needs to be performed. Moreover, NH_3-TPD analysis shows that the catalyst obtained has an acid density of 15.88 µmol/m^2, even higher than tetragonal or monoclinic ZrO_2. However, it has a really low basic density.

Table12. Nature, specific surface areas and acid and basic densities of Ti/Zr/O.

Catalyst	SSA (m^2/g)	Crystalline phase (XRD)	Acid density (µmol/m^2)	T max desorption (°C)	Basic density (µmol/m^2)	T max desorption °C
Synthesized Ti/Zr/O	125	Amorphous	15.88	Wide band from 200 to 400°C	0.03	-
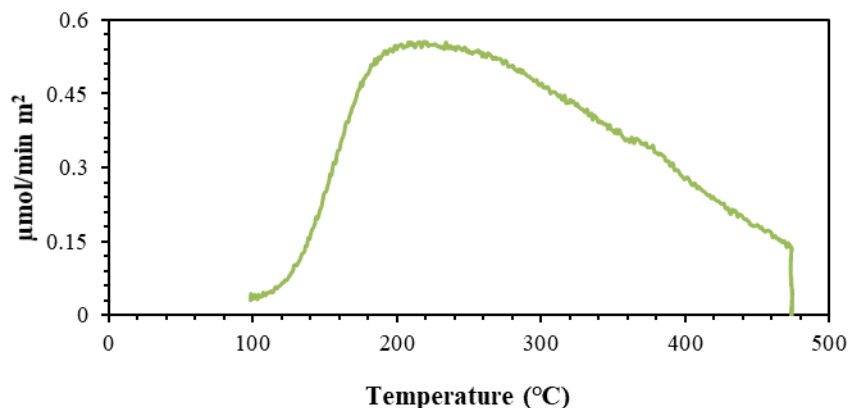
Figure 38. NH_3 -TPD profile of synthesized Ti/Zr/O.

In order to understand the catalytic behaviour of Ti/Zr/O for the CTH of ML with ethanol as H-donor, tests were performed at different temperatures by feeding a mixture of ethanol and ML (ethanol/ML molar ratio = 10) in a stream of nitrogen (% mol organic mixture: 10%) with a 1 s residence time, for 4.5 h, using always a fresh sample of pre-treated catalyst (figure 39). The catalyst was treated in-situ inside the reactor under an air flow (30 mL/min) for 1 h at 400°C in order to clean the surface from adsorbed water and CO_2.


Figure 39. Catalytic results obtained in the CTH of ML using ethanol as H-donor over Ti/Zr/O in the gas-phase. Reaction conditions: ML:EtOH=1:10 (molar ratio), t = 4.5 h, τ = 1 s, %mol N_2:ML:EtOH=90.1:0.9:9.

In the chosen range of temperatures, the catalyst provides an almost complete conversion, demonstrating to be quite active. Interestingly, at 200 °C the catalyst provided not only an almost complete conversion of ML (98%), but also a good selectivity towards GVL, reaching a yield of approximately 60%. In addition, a good carbon balance was obtained, and the main by-products where EL and ethyl pentenoates. These last ones, as previously explained, might come from further ring opening of GVL to produce ethyl 4-hydroxypentanoate (not detected) that can then undergo dehydration to ethyl pentenoate. These results are of value since they have showed that by

introducing TiO_2 in the structure of the catalyst (ZrO_2) the operating temperature can be decreased from 250 to 200 °C obtaining similar results.

Moreover, as the temperature is further increase to 250 °C, GVL yield decreases to around 25% and the amount of detected ethyl penten/anoates increased to a value of 65%. This means that under these conditions Ti/Zr/O is too active for the proposed reaction, leading to consecutive reactions over GVL. The same behaviour is seen when further increasing the temperature to 300 °C. However, in this case the carbon balance is affected by the high temperatures, decreasing to a value of 65%. This is most probably due to both the formation of heavy carbonaceous material on the surface of the catalyst and the formation of light non-condensable products that can be formed from consecutive reactions over GVL as previously seen. In fact, table 13 shows TGA analysis performed on the spent Ti/Zr/O, and it can be seen that as the reaction temperature increases, the amount of heavy carbonaceous material accumulated on the surface of the catalyst increases. Therefore, it can be concluded that the increment of the carbon loss as the reaction temperature increases is mainly due to the formation of heavy carbonaceous material on the surface of the catalyst.

Table 13. TGA of the spent $TiZrO_4$ performed under flow of air.

Reaction temperature (°C)	Reaction time (min)	Weight loss (%)	Max Desorption Temperature (°C)
200	270	4.14	310
250	270	5.05	380
300	270	8.23	376

Given the remarkable activity obtained while working at 250 °C, it was decided to modify the contact time in order to see if it was possible to limit the activity of the catalyst and avoiding consecutive reactions over GVL. Hence, a test using a lower contact time was performed and results can be seen in figure 42.
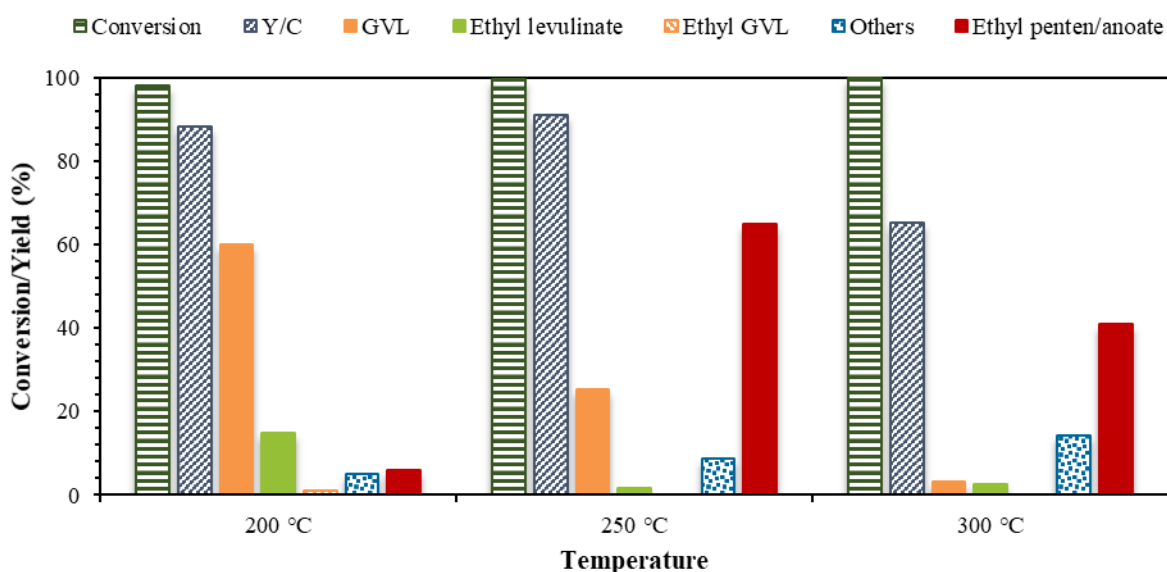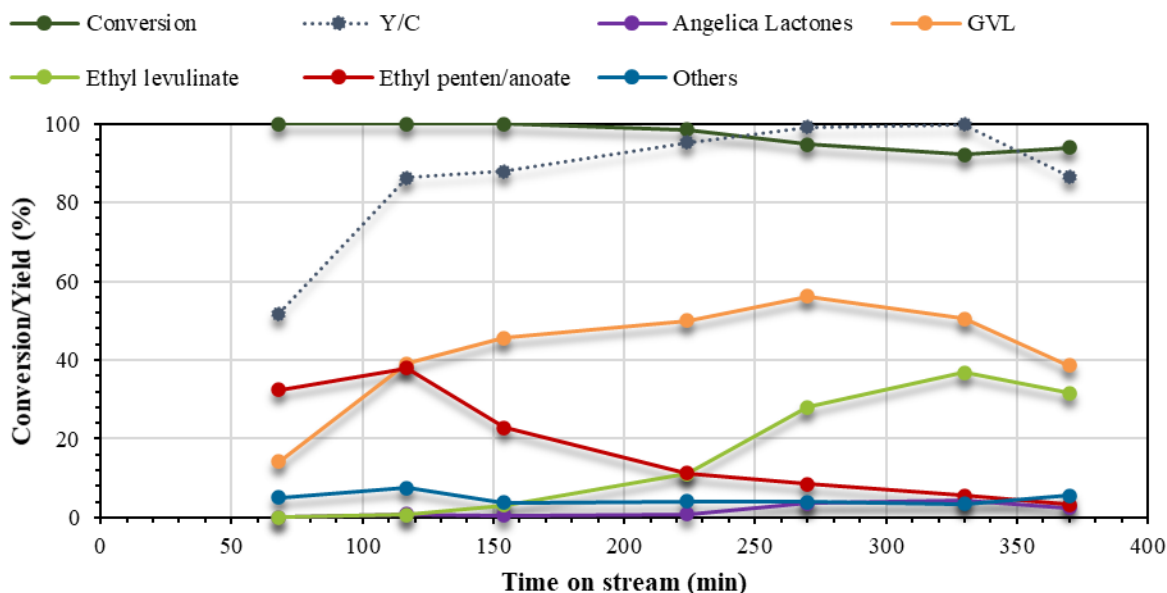
Figure 40. Catalytic results obtained in the CTH of ML using ethanol as H-donor over TiZrO$_4$ in the gas-phase. Reaction conditions: ML:EtOH=1:10 (molar ratio), T = 250 °C, τ = 0.3 s, %mol N$_2$:ML:EtOH=90.1:0.9:9.

In fact, when lowering the contact time to 0.3 s (figure 40), the amount of pentenoates coming from consecutive reaction undergone by GVL was limited. It can be seen that during the first 100 minutes of reactions, the main products is still the pentenoates. However, as time passes, the yield for ethyl pentenoates starts to decrease, and GVL starts to increase until it reaches a maximum value of 56% yield at 270 minutes. Moreover, as GVL yield starts to increase, ML conversion starts to decrease until it appears to reach a steady value around 90%. Just as when ZrO$_2$ is used, when the catalyst starts to deactivate both the yield for EL and ALs starts to increase. As previously discussed, this might be due to the deposition of heavy carbonaceous material on the surface of the catalyst which block the active sites for CTH to take place, therefore a decrease in GVL yield starts to occur, instead the alcoholysis of ALs takes place, producing EL.

3.2. Bio-ethanol: hydrogenolysis of polyols

3.2.1. Catalytic tests.

Following the trend of the so far published studies on the production of ethanol from the hydrogenolysis of polyols, a Pd/Fe_3O_4 catalyst was synthesized following a co-precipitation methodology. In addition, Pd/ZrO_2 was also synthesized by co-precipitation and was tested for the hydrogenolysis of polyols.

It was decided to firstly start testing the catalysts for the simplest form of diols, EG and 1,2-PDO. Results are summarized in table 14. It can be clearly seen that Pd/Fe_3O_4 was found to be active for the hydrogenolysis of 1,2-PDO and EG, confirming what has already been reported so far in the literature[136,137]. In addition, Pd/ZrO_2 was found to be mildly active, reaching a conversion of 26% and a selectivity for ethanol of 30%.

Table 14. Conversion of 1,2-PDO and EG promoted by Pd supported catalyst. Reaction conditions: 0.1 g catalyst; 15 ml aqueous solution (4 wt%), 5 bar H_2, 250 $^{\circ}$C, 24 h. [*]in addition 1-propanol.

Substrate	Catalyst	Conversion (%)	Ethanol selectivity (%)
1,2-PDO	Pd/ZrO_2	26	30
	Pd/C	17	49
	Pd/Fe_3O_4	81	52[*]
EG	Pd/ZrO_2	27	0
	Pd/C	16	74
	Pd/Fe_3O_4	49	76

Moreover, it was decided to substitute Pd with different metals (Ru, Co and Pt) in order to see if a similar or an enhanced activity could be obtained. Results can be seen in table 15. It can be seen that Ru appears to be the only active metal towards the conversion of 1,2-PDO giving a high selectivity towards the production of ethanol. This means that Ru was able to activate mainly the dehydrogenation/decarbonylation of 1,2-PDO and only in small part the dehydration

/hydrogentation. Moreover, no activity was seen when using EG as substrate. This could mean that the hydrogenlysis of glycerol could be oriented mainly toward the production of EG and on the other hand, to a lower extend, towards the production of 1,2-PDO that could mainly react to produce ethanol.

In addition, Ru/ZrO$_2$ was synthesized and tested for the hydrogenolysis of both EG and 1,2-PDO. However, in this case HPLC results showed no peaks after reaction implying a complete conversion of the substrate with no detectable products. Noteworthy, during the reaction, a slight pressure increase of around 5 bar was observed. In fact, the post reaction liquid had a turbid consistency and the filtration of the sample for analysis was particularly difficult. This was probably due to a polymerization of the substrate.

Table 15. Conversion of 1,2-PDO and EG promoted by X/Fe$_3$O$_4$ (X = Ru, Co, Pt). Conditions: 0.1 g catalyst; 15 ml aqueous solution (4 wt%), 5 bar H$_2$, 250 ^{o}C, 24 h. [*]In addition 1-propanol.

Substrate	Catalyst	Conversion (%)	Ethanol selectivity (%)
1,2-PDO	Ru/Fe$_3$O$_4$	42	77[*]
	Pt/ Fe$_3$O$_4$	32	12[*]
	Co/ Fe$_3$O$_4$	0	0
EG	Ru/ Fe$_3$O$_4$	2	0
	Pt/ Fe$_3$O$_4$	2	0
	Co/ Fe$_3$O$_4$	0	0

In addition to the co-precipitated Pd/Fe$_3$O$_4$ and Ru/Fe$_3$O$_4$, an additional synthesis was carried out following the activated carbon route (denominated Pd/Fe$_3$O$_4$-AC and Ru/Fe$_3$O$_4$-AC) proposed by Schwickardi et al.[193] These last catalysts, Pd/Fe$_3$O$_4$, Ru/Fe$_3$O$_4$ and Pd/ZrO$_2$ were then tested for the hydrogenolysis of glycerol in order to further understand their behaviour. Results can be seen in figure 41.

With Pd/Fe$_3$O$_4$ and Pd/Fe$_3$O$_4$-AC a conversion of 99% and 83% was achieved and selectivity for ethanol of 37% and 28%, respectively. Besides ethanol, the other products obtained were EG, 1,2-PDO and 1-propanol. These results confirm what was already stated in the literature[122,127,128,138,165]; Pd/Fe$_3$O$_4$ has the ability of promoting dehydration/hydrogenation of glycerol to yield 1,2-PDO which then suffers both of dehydration/hydrogenation and dehydrogenation/decarbonylation to yield 1-propanol and ethanol, respectively. Even though it was expected for the catalyst synthesized through the activated carbon route to be more active, this was not the case. In fact, glycerol conversion and ethanol selectivity were lower, but a higher selectivity was achieved for 1,2-PDO, implying that the catalyst was not as active for the dehydration/hydrogenation of 1,2-PDO. Moreover, a higher selectivity towards EG was achieved, meaning that in comparison to Pd/Fe$_3$O$_4$, the catalyst through the activated carbon route was more able to promote the dehydrogenation/decarbonylation of glycerol.

When using Pd/ZrO$_2$, glycerol conversion reached 54% and a 25% selectivity for ethanol was achieved. Once again, the by-products obtained were EG, 1,2-PDO and 1-propanol. Even though the conversion reached was lower, it appears that Pd/ZrO$_2$ has a similar behaviour to Pd/Fe$_3$O$_4$-AC, as it seems to also promote to a greater extent than Pd/Fe$_3$O$_4$ the dehydrogenation/decarbonylation of glycerol to yield EG.

When using Ru/Fe$_3$O$_4$ for the hydrogenolysis of glycerol, contrary to what was expected, it was more active towards the dehydration/hydrogentation to yield 1,2-PDO, and just in part towards the deydration/decarbonilation to yield EG. In this case, the catalyst does not seem to be active enough to be able to continue with the reaction and move towards the production of ethanol. However, small quantities of 1-propanol derived from the dehydration/hydrogentation of 1,2-PDO were detected. Along the same line, Ru/Fe$_3$O$_4$-AC was tested for the hydrogenolysis of glycerol, however, once again HPLC analysis showed no peaks after reaction implying a complete conversion of the substrate with no detectable products. Just as for Ru/ZrO$_2$, a slight pressure increase of around 5 bar was observed during reaction and the post reaction solutions has a turbid consistency, which once again could be due to the polymerization of the substrate.
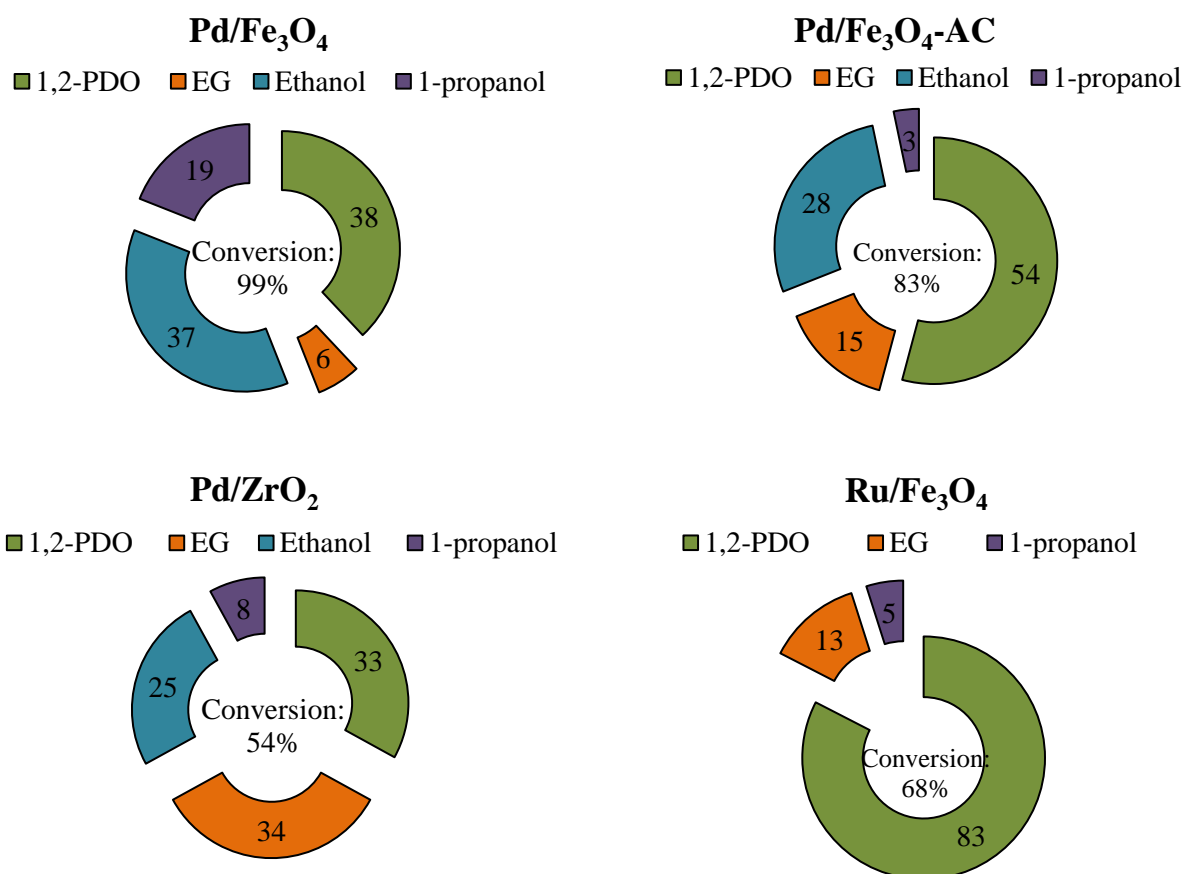
Figure 41. Catalytic results obtained in the hydrogenolysis of glycerol promoted by Pd and Ru supported catalyst, selectivities reported. Reaction conditions: 0.1 g catalyst; 15 ml aqueous solution (4 wt%), 5 bar H_2, 250 ℃, 24 h.

With the results obtained, and what has been reported in literature, a reaction scheme for the hydrogenolysis of glycerol can be proposed (scheme 10). The main reactions involved are dehydration/hydrogenation and dehydrogenation/decarbonylation. However, the gas-phase products were not analysed in order to confirm APR and WGS.
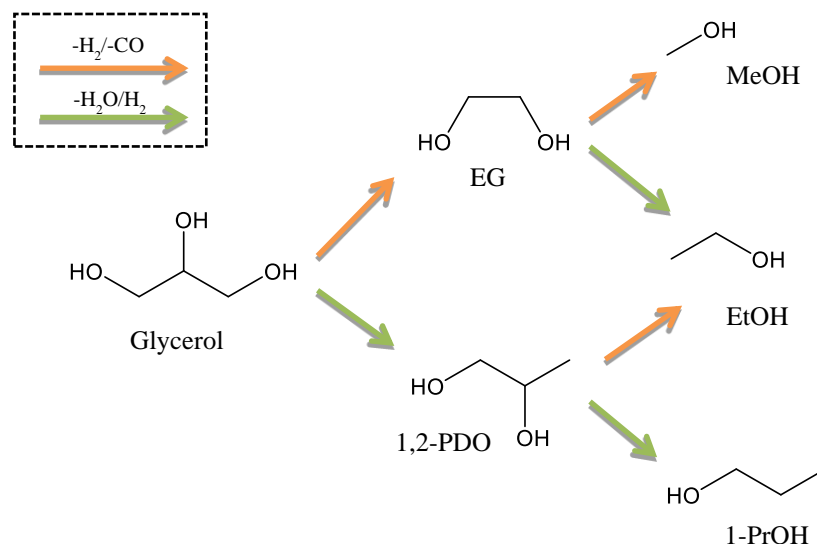
Scheme 10. Path followed during hydrogenolysis of glycerol over Pd supported catalysts.

According to Mauriello et al.[138,166] in the reaction path that leads to 1,2-PDO, firstly, two adjacent alcoholic groups of glycerol adsorb onto PdFe bimetallic sites to then lead to the breakage of the C-OH bond promoted by Pd. Subsequently, due to the instability of the formed enol, hydroxyacetone is formed, which is then hydrogenated to 1,2-PDO. On the other hand, the formation of EG is obtained though the dissociation of a primary alcoholic groups proceeding by C–H bond breaking promoted by Pd sites, forming glyceraldehyde. This then undergoes C–CO breaking leading to formation of EG and CO. This can be seen in scheme 11.
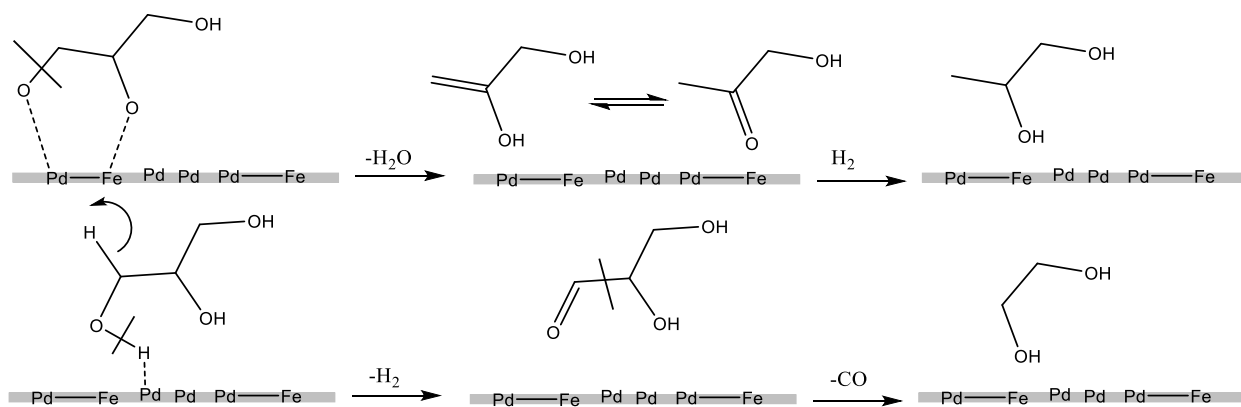
Scheme 11. Initial steps in the hydrogenolysis of glycerol over Pd-Fe catalyst; dehydration/hydrogenation and dehydrogenation/decarbonylation routes.

3.2.2. *Catalyst characterization*

As seen in the previous section, Pd/Fe_3O_4, Ru/Fe_3O_4, Pd/ZrO_2 synthesized following a co-precipitation methodology, were found to be active for the hydrogenolysis of different polyols. In addition, Pd/Fe_3O_4 synthesized following the activated carbon route (denominated Pd/Fe_3O_4-AC) was found to be active for hydrogenolysis of glycerol. The activated carbon route methodology proposed by y Schwickardi et al.[193] relies on impregnating with a highly concentrated metal salt solutions a sample of activated carbon, which is then calcinated in order to burn off the carbon. According to the literature, given the high porosity of the activated carbons, this methodology allows to obtain high-surface-area materials with a small-particle-size and a good metal distribution. Specific surface area, metal loading and mean particle size can be seen in table 16.

Table 16. Main characteristics of synthesized catalysts. (Metal loading and mean particle size from TEM)

Catalyst	$S_{BET}(m^2/g)$	d_n (nm)
Pd/Fe_3O_4	41	1.5
Pd/Fe_3O_4-AC	40	7.2
Pd/ZrO_2	222	-
Ru/Fe_3O_4	18	50.9

XRD analyses of the synthesized catalysts are shown in figure 42. XRD for Pd/Fe_3O_4 showed diffraction patterns characteristic of Fe_3O_4. In addition, a diffraction signal at $2\theta = 44.5°$ was observed, which corresponds to Fe (0)[194]. No diffraction signals were detected for Pd, hinting that the metal was well distributed along the support and the particle size of the metal was indeed quite small. In the case of Pd/Fe_3O_4-AC, the diffraction patterns obtained are basically the same as those for Pd/Fe_3O_4, showing diffraction patterns characteristic of Fe_3O_4 and in addition the diffraction signal at $2\theta = 44.5°$ and an additional one at $2\theta = 65°$ corresponding to Fe^0. Moreover, in this case a small diffraction signal can be seen between $40°$ and $41°$ and according to the literature, this might be either correlated to the diffraction peaks of Pd that appears at $40.01°$ or the one for PdFe

appearing at 40.79°.[121] These results together with BET analyses suggest, so far, that the activated carbon route was not able to provide a smaller particle size and a higher specific surface area.
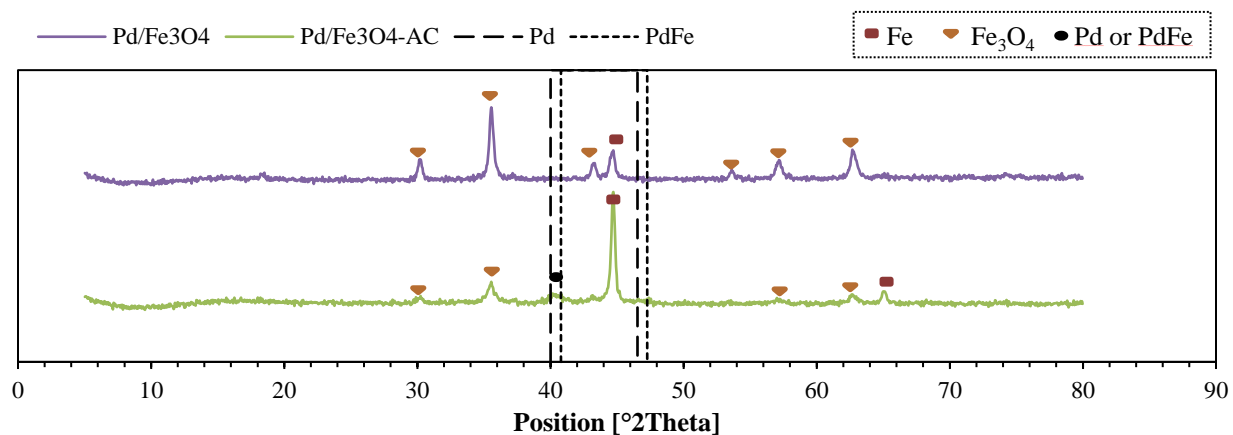
Figure 42. XRD for Pd/Fe$_3$O$_4$ synthesized catalysts.

Along this line, figure 43 and figure 44 show the particle size distribution of Pd/Fe$_3$O$_4$ and Pd/Fe$_3$O$_4$-AC, respectively. In fact, the activated carbon route was not able to promote a smaller mean particle size for Pd, reaching a value of 7.2 nm while Pd/Fe$_3$O$_4$ synthesized by co-precipitation method gave a value of 1.5 nm. This strange behaviour might be due to the excess of water used during the synthesis procedure, which might block the pores of the activated carbon this way making it harder for Pd to be evenly distributed along the pores of the activate carbon. In fact, EDX maps show a significant difference in the distribution of Pd over the catalyst. Catalyst synthesized through a traditional co-precipitation methodology shows well distributed Pd nanoparticles (figure 43 C). On the other hand, the activated carbon route methodology did not provide a uniform distribution of the Pd nanoparticles (figure 44 C).
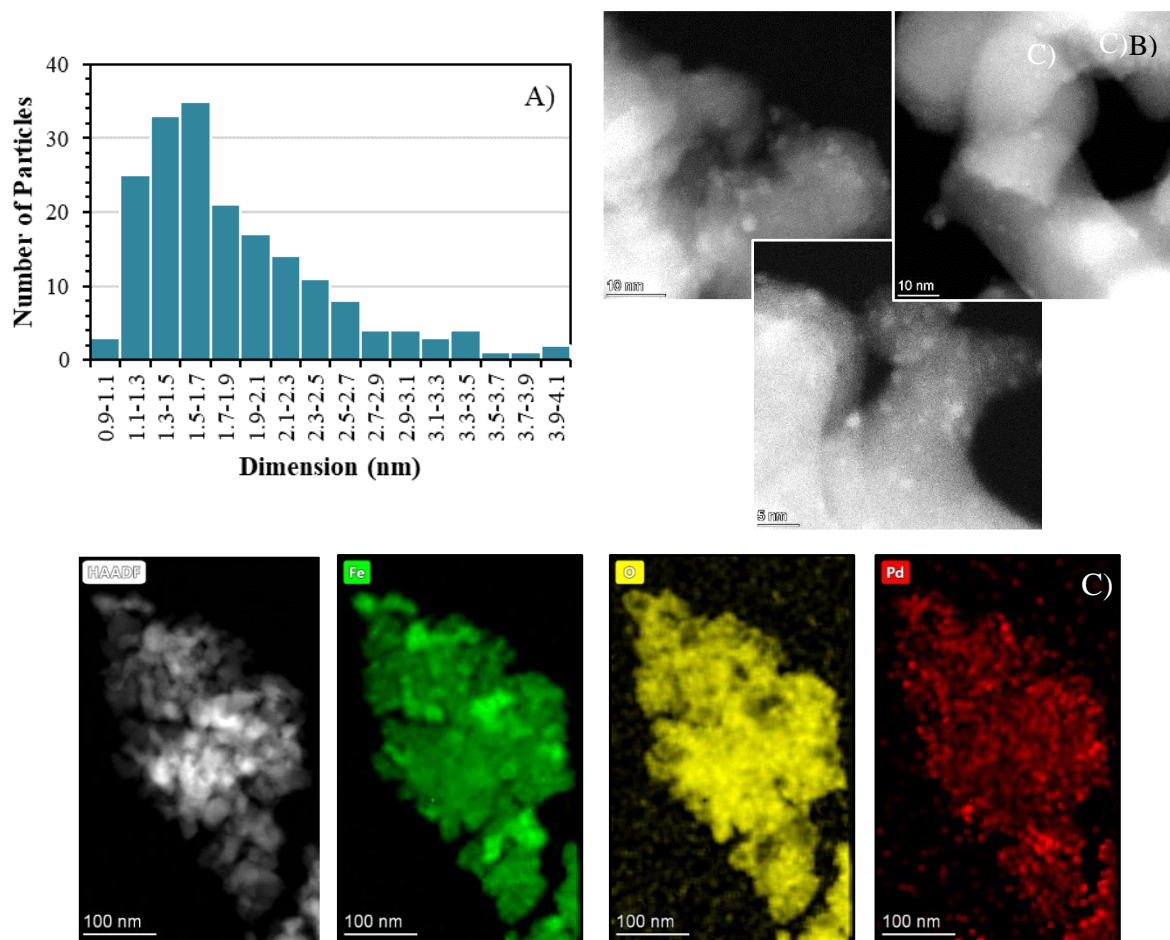
Figure 43. Particle size distribution A), high resolution TEM images B), and EDX maps C) of Pd/Fe$_3$O$_4$ catalyst.
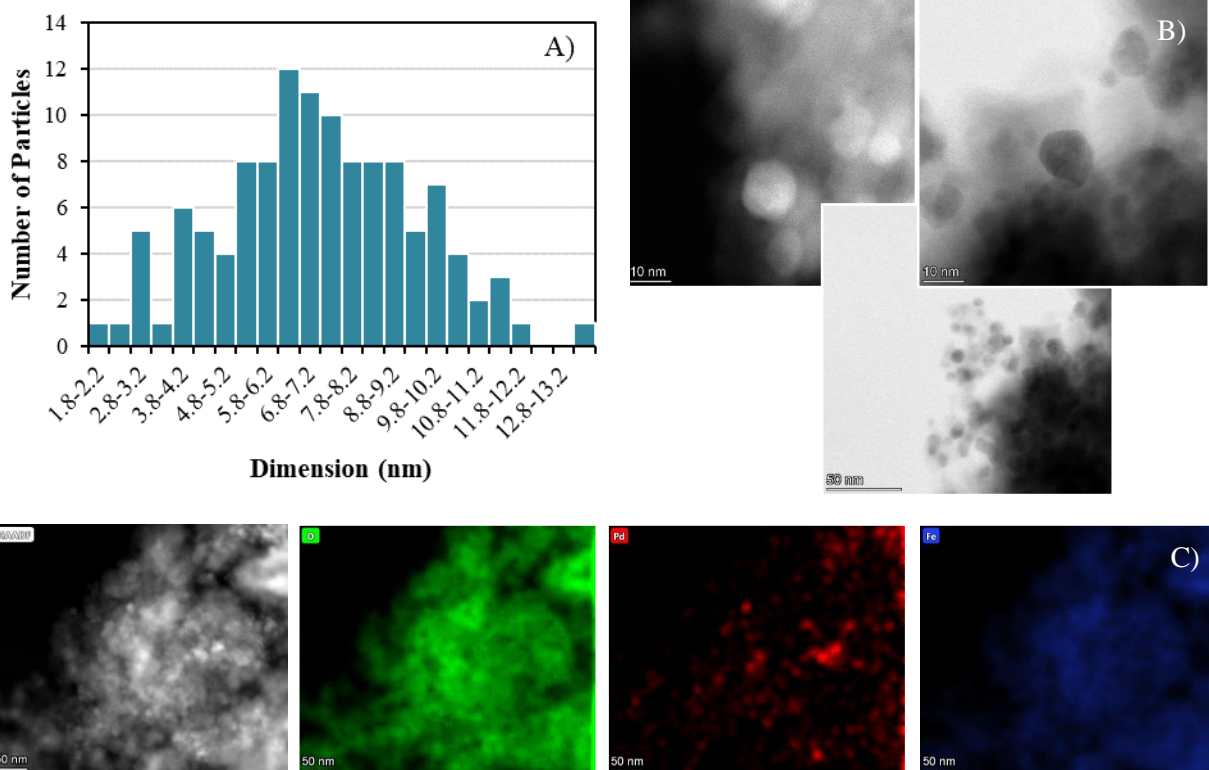
Figure 44. Particle size distribution A), high resolution TEM images B), and EDX maps C) of Pd/Fe$_3$O$_4$-AC catalyst.
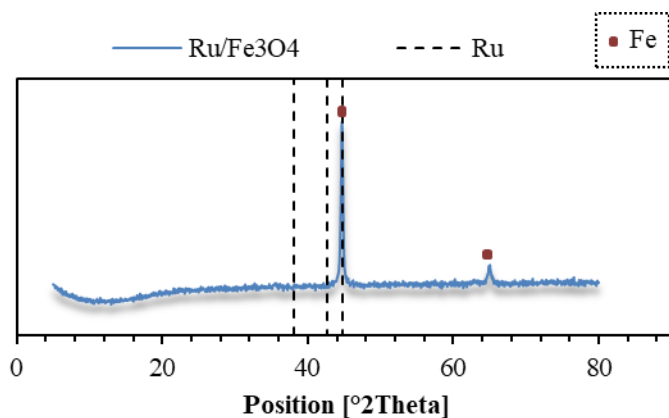
Figure 45. XRD for synthesized Ru/Fe$_3$O$_4$ catalysts.

In the case of the XRD for Ru/Fe$_3$O$_4$ (figure 45), only the diffraction patterns related to Fe^0 were seen. This could indicate that Fe$_2$O$_3$ support was completely reduced to Fe^0 and, since no signal related to Ru was seen, that it could be well distributed along the surface of the support in the form of nanoparticles.

In order to further analyse the material and confirm if in fact a good particle distribution was achieved during the synthesis, TEM analyses were also performed for the Ru/Fe$_3$O$_4$ catalyst. Even

though the diffractogram in figure 45 could indicate the presence of nanoparticles and a good distribution, figure 46 shows that the mean particle size of the Ru particles was higher than expected, reaching a value of 50.9 nm. However, the EDX maps shown in figure 46 C) do confirm a good distribution of the particles of Ru along the surface of the catalyst.
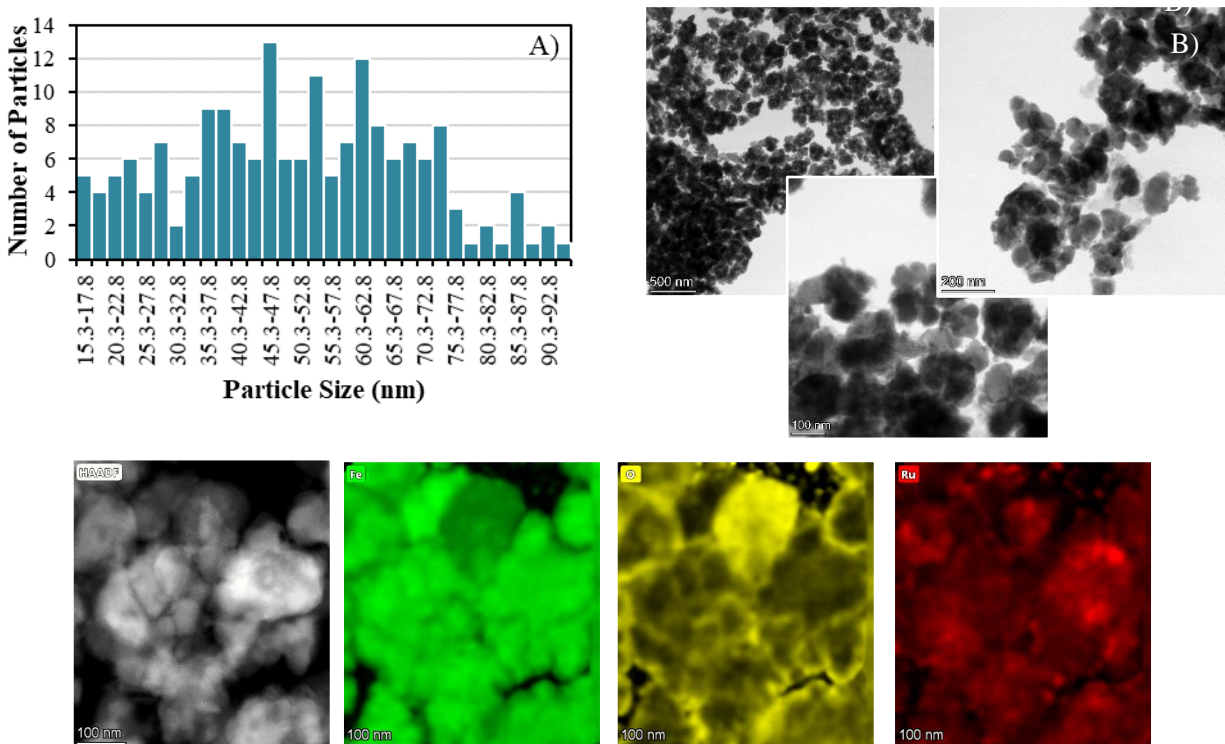
**Figure 46.** Particle size distribution A), high resolution TEM images B), and EDX maps C) of Ru/Fe_3O_4 catalyst.

According to the literature, reduction of pure Fe_2O_3 samples is observed at about 340 °C[121,166], however hydrogen TPR for Pd/Fe_3O_4 (figure 47 left) shows two peaks at around 80 and 150 °C, and another broad peak around 600 °C. First peak corresponds to the reduction of Pd^{2+} to Pd^0 and the second peak to the reduction of Fe_2O_3 to Fe_3O_4. Lastly, the broad peak corresponds to the further reduction of Fe_3O_4 to Fe^0. These results suggest that the presence of Pd under the pre-reduction/pre-treatment conditions seems to promote the reduction of Fe_2O_3 towards Fe_3O_4, shifting its reduction to lower temperatures[121,166]. Moreover, according to Bhogeswararao et al.[195], PdO reduces at around 25 °C in H_2 atmosphere and tends to form β-PdH. These hydrides

decompose at higher temperatures and show a negative peak. However, H_2-TPR did not show any negative peaks which could have been attributed to the decomposition of β-PdH. In fact, this suggests that a possible metal–support interaction might be taking place, such as the formation of PdFe bimetallic nanoparticles[121,122,196].
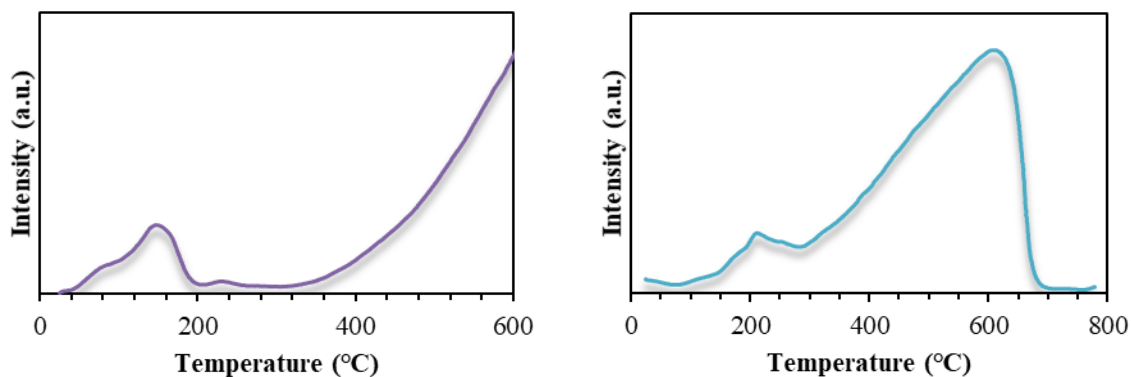
Figure 47. TPR analyses for Pd/Fe$_3$O$_4$ (left) and Ru/Fe$_3$O$_4$ (right).

H_2-TPR for Ru/Fe$_3$O$_4$ (figure 47 right) appears to show two peaks, the first one around 200 °C and the second one broad starting at around 500 °C. According to the literature, the first peak is actually composed by two different peaks; a first one at 207 °C which appears to be related the reduction of Ru oxide to Ru^0 and a second one at 250 °C related to the reduction of Fe$_2$O$_3$ to Fe$_3$O$_4$. Instead, the second broad peak is related to both the reduction of Fe$_3$O$_4$ to Fe^0 at around 500 °C. According to the literature, after exposing the catalyst to further reduction cycles, the peak related to the reduction of Ru oxide to Ru^0 disappears. Because of this, it is suggested that the reduced Ru becomes part of a bimetallic nanoparticle which remains dispersed in the support[197].

In addition, given the high stability of ZrO$_2$ and the optimized synthesis established in the previous sections of this manuscript, it was decided to test it as a support. This catalyst was synthetized following a co-precipitation methodology. As seen on figure 48, the material obtained is a highly amorphous catalyst. The XRD diffractogram shows two broad reflexes instead of the two main diffraction signals related to tetragonal ZrO$_2$. The signal on the left corresponds to tetragonal ZrO$_2$ with Miller index (111) and the broad shoulder on right is related to the (220) crystal plane also

present in tetragonal ZrO_2[198]. Nonetheless, further characterization such TEM and EDX maps still needs to be performed.

Figure 48. XRD for Pd/ZrO_2 synthesized catalysts.

4. Conclusions

The results obtained are a promising starting point for the gas-phase CTH of alkyl levulinates with alcohols over heterogeneous catalysts. And in fact, these results were published, for the first time, in two different articles[199,200].
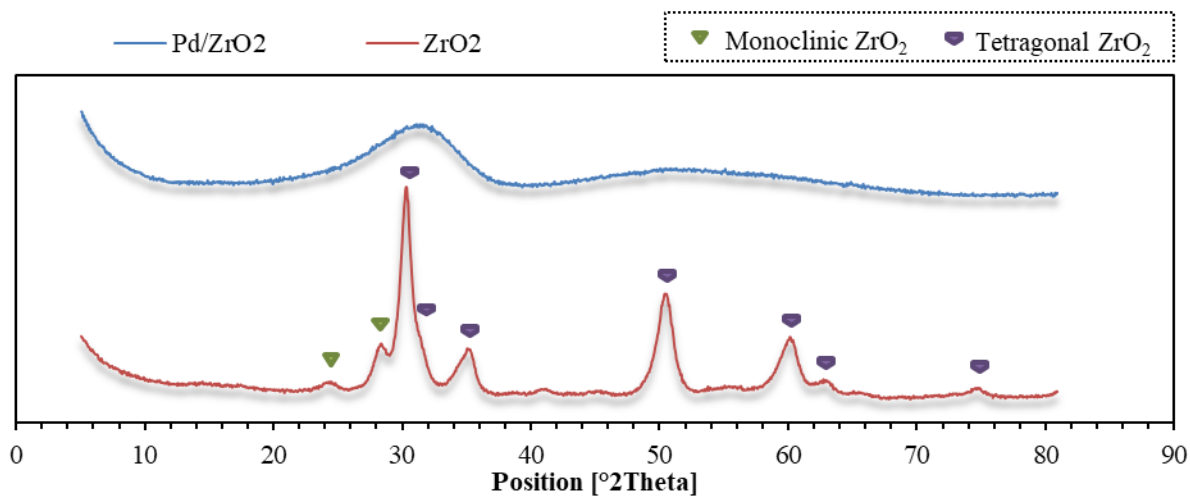
A high surface (120m^2/g) tetragonal ZrO_2 was synthesize by means of coprecipitation and the result was an amphoteric material containing Lewis acid and basic sites. It was then tested, and it was proven to be a suitable catalyst for the CTH of ML with ethanol as H-donor in the gas-phase. Tests performed with ethanol at different temperatures, provided a complete conversion of ML in all of the cases. As the temperature increased, GVL yield started to decrease, with a corresponding decrease in the carbon balance. This carbon loss was found to be mainly due to the formation of light compounds such as C3 and C4 unsaturated compounds. The main by-products observed were ethyl GVL and ethyl pentenoate, generated from the hydroxyalkylation of ALs by acetaldehyde (followed by dehydration of the intermediate and reduction of the double bond) and the alcoholysis of GVL, respectively. It was found that the optimized temperature for the reaction was 250°C, reaching a complete conversion of ML and a GVL yield of 67%. In addition, tests performed with EL as substrate confirm the absence of an equilibrium limitation for the intramolecular cyclization. A complete conversion of the ester was achieved, and both GVL and ethyl-GVL were the main products.

In addition, in order to compre the catalytic activity of the different crystalline phases, commercial monoclinic ZrO_2 was tested at different temperatures, however, the results obtained where not optimal. ML conversion was around 30% when working at 250 and 300 °C, with a low carbon balance, and low yields for GVL (>5%). When increasing the temperature to 400 °C ML conversion increased to 96%, however, carbon balance was still poor and GVL yield was 23%. Nonetheless, this comparison is not accurate given the low surface area of the commercial monoclinic ZrO_2 (3 m^2/g). Therefore, a high surface (117 m^2/g) monoclinic ZrO_2 was synthesized and, surprisingly, the result was a catalyst having a much higher basic density than tetragonal ZrO_2. It was then tested for the CTH of ML with ethanol as H-donor in the gas-phase at the previously

optimized conditions (250 °C). The results obtained were quite similar to those using tetragonal ZrO_2, however GLV yield reached a lower value (45%) and it yielded higher amount of EL. In addition, and noteworthy, ALs were seen in small quantities.

The catalytic tests performed using methanol and isopropanol as H-donor over tetragonal ZrO_2 lead to conclude the following:

- When using methanol as H-donor ML conversion reached a value of 35%, with low GVL yield (4%) and high carbon loss. EL shows a higher reactivity (conversion of 90%), however, is due to the transesterification of EL with methanol to form ML. Therefore, demonstrating that methanol is the least active alcohol for the CTH of alkyl levulinates.

- Isopropanol, on the other, is an excellent H-donor, achieving complete conversions of both ML and EL and high yields of GVL (80% and 50%, respectively). No ethyl GVL is formed since no hydroxyalkylating agent such as acetaldehyde is formed. Noteworthy, no isopropyl levulinate was detected, probably due to the higher steric hindrance of the secondary alcohol, which limits the transesterification.

The stability test at the optimized conditions in the gas-phase configuration (250°C and EtOH) using tetragonal ZrO_2 showed that the reaction is selective towards GVL for at least 300 min (yields of around 70%). After this, a progressive change in chemo-selectivity was seen. Moreover, when using monoclinic ZrO_2, the catalytic behaviour was quite similar, however the maximum yield for GVL (63%) was achieved faster, after 200 min. However, after this a sudden drop in both ML conversion and GVL yield was observed, followed by a change in chemo-selectivity of the reaction. With monoclinic ZrO_2, the yield of GVL and EL are equal when 250 minutes on stream have passed, while when using tetragonal ZrO_2, this only occurs after 430 minutes on stream. This difference in behaviour appears to be a consequence of the different acid and basic density presented in the catalysts.

Moreover, the characterization of the post reaction catalyst (tetragonal ZrO_2) showed the deposition of heavy compounds over the catalyst and a progressive loss of Lewis acid sites are

responsible of this progressive change in chemo-selectivity. In addition, the catalyst was successfully regenerated *in situ.* An almost complete recovery of the initial catalytic behaviour was achieved and DRIFT analyses with absorbed pyridine showed that a partial recovery of its Lewis acid sites was achieved.

The results obtained when using methanol as H-donor in the liquid-phase were in agreement with the ones from gas-phase tests, reaching a conversion of less than 5% and a yield for GVL of less than 1%. When using EL as substrate a higher conversion is achieved (25%), however, this is mainly due to the transesterification of EL to yield ML, only traces of GVL were detected. When using ethanol, the results are not comparable to those of the gas-phase. Indeed, a modest ML conversion of 22% was achieved and the selectivity of the reaction is once again oriented towards the formation of EL. On the other hand, starting from EL the conversion value was lower compared with ML (around 12%), but the transformation was selective towards GVL. Lastly, when using isopropanol, once again it was proven to be the most active as H-donor for CTH, reaching higher conversions and providing a higher selectivity towards GVL. ML and EL were converted (21% and 31%, respectively) quite selectively into GVL reaching higher yields (17% and 27%, respectively) after 8 h at 250 °C.

After testing the reusability and stability of catalysts in the liquid-phase configuration, it was seen that the selectivity of the reaction did not suffer any changes after recycling. However, there was a significant reduction of the activity. The spent catalyst was successfully regenerated achieving to recover the initial catalytic behaviour.

Moreover, the results obtained in the liquid-phase configuration lead to conclude that the gas-phase approach allows us to obtained better results in terms of productivity and GVL selectivity. In addition, it also allows us to work with a lower excess of alcohol and still obtain remarkable results in terms of conversion of the alkyl levulinates and GVL yield.

Catalytic tests performed by feeding the intermediate, α-AL, and main product, GVL, gave an insight of the overall reaction mechanism. In addition, it was possible to confirm that a change in chemoselectivity promoted side reactions such as the alcoholysis of ALs to EL.

In addition, a true sample of bio-ethanol was used as H-donor in the CTH of ML in the has-phase. A similar catalytic behaviour to that observed using pure ethanol was obtained. However, deactivation was seen earlier and at a faster rate, indicating the possible role played by impurities on the deactivation of the catalyst.

Moreover, the CTH of LA with ethanol provided remarkable results, achieving high yields in GVL. However, the same change in the chemo-selectivity (from GVL to EL) was observed at 250 °C. Nonetheless, increasing the reaction temperature, these phenomena were limited, reaching a steady GVL yield of around 50 %.

To try to improve the catalytic performance of the catalyst, Ti/Zr/O mixed oxide was synthesized and tested for the CTH of ML with ethanol. In this case the catalyst obtained had an acid density much higher than both tetragonal and monoclinic ZrO_2. However, the basic density was quite low, and it was not possible to quantify it by means of CO_2-TPD. Test conducted at different temperatures allowed a complete ML conversion in all of the cases. Interestingly, when working at 200 °C a high yield was achieved for GVL (60%), showing a similar behaviour to that obtained when using ZrO_2 at 250 °C. As the temperature increases, consecutive reaction over GVL start to occur, yielding high quantities of ethyl pentenoates.

Lastly, as reported in the literature, Pd/Fe_3O_4 was found to be active for the liquid-phase hydrogenolysis of 1,2-PDO, EG and glycerol, being selective for the production of ethanol. In addition, Pd/ZrO_2 was also found to be active for glycerol hydrogenolysis, reaching a conversion of 54% and an ethanol selectivity of 25%. Other products obtained where EG, 1,2-PDO and 1-propanol confirming that dehydration/hydrogenation and dehydrogenation/decarbonylation are the main reaction involved in the process. Moreover, substituting Pd with Ru over Fe_3O_4 was found to be also active for the hydrogenolysis of 1,2-PDO reaching a conversion of 42% and a selectivity

towards ethanol of 77%. However, when used for the hydrogenolysis of glycerol, the products obtained were 1,2-PDO corresponding to the dehydration/hydrogenation, low quantities of 1-propanol from further dehydration/hydrogenation of 1,2-PDO and low selectivity towards EG from the dehydrogenation/decarbonylation, but no ethanol was detected.

5. References

1. Anastas, P. T.; Warner, J. C. *Green Chemistry: Theory and Practice*. (1998).

2. Anastas, P. T.; Eghbali, N. Green Chemistry: Prinples and Practice. *Chem. Soc. Rev.* **39**, 301–312 (2010).

3. American Chemistry Society. What is Green Chemistry? https://www.acs.org/content/acs/en/greenchemistry/what-is-green-chemistry.html (2016).

4. Hilbold Nicolas-Julian, S. F. Bio-Based Building Blocks, Case Study of a Large-Scale Manufacturing Process. *Sustain. Green Chem.* **31**, 28–32 (2013).

5. Ghosh, D. *et al.* Fuels and chemicals from lignocellulosic biomass: An integrated biorefinery approach. *Energy and Fuels* **29**, 3149–3157 (2015).

6. Wettstein, S. G., Martin Alonso, D., Gürbüz, E. I. & Dumesic, J. A. A roadmap for conversion of lignocellulosic biomass to chemicals and fuels. *Curr. Opin. Chem. Eng.* **1**, 218–224 (2012).

7. Ahorsu, R., Medina, F. & Constantí, M. Significance and challenges of biomass as a suitable feedstock for bioenergy and biochemical production: A review. *Energies* **11**, (2018).

8. *S2Biom D8.2 Vision for 1 billion dry tonnes lignocellulosic biomass as a contribution to biobased economy by 2030 in Europe. 2016.*

9. Perlack, R. D. *et al. US Billion-Ton Update*. (2011).

10. Liu, W., Jiang, H. & Yu, H. Thermochemical conversion of lignin to functional materials: a review and future directions. *Green Chem.* **17**, 4888–4907 (2015).

11. Pileidis, F. D. & Titirici, M. M. Levulinic Acid Biorefineries: New Challenges for Efficient Utilization of Biomass. *ChemSusChem* **9**, 562–582 (2016).

12. Cherubini, F. The biorefinery concept: Using biomass instead of oil for producing energy and chemicals. *Energy Convers. Manag.* **51**, 1412–1421 (2010).

13.   Bridgwater, A. V & Peacocke, G. V. C. Fast pyrolysis processes for biomass. **4**, 1–73 (2000).

14.   Conti, R. Analytical pyrolysis and microextraction methods to characterize oil and biochar from thermal and catalytic cracking of biomass. (Alma Mater Studiorum – Università di Bologna, 2016).

15.   Marris, E. Black is the new green. *Nature* **442**, 624–626 (2006).

16.   Lehmann, J. & Joseh, S. Biochar for Environmental Management. in (eds. Lehmann, J. & Joseph, S.) 1–9 (Earthscan).

17.   Torri, C. *et al.* Preliminary investigation on the production of fuels and bio-char from Chlamydomonas reinhardtii biomass residue after bio-hydrogen production. *Bioresour. Technol.* **102**, 8707–8713 (2011).

18.   Manyà, J. J. Pyrolysis for biochar purposes: A review to establish current knowledge gaps and research needs. *Environ. Sci. Technol.* **46**, 7939–7954 (2012).

19.   Spath, P. L. & Dayton, D. C. Preliminary Screening -- Technical and Economic Assessment of Synthesis Gas to Fuels and Chemicals with Emphasis on the Potential for Biomass-Derived Syngas. (2003) doi:10.2172/15006100.

20.   Hamelinck, C. N., Van Hooijdonk, G. & Faaij, A. P. C. Ethanol from lignocellulosic biomass: Techno-economic performance in short-, middle- and long-term. *Biomass and Bioenergy* **28**, 384–410 (2005).

21.   Sun, Y. & Cheng, J. Hydrolysis of lignocellulosic materials for ethanol production: A review. *Bioresour. Technol.* **83**, 1–11 (2002).

22.   Demirbaş, A. Biodiesel fuels from vegetable oils via catalytic and non-catalytic supercritical alcohol transesterifications and other methods: A survey. *Energy Convers. Manag.* **44**, 2093–2109 (2003).

23.   Kamm, M., Kamm, B. & Gruber, P. R. *Biorefineries-Industrial Processes and Products: Status Quo and Future Directions*. (WILEY-VCH Verlag GmbH & Co. KGaA, 2008).

doi:10.1002/9783527619849.

24. Werpy, T. & Petersen, G. Top Value Added Chemicals from Biomass Volume I — Results of Screening for Potential Candidates from Sugars and Synthesis Gas. *U.S. Dep. Energy* (2004) doi:10.2172/15008859.

25. Kucharska, K. *et al.* Pretreatment of lignocellulosic materials as substrates for fermentation processes. *Molecules* **23**, 1–32 (2018).

26. Jørgensen, H., Kristensen, J. B. & Felby, C. Enzymatic conversion of lignocellulose into fermentable sugars: challenges and opportunities Henning. *Biofuels, Bioprod. Biorefining* **1**, 119–134 (2007).

27. Van de Vyver, S. *et al.* Catalytic production of levulinic acid from cellulose and other biomass-derived carbohydrates with sulfonated hyperbranched poly(arylene oxindole)s. *Energy Environ. Sci.* **4**, 3601 (2011).

28. Girisuta, B., Janssen, L. P. B. M. & Heeres, H. J. Green chemicals: A kinetic study on the conversion of glucose to levulinic acid. *Chem. Eng. Res. Des.* **84**, 339–349 (2006).

29. Yan, K., Jarvis, C., Gu, J. & Yan, Y. Production and catalytic transformation of levulinic acid: A platform for speciality chemicals and fuels. *Renew. Sustain. Energy Rev.* **51**, 986–997 (2015).

30. Girisuta, B., Janssen, L. P. B. M. & Heeres, H. J. Kinetic Cellulose to Levulinic acid.pdf. 1696–1708 (2007).

31. Yan, L., Yang, N., Pang, H. & Liao, B. Production of levulinic acid from bagasse and paddy straw by liquefaction in the presence of hydrochloride acid. *Clean - Soil, Air, Water* **36**, 158–163 (2008).

32. Lange, J. P. *et al.* Valeric biofuels: A platform of cellulosic transportation fuels. *Angew. Chemie - Int. Ed.* **49**, 4479–4483 (2010).

33. Serrano-Ruiz, J. C., Braden, D. J., West, R. M. & Dumesic, J. A. Conversion of cellulose to hydrocarbon fuels by progressive removal of oxygen. *Appl. Catal. B Environ.* **100**,

184–189 (2010).

34.   Cha, J. Y. & Hanna, M. A. Levulinic acid production based on extrusion and pressurized batch reaction. *Ind. Crops Prod.* **16**, 109–118 (2002).

35.   Bozell, J. J. *et al.* Production of levulinic acid and use as a platform chemical for derived products. *Resour. Conserv. Recycl.* **28**, 227–239 (2000).

36.   Hayes, D. J., Fitzpatrick, S., Hayes, M. H. B. & Ross, J. R. H. *Biorefineries: Industrial Processes and Products*. (Wiley-VCH, 2006).

37.   Huber, G. W., Iborra, S. & Corma, A. Synthesis of transportation fuels from biomass: Chemistry, catalysts, and engineering. *Chem. Rev.* **106**, 4044–4098 (2006).

38.   Uslu, H., Bayat, C., Gökmen, S. & Yorulmaz, Y. Reactive extraction of formic acid by amberlite LA-2 extractant. *J. Chem. Eng. Data* **54**, 48–53 (2009).

39.   Wang, P., Zhan, S. H. & Yu, H. B. *Advance in Ecological Environment Functional Materials and Ion Industry*. (2010).

40.   Redmon, B. C. Process for the production of levulinic acid. (1956).

41.   Hu, X. & Li, C. Z. Levulinic esters from the acid-catalysed reactions of sugars and alcohols as part of a bio-refinery. *Green Chem.* **13**, 1676–1679 (2011).

42.   Peng, L. *et al.* Catalytic conversion of cellulose to levulinic acid by metal chlorides. *Molecules* **15**, 5258–5272 (2010).

43.   Pratama, A. P., Rahayu, D. U. C. & Krisnandi, Y. K. Levulinic acid production from delignified rice husk waste over manganese catalysts: Heterogeneous versus homogeneous. *Catalysts* **10**, (2020).

44.   Krisnandi, Y. K. *et al.* Hierarchical MnOx/ZSM-5 as heterogeneous catalysts in conversion of delignified rice husk to levulinic acid. *Indones. J. Chem.* **19**, 115–123 (2019).

45.   Rackemann, D. W. & Doherty, W. O. The conversion of lignocellulosics to levulinic acid. *Biofuels, Bioprod. Biorefining* **5**, 198–214 (2011).

46. Osatiashtiani, A., Lee, A. F. & Wilson, K. Recent advances in the production of γ-valerolactone from biomass-derived feedstocks via heterogeneous catalytic transfer hydrogenation. *J. Chem. Technol. Biotechnol.* **92**, 1125–1135 (2017).

47. Andrew P Dunlop, S. S. Preparation of succinic acid. (1952).

48. Podolean, I. *et al.* Ru-based magnetic nanoparticles (MNP) for succinic acid synthesis from levulinic acid. *Green Chem.* **15**, 3077 (2013).

49. Carnevali, D., Rigamonti, M. G., Tabanelli, T., Patience, G. S. & Cavani, F. Levulinic acid upgrade to succinic acid with hydrogen peroxide. *Appl. Catal. A Gen.* **563**, 98–104 (2018).

50. Joshi, H., Moser, B. R., Toler, J., Smith, W. F. & Walker, T. Ethyl levulinate: A potential bio-based diluent for biodiesel which improves cold flow properties. *Biomass and Bioenergy* **35**, 3262–3266 (2011).

51. Lomba, L., Giner, B., Bandrés, I., Lafuente, C. & Pino, M. R. Physicochemical properties of green solvents derived from biomass. *Green Chem.* **13**, 2062 (2011).

52. Negus, M. P., Mansfield, A. C. & Leadbeater, N. E. The preparation of ethyl levulinate facilitated by flow processing: The catalyzed and uncatalyzed esterification of levulinic acid. *J. Flow Chem.* **5**, 148–150 (2015).

53. Pileidis, F. D., Tabassum, M., Coutts, S. & Titirici, M. Esterification of levulinic acid into ethyl levulinate catalysed by sulfonated hydrothermal carbons. *Chinese J. Catal.* **35**, 929–936 (2014).

54. Démolis, A., Essayem, N. & Rataboul, F. Synthesis and applications of alkyl levulinates. *ACS Sustain. Chem. Eng.* **2**, 1338–1352 (2014).

55. Wright, W. R. H. & Palkovits, R. Development of heterogeneous catalysts for the conversion of levulinic acid to γ-valerolactone. *ChemSusChem* **5**, 1657–1667 (2012).

56. Omoruyi, U., Page, S., Hallett, J. & Miller, P. W. Homogeneous catalyzed reactions of levulinic acid: To Γ-valerolactone and beyond. *ChemSusChem* **9**, 2037–2047 (2016).

57.   Upare, P. P. *et al.* Selective hydrogenation of levulinic acid to γ-valerolactone over carbon-supported noble metal catalysts. *J. Ind. Eng. Chem.* **17**, 287–292 (2011).

58.   Yan, K., Yang, Y., Chai, J. & Lu, Y. Catalytic reactions of gamma-valerolactone: A platform to fuels and value-added chemicals. *Appl. Catal. B Environ.* **179**, 292–304 (2015).

59.   Horváth, I. T., Mehdi, H., Fábos, V., Boda, L. & Mika, L. T. γ-Valerolactone-a sustainable liquid for energy and carbon-based chemicals. *Green Chem.* **10**, 238–242 (2008).

60.   Dutta, S. *et al.* Green synthesis of gamma-valerolactone (GVL) through hydrogenation of biomass-derived levulinic acid using non-noble metal catalysts: A critical review. *Chem. Eng. J.* **372**, 992–1006 (2019).

61.   Bereczky, Á., Lukács, K., Farkas, M. & Dóbé, S. Effect of γ-Valerolactone Blending on Engine Performance, Combustion Characteristics and Exhaust Emissions in a Diesel Engine. *Nat. Resour.* **05**, 177–191 (2014).

62.   Prat, D. *et al.* CHEM21 selection guide of classical- and less classical-solvents. *Green Chem.* **18**, 288–296 (2015).

63.   Fábos, V., Koczó, G., Mehdi, H., Boda, L. & Horváth, I. T. Bio-oxygenates and the peroxide number: A safety issue alert. *Energy Environ. Sci.* **2**, 767–769 (2009).

64.   Alonso, D. M., Wettstein, S. G. & Dumesic, J. A. Gamma-valerolactone, a sustainable platform molecule derived from lignocellulosic biomass. *Green Chem.* **15**, 584 (2013).

65.   Gilkey, M. J. & Xu, B. Heterogeneous Catalytic Transfer Hydrogenation as an Effective Pathway in Biomass Upgrading. *ACS Catal.* **6**, 1420–1436 (2016).

66.   Neves, P. *et al.* Production of biomass-derived furanic ethers and levulinate esters using heterogeneous acid catalysts. *Green Chem.* **15**, 3367 (2013).

67.   Zhang, P., Zhu, H. & Dai, S. Porous Carbon Supports: Recent Advances with Various Morphologies and Compositions. *ChemCatChem* **7**, 2788–2805 (2015).

68. He, J. *et al.* Cascade catalytic transfer hydrogenation – cyclization of ethyl levulinate to - valerolactone with Al – Zr mixed oxides. *Appl. Catal. A Gen.* **510**, 11–19 (2016).

69. Osakada, K., Ikariya, T. & Yoshikawa, S. Preparation and properties of hydride triphenyl-phosphine ruthenium complexes with 3-formyl (or acyl) propionate [RuH(ocochrchrcor′)(PPh3)3] (R H, CH3, C2H5;... *J. Organomet. Chem.* **231**, 79–90 (1982).

70. Mehdi, H. *et al.* Integration of homogeneous and heterogeneous catalytic processes for a multi-step conversion of biomass: From sucrose to levulinic acid, γ-valerolactone, 1,4-pentanediol, 2-methyl-tetrahydrofuran, and alkanes. *Top. Catal.* **48**, 49–54 (2008).

71. Phanopoulos, A., White, A. J. P., Long, N. J. & Miller, P. W. Catalytic Transformation of Levulinic Acid to 2-Methyltetrahydrofuran Using Ruthenium - N-Triphos Complexes. *ACS Catal.* **5**, 2500–2512 (2015).

72. Yan, Z. P., Lin, L. & Liu, S. Synthesis of γ-valerolactone by hydrogenation of biomass-derivedLevulinic acid over Ru/C catalyst. *Energy and Fuels* **23**, 3853–3858 (2009).

73. Schuette, H. A. & Thomas, R. W. NORMAL VALEROLACTONE. III. ITS PREPARATION BY THE CATALYTIC REDUCTION OF LEVULINIC ACID WITH HYDROGEN IN THE PRESENCE OF PLATINUM OXIDE. *J. Am. Chem. Soc.* **52**, 3010–3012 (1930).

74. Kyrides, L. P. & Craver, J. K. Process for the production of lactones. (1942).

75. Christian Jr, R. V., Brown, H. D. & Hixon, R. M. Derivatives of γ-Valerolactone, 1,4-Pentanediol and 1,4-Di-(β-cyanoethoxy)-pentane1. *J. Am. Chem. Soc.* **69**, 1961–1963 (1947).

76. Broadbent, H. S., Campbell, G. C., Bartley, W. J. & Johnson, J. H. Rhenium and Its Compounds as Hydrogenation Catalysts. III. Rhenium Heptoxide. *J. Org. Chem.* **24**, 1847–1854 (1959).

77. Manzer, L. E. Catalytic synthesis of α-methylene-γ-valerolactone: a biomass-derived acrylic monomer. *Appl. Catal. A Gen.* **272**, 249–256 (2004).

78. Manzer, L. E. No Title.

79. Dunlop, A. P. & Madden, J. W. Process of preparing gammavalerolactone. (1957).

80. Al-Shaal, M. G., Wright, W. R. H. & Palkovits, R. Exploring the ruthenium catalysed synthesis of γ-valerolactone in alcohols and utilisation of mild solvent-free reaction conditions. *Green Chem.* **14**, 1260–1263 (2012).

81. L. E. Manzer & Hutchenson, K. W. Production of 5-methyl-dihydro-furan-2-one from levulinic acid in supercritical media. (2004).

82. Galletti, A. M. R., Antonetti, C., De Luise, V. & Martinelli, M. A sustainable process for the production of γ-valerolactone by hydrogenation of biomass-derived levulinic acid. *Green Chem.* **14**, 688–694 (2012).

83. Chia, M. & Dumesic, J. A. Liquid-phase catalytic transfer hydrogenation and cyclization of levulinic acid and its esters to γ-valerolactone over metal oxide catalysts. *Chem. Commun.* **47**, 12233 (2011).

84. Gürbüz, E. I., Alonso, D. M., Bond, J. Q. & Dumesic, J. A. Reactive extraction of levulinate esters and conversion to γ-Valerolactone for production of liquid fuels. *ChemSusChem* **4**, 357–361 (2011).

85. Du, X. L. *et al.* Hydrogen-independent reductive transformation of carbohydrate biomass into ??-valerolactone and pyrrolidone derivatives with supported gold catalysts. *Angew. Chemie - Int. Ed.* **50**, 7815–7819 (2011).

86. Du, X. L., Bi, Q. Y., Liu, Y. M., Cao, Y. & Fan, K. N. Conversion of biomass-derived levulinate and formate esters into γ-valerolactone over supported gold catalysts. *ChemSusChem* **4**, 1838–1843 (2011).

87. Sudhakar, M. *et al.* Vapor phase hydrogenation of aqueous levulinic acid over hydroxyapatite supported metal (M=Pd, Pt, Ru, Cu, Ni) catalysts. *Appl. Catal. B Environ.* **180**, 113–120 (2016).

88. Balla, P., Perupogu, V., Vanama, P. K. & Komandur, V. R. C. Hydrogenation of biomass-

derived levulinic acid to γ-valerolactone over copper catalysts supported on ZrO2. *J. Chem. Technol. Biotechnol.* **91**, 769–776 (2016).

89. Boddien, A., Loges, B., Junge, H. & Beller, M. Hydrogen generation at ambient conditions: Application in fuel cells. in *ChemSusChem* vol. 1 751–758 (2008).

90. Holladay, J. D., Hu, J., King, D. L. & Wang, Y. An overview of hydrogen production technologies. *Catalysis Today* vol. 139 244–260 (2009).

91. Kuwahara, Y., Kaburagi, W., Osada, Y., Fujitani, T. & Yamashita, H. Catalytic transfer hydrogenation of biomass-derived levulinic acid and its esters to γ-valerolactone over ZrO2 catalyst supported on SBA-15 silica. *Catal. Today* **281**, 418–428 (2017).

92. Scholz, D., Aellig, C. & Hermans, I. Catalytic transfer hydrogenation/hydrogenolysis for reductive upgrading of furfural and 5-(hydroxymethyl)furfural. *ChemSusChem* **7**, 268–275 (2014).

93. Yang, Z., Huang, Y.-B., Guo, Q.-X. & Fu, Y. RANEY® Ni catalyzed transfer hydrogenation of levulinate esters to γ-valerolactone at room temperature. *Chem. Commun.* **49**, 5328 (2013).

94. Kuwahara, Y., Kaburagi, W. & Fujitani, T. Catalytic transfer hydrogenation of levulinate esters to γ-valerolactone over supported ruthenium hydroxide catalysts. *RSC Adv.* **4**, 45848–45855 (2014).

95. Yun, W. C., Lin, T. Y., Chiu, H. Y. & Lin, K. Y. A. Microwave Irradiation-Enhanced Catalytic Transfer Hydrogenation of Levulinic Acid to γ-Valerolactone Using Ruthenium: A Comparative Study with Conventional Heating Processes. *Waste and Biomass Valorization* **11**, 2783–2793 (2020).

96. Tanwongwan, W. *et al.* Simultaneous activation of copper mixed metal oxide catalysts in alcohols for gamma-valerolactone production from methyl levulinate. *Appl. Catal. A Gen.* **579**, 91–98 (2019).

97. Yu, Z. *et al.* Catalytic Transfer Hydrogenation of Levulinic Acid to γ-Valerolactone over Ni3P-CePO4 Catalysts. *Ind. Eng. Chem. Res.* **59**, 7416–7425 (2020).

98. Yu, Z. *et al.* Aqueous Phase Hydrodeoxygenation of Phenol over Ni3P-CePO4 Catalysts. *Ind. Eng. Chem. Res.* **57**, 10216–10225 (2018).

99. Komanoya, T., Nakajima, K., Kitano, M. & Hara, M. Synergistic Catalysis by Lewis Acid and Base Sites on ZrO2 for Meerwein-Ponndorf-Verley Reduction. *J. Phys. Chem. C* **119**, 26540–26546 (2015).

100. Tang, X. *et al.* Conversion of biomass to γ-valerolactone by catalytic transfer hydrogenation of ethyl levulinate over metal hydroxides. *Appl. Catal. B Environ.* **147**, 827–834 (2014).

101. Leng, Y., Shi, L., Du, S., Jiang, J. & Jiang, P. A tannin-derived zirconium-containing porous hybrid for efficient Meerwein-Ponndorf-Verley reduction under mild conditions. *Green Chem.* **22**, 180–186 (2020).

102. Song, J. *et al.* A new porous Zr-containing catalyst with a phenate group: An efficient catalyst for the catalytic transfer hydrogenation of ethyl levulinate to γ-valerolactone. *Green Chem.* **17**, 1626–1632 (2015).

103. Valvekens, P., Vandichel, M., Waroquier, M., Van Speybroeck, V. & De Vos, D. Metal-dioxidoterephthalate MOFs of the MOF-74 type: Microporous basic catalysts with well-defined active sites. *J. Catal.* **317**, 1–10 (2014).

104. Gliński, M. & Ulkowska, U. Reactivity of alcohols in chemoselective transfer hydrogenation of acrolein over magnesium oxide as the catalyst. *Catal. Letters* **141**, 293–299 (2011).

105. Grazia, L. *et al.* Gas-phase cascade upgrading of furfural to 2-methylfuran using methanol as a H-transfer reactant and MgO based catalysts. *Catal. Sci. Technol.* **6**, 4418–4427 (2016).

106. Li, F. *et al.* Catalytic transfer hydrogenation of butyl levulinate to Γ-valerolactone over zirconium phosphates with adjustable Lewis and BrØnsted acid sites. *Appl. Catal. B Environ.* **214**, 67–77 (2017).

107. Cirujano, F. G., Corma, A. & Llabrés i Xamena, F. X. Conversion of levulinic acid into

chemicals: Synthesis of biomass derived levulinate esters over Zr-containing MOFs. *Chem. Eng. Sci.* **124**, 52–60 (2015).

108. Wang, J., Jaenicke, S. & Chuah, G. K. Zirconium-Beta zeolite as a robust catalyst for the transformation of levulinic acid to γ-valerolactone via Meerwein-Ponndorf-Verley reduction. *RSC Adv.* **4**, 13481–13489 (2014).

109. Lai, J. *et al.* Catalytic Transfer Hydrogenation of Biomass-Derived Ethyl Levulinate into Gamma-Valerolactone Over Graphene Oxide-Supported Zirconia Catalysts. *Catal. Letters* **149**, 2749–2757 (2019).

110. Sakakibara, K., Endo, K. & Osawa, T. Facile synthesis of Γ-valerolactone by transfer hydrogenation of methyl levulinate and levulinic acid over Ni/ZrO2. *Catal. Commun.* **125**, 52–55 (2019).

111. Zhou, S. *et al.* Zirconium–lignosulfonate polyphenolic polymer for highly efficient hydrogen transfer of biomass-derived oxygenates under mild conditions. *Appl. Catal. B Environ.* **248**, 31–43 (2019).

112. Tang, X. *et al.* Conversion of biomass-derived ethyl levulinate into γ-valerolactone via hydrogen transfer from supercritical ethanol over a ZrO2 catalyst. *RSC Adv.* **3**, 10277 (2013).

113. Grazia, L. *et al.* Exploiting H-transfer as a tool for the catalytic reduction of bio-based building blocks: The gas-phase production of 2-methylfurfural using a FeVO4 catalyst. *Green Chem.* **19**, 4412–4422 (2017).

114. Di Cosimo, J. I., Acosta, A. & Apesteguía, C. R. Allylic alcohol synthesis by gas-phase hydrogen transfer reduction of unsaturated ketones. *J. Mol. Catal. A Chem.* **234**, 111–120 (2005).

115. Cosimo, J. I. D., Acosta, A. & Apesteguía, C. R. Gas-phase hydrogen transfer reduction of α,β-unsaturated ketones on Mg-based catalysts. *J. Mol. Catal. A Chem.* **222**, 87–96 (2004).

116. Kobayashi, H. & Fukuoka, A. Synthesis and utilisation of sugar compounds derived from

lignocellulosic biomass. *Green Chem.* **15**, 1740–1763 (2013).

117. Isikgor, F. H. & Becer, C. R. Lignocellulosic biomass: a sustainable platform for the production of bio-based chemicals and polymers. *Polym. Chem.* **6**, 4497–4559 (2015).

118. Zaldivar, J., Nielsen, J. & Olsson, L. Fuel ethanol production from lignocellulose: A challenge for metabolic engineering and process integration. *Appl. Microbiol. Biotechnol.* **56**, 17–34 (2001).

119. Kennes, D., Abubackar, H. N., Diaz, M., Veiga, M. C. & Kennes, C. Bioethanol production from biomass: Carbohydrate vs syngas fermentation. *J. Chem. Technol. Biotechnol.* **91**, 304–317 (2016).

120. Song, H. *et al.* Direct conversion of cellulose into ethanol catalysed by a combination of tungstic acid and zirconia-supported Pt nanoparticles. *Chem. Commun.* **55**, 4303–4306 (2019).

121. Wu, C. T. *et al.* A non-syn-gas catalytic route to methanol production. *Nat. Commun.* **3**, (2012).

122. Musolino, M. G., Scarpino, L. A., Mauriello, F. & Pietropaolo, R. Glycerol hydrogenolysis promoted by supported palladium catalysts. *ChemSusChem* **4**, 1143–1150 (2011).

123. Luque, R. *et al.* Biofuels: A technological perspective. *Energy Environ. Sci.* **1**, 542–564 (2008).

124. Liao, F. *et al.* Tunability of catalytic properties of Pd-based catalysts by rational control of strong metal and support interaction (SMSI) for selective hydrogenolyic C-C and C-O bond cleavage of ethylene glycol units in biomass molecules. *Catal. Sci. Technol.* **5**, 3491–3495 (2015).

125. Bozell, J. J. & Petersen, G. R. Technology development for the production of biobased products from biorefinery carbohydrates - The US Department of Energy's 'top 10' revisited. *Green Chem.* **12**, 539–554 (2010).

126. Nda-Umar, U. I., Ramli, I., Taufiq-Yap, Y. H. & Muhamad, E. N. An overview of recent research in the conversion of glycerol into biofuels, fuel additives and other bio-based chemicals. *Catalysts* **9**, (2019).

127. Gumina, B., Mauriello, F., Pietropaolo, R., Galvagno, S. & Espro, C. Hydrogenolysis of sorbitol into valuable C3-C2 alcohols at low H2pressure promoted by the heterogeneous Pd/Fe3O4catalyst. *Mol. Catal.* **446**, 152–160 (2018).

128. Gumina, B., Espro, C., Galvagno, S., Pietropaolo, R. & Mauriello, F. Bioethanol Production from Unpretreated Cellulose under Neutral Selfsustainable Hydrolysis/Hydrogenolysis Conditions Promoted by the Heterogeneous Pd/Fe3O4 Catalyst. *ACS Omega* **4**, 352–357 (2019).

129. De, S., Saha, B. & Luque, R. Hydrodeoxygenation processes: Advances on catalytic transformations of biomass-derived platform chemicals into hydrocarbon fuels. *Bioresour. Technol.* **178**, 108–118 (2015).

130. Connor, R. & Adkins, H. Hydrogenolysis of oxygenated organic compounds. *J. Am. Chem. Soc.* **54**, 4678–4690 (1932).

131. Ruppert, A. M., Weinberg, K. & Palkovits, R. Hydrogenolysis goes bio: From carbohydrates and sugar alcohols to platform chemicals. *Angew. Chemie - Int. Ed.* **51**, 2564–2601 (2012).

132. Zhang, J., Li, J. B., Wu, S. Bin & Liu, Y. Advances in the catalytic production and utilization of sorbitol. *Ind. Eng. Chem. Res.* **52**, 11799–11815 (2013).

133. Gallegos-Suarez, E., Guerrero-Ruiz, A., Rodriguez-Ramos, I. & Arcoya, A. Comparative study of the hydrogenolysis of glycerol over Ru-based catalysts supported on activated carbon, graphite, carbon nanotubes and KL-zeolite. *Chem. Eng. J.* **262**, 326–333 (2015).

134. Menchavez, R. N., Morra, M. J. & He, B. B. Co-production of ethanol and 1,2-propanediol via glycerol hydrogenolysis using Ni/Ce-Mg catalysts: Effects of catalyst preparation and reaction conditions. *Catalysts* **7**, 1–14 (2017).

135. Wang, X., Hao, Y. & Keane, M. A. Selective gas phase hydrogenation of p -

nitrobenzonitrile to p -aminobenzonitrile over zirconia supported gold. **510**, 171–179 (2016).

136. Espro, C., Gumina, B., Paone, E. & Mauriello, F. Upgrading lignocellulosic biomasses: Hydrogenolysis of platform derived molecules promoted by heterogeneous Pd-Fe catalysts. *Catalysts* **7**, (2017).

137. Espro, C., Gumina, B., Szumelda, T., Paone, E. & Mauriello, F. Catalytic transfer hydrogenolysis as an effective tool for the reductive upgrading of cellulose, hemicellulose, lignin, and their derived molecules. *Catalysts* **8**, (2018).

138. Mauriello, F. *et al.* Exploring the catalytic properties of supported palladium catalysts in the transfer hydrogenolysis of glycerol. *Appl. Catal. B Environ.* **166–167**, 121–131 (2015).

139. Vilcocq, L., Cabiac, A., Especel, C., Guillon, E. & Duprez, D. Transformation du sorbitol en biocarburants par catalyse hétérogène: Considerations chimiques et industrielles. *Oil Gas Sci. Technol.* **68**, 841–860 (2013).

140. Van Ryneveld, E., Mahomed, A. S., Van Heerden, P. S., Green, M. J. & Friedrich, H. B. A catalytic route to lower alcohols from glycerol using Ni-supported catalysts. *Green Chem.* **13**, 1819–1827 (2011).

141. Yang, C. *et al.* Hydrogenolysis of methyl glycolate to ethanol over a Pt-Cu/SiO 2 single-atom alloy catalyst: A further step from cellulose to ethanol. *Green Chem.* **20**, 2142–2150 (2018).

142. Zhu, S. *et al.* Promoting effect of boron oxide on Cu/SiO2 catalyst for glycerol hydrogenolysis to 1,2-propanediol. *J. Catal.* **303**, 70–79 (2013).

143. Zhu, Y. *et al.* Construction of Cu/ZrO 2 /Al 2 O 3 composites for ethanol synthesis: Synergies of ternary sites for cascade reaction. *Appl. Catal. B Environ.* **166–167**, 551–559 (2015).

144. Tronci, S. & Pittau, B. Conversion of glucose and sorbitol in the presence of Ru/C and Pt/C catalysts. *RSC Adv.* **5**, 23086–23093 (2015).

145. Miyazawa, T., Kusunoki, Y., Kunimori, K. & Tomishige, K. Glycerol conversion in the aqueous solution under hydrogen over Ru/C + an ion-exchange resin and its reaction mechanism. *J. Catal.* **240**, 213–221 (2006).

146. Mane, R., Patil, S., Shirai, M., Rayalu, S. & Rode, C. Influence of carbon based supports on selectivity behavior of diols and propanol in Ru catalyzed glycerol hydrogenolysis. *Appl. Catal. B Environ.* **204**, 134–146 (2017).

147. Zhao, H., Zheng, L., Li, X., Chen, P. & Hou, Z. Hydrogenolysis of glycerol to 1,2-propanediol over Cu-based catalysts: A short review. *Catal. Today* 0–1 (2019) doi:10.1016/j.cattod.2019.03.011.

148. Jin, X. *et al.* Sorbitol Hydrogenolysis over Hybrid Cu/CaO-Al2O3 Catalysts: Tunable Activity and Selectivity with Solid Base Incorporation. *ACS Catal.* **5**, 6545–6558 (2015).

149. Guo, L., Zhou, J., Mao, J., Guo, X. & Zhang, S. Supported Cu catalysts for the selective hydrogenolysis of glycerol to propanediols. *Appl. Catal. A Gen.* **367**, 93–98 (2009).

150. Shozi, M. L. *et al.* An investigation of Cu-Re-ZnO catalysts for the hydrogenolysis of glycerol under continuous flow conditions. *Sustain. Energy Fuels* **1**, 1437–1445 (2017).

151. Li, N. & Huber, G. W. Aqueous-phase hydrodeoxygenation of sorbitol with Pt/SiO2-Al2O3: Identification of reaction intermediates. *J. Catal.* **270**, 48–59 (2010).

152. Seretis, A. & Tsiakaras, P. Aqueous phase reforming (APR) of glycerol over platinum supported on Al2O3 catalyst. *Renew. Energy* **85**, 1116–1126 (2016).

153. Li, C. *et al.* One-pot chemocatalytic transformation of cellulose to ethanol over Ru-WOx/HZSM-5. *Green Chem.* **21**, 2234–2239 (2019).

154. Ji, N. *et al.* Direct catalytic conversion of cellulose into ethylene glycol using nickel-promoted tungsten carbide catalysts. *Angew. Chemie - Int. Ed.* **47**, 8510–8513 (2008).

155. Zheng, M. Y. *et al.* Transition metal-tungsten bimetallic catalysts for the conversion of cellulose into ethylene glycol. *ChemSusChem* **3**, 63–66 (2010).

156. Zhang, Y., Wang, A. & Zhang, T. A new 3D mesoporous carbon replicated from

commercial silica as a catalyst support for direct conversion of cellulose into ethylene glycol. *Chem. Commun.* **46**, 862–864 (2010).

157. Tai, Z., Zhang, J., Wang, A., Zheng, M. & Zhang, T. Temperature-controlled phase-transfer catalysis for ethylene glycol production from cellulose. *Chem. Commun.* **48**, 7052–7054 (2012).

158. Liu, Y., Luo, C. & Liu, H. Tungsten trioxide promoted selective conversion of cellulose into propylene glycol and ethylene glycol on a ruthenium catalyst. *Angew. Chemie - Int. Ed.* **51**, 3249–3253 (2012).

159. Ji, N., Zheng, M., Wang, A., Zhang, T. & Chen, J. G. Nickel-promoted tungsten carbide catalysts for cellulose conversion: Effect of preparation methods. *ChemSusChem* **5**, 939–944 (2012).

160. Wang, A. & Zhang, T. One-pot conversion of cellulose to ethylene glycol with multifunctional tungsten-based catalysts. *Acc. Chem. Res.* **46**, 1377–1386 (2013).

161. Liu, Q. *et al.* Selective Cellulose Hydrogenolysis to Ethanol Using Ni@C Combined with Phosphoric Acid Catalysts. *ChemSusChem* 3977–3987 (2019) doi:10.1002/cssc.201901110.

162. Deng, J., Ren, P., Deng, D. & Bao, X. Enhanced electron penetration through an ultrathin graphene layer for highly efficient catalysis of the hydrogen evolution reaction. *Angew. Chemie - Int. Ed.* **54**, 2100–2104 (2015).

163. Su, J. *et al.* Ruthenium-cobalt nanoalloys encapsulated in nitrogen-doped graphene as active electrocatalysts for producing hydrogen in alkaline media. *Nat. Commun.* **8**, 1–10 (2017).

164. Liao, F. *et al.* PdFe nanoparticles as selective catalysts for C-C cleavage in hydrogenolysis of vicinal diol units in biomass-derived chemicals. *Catal. Sci. Technol.* **5**, 887–896 (2015).

165. Musolino, M. G., Scarpino, L. A., Busacca, C. & Mauriello, F. Selective Hydrogenolysis of Glycerol to Propylene glycol over supported Palladium Catalysts : Effect of Support. **1727**, 2008 (2008).

166. Mauriello, F. *et al.* Hydrogenolysis vs. aqueous phase reforming (APR) of glycerol promoted by a heterogeneous Pd/Fe catalyst. *Catal. Sci. Technol.* **5**, 4466–4473 (2015).

167. Liao, F., Lo, T. W. B. & Tsang, S. C. E. Recent Developments in Palladium-Based Bimetallic Catalysts. *ChemCatChem* **7**, 1998–2014 (2015).

168. G.K. Chuah , S. Jaenicke, S.A. Cheong, K. S. C. The influence of preparation conditions on the surface area of zirconia. *Science (80-.).* **131**, 267–284 (1996).

169. Afanasiev, P. Mixed TiO2-ZrO2 support for hydrotreating, obtained by co-precipitation from Zr basic carbonate and Ti oxosulfate. *Catal. Commun.* **9**, 734–739 (2008).

170. Trevisanut, C., Mari, M., Millet, J.-M. M. & Cavani, F. Chemical-loop reforming of ethanol over metal ferrites: An analysis of structural features affecting reactivity. *Int. J. Hydrogen Energy* **40**, 5264–5271 (2015).

171. Chuah, G. K. & Jaenicke, S. The preparation of high surface area zirconia — Influence of precipitating agent and digestion. *Appl. Catal. A Gen.* **163**, 261–273 (1997).

172. Srinivasan, R., Harris, M., Simpson, S. F., Deangelis, R. J. & Davis, B. Zirconium oxide crystal phase: The role of the pH and time to attain the final pH for precipitation of the hydrous oxide. **3**, 787–797 (1988).

173. Gazzoli, D., Mattei, G. & Valigi, M. Raman and X-ray investigations of the incorporation of Ca2+ and Cd2+ in the ZrO2 structure. *J. Raman Spectrosc.* **38**, 824–831 (2007).

174. Murugendrappa, M. V. *et al.* Effect of fuels on conductivity, dielectric and humidity sensing properties of ZrO2 nanocrystals prepared by low temperature solution combustion method. *J. Asian Ceram. Soc.* **4**, 309–318 (2016).

175. Phillipp.Cm & Mazdiyas.Ks. Infrared and raman spectra of zirconia polymorphs. *J. Am. Ceram. Soc.* **54**, 254–258 (1971).

176. Clearfield, A., Serrette, G. P. D. & Khazi-Syed, A. H. Nature of hydrous zirconia and sulfated hydrous zirconia. *Catal. Today* **20**, 295–312 (1994).

177. Chuah, G. K. An Investigation into the Preparation of High Surface Area Zirconia. *Catal.*

Today **49**, 131–139 (1999).

178. Arena, F., Chio, R. Di & Trunfio, G. An experimental assessment of the ammonia temperature programmed desorption method for probing the surface acidic properties of heterogeneous catalysts . *Appl. Catal. A-Gen.* **503**, 227–236 (2015).

179. Busca, G. The surface acidity of solid oxides and its characterization by IR spectroscopic methods. An attempt at systematization. *Phys. Chem. Chem. Phys.* **1**, 723–736 (1999).

180. Oliviero, L. *et al.* 2,6-Dimethylpyridine as a probe of the strength of Brønsted acid sites: Study on zeolites. Application to alumina. *Phys. Chem. Chem. Phys.* **7**, 1861–1869 (2005).

181. Cheng, Y., Zhang, H., Jaenicke, J. A., Tan, E. C. P. & Chuah, G. K. Minimalistic Synthesis of α-Zirconium Diammonium Phosphate and Zirconia for Applications in Ion Exchange and Catalysis. *ACS Sustain. Chem. Eng.* **7**, 895–904 (2019).

182. Albuquerque, E. M., Borges, L. E. P., Fraga, M. A. & Sievers, C. Relationship between Acid–Base Properties and the Activity of ZrO2-Based Catalysts for the Cannizzaro Reaction of Pyruvaldehyde to Lactic Acid. *ChemCatChem* **9**, 2675–2683 (2017).

183. Sun, D., Takahashi, Y., Yamada, Y. & Sato, S. Efficient formation of angelica lactones in a vapor-phase conversion of levulinic acid. *Appl. Catal. A Gen.* **526**, 62–69 (2016).

184. Xin, J. *et al.* Formation of C-C bonds for the production of bio-alkanes under mild conditions. *Green Chem.* **16**, 3589–3595 (2014).

185. Lima, C. G. S., Monteiro, J. L., de Melo Lima, T., Weber Paixão, M. & Corrêa, A. G. Angelica Lactones: From Biomass-Derived Platform Chemicals to Value-Added Products. *ChemSusChem* (2017) doi:10.1002/cssc.201701469.

186. Zhao, Y., Li, W., Zhang, M. & Tao, K. A comparison of surface acidic features between tetragonal and monoclinic nanostructured zirconia. *Catal. Commun.* **3**, 239–245 (2002).

187. Franchini, C. A., Duarte de Farias, A. M., Albuquerque, E. M., dos Santos, R. & Fraga, M. A. Single-stage medium temperature water-gas shift reaction over Pt/ZrO 2 - Support structural polymorphism and catalyst deactivation. *Appl. Catal. B Environ.* **117**–**118**, 302–

309 (2012).

188. Jacob, K. H., Knözinger, E. & Benier, S. Adsorption sites on polymorphic zirconia. *J. Mater. Chem.* **3**, 651–657 (1993).

189. Wang, Y. *et al.* Transfer Hydrogenation of Alkenes Using Ethanol Catalyzed by a NCP Pincer Iridium Complex: Scope and Mechanism. *J. Am. Chem. Soc.* **140**, 4417–4429 (2018).

190. Chen, T. *et al.* Degradable polymers from ring-opening polymerization of α-angelica lactone, a five-membered unsaturated lactone. *Polym. Chem.* **2**, 1190–1194 (2011).

191. Kon, K., Onodera, W. & Shimizu, K. Selective hydrogenation of levulinic acid to valeric acid and valeric biofuels by a Pt/HMFI catalyst. *Catal. Sci. Technol.* **4**, 3227–3234 (2014).

192. Lahousse, C., Aboulayt, A., Maugé, F., Bachelier, J. & Lavalley, J. C. Acidic and basic properties of zirconia-alumina and zirconia-titania mixed oxides. *J. Mol. Catal.* **84**, 283–297 (1993).

193. Schwickardi, M., Johann, T., Schmidt, W. & Schu, F. High-Surface-Area Oxides Obtained by an Activated Carbon Route. 3913–3919 (2002).

194. Thi, N., Huyen, T., Nhung, N. H., Thanh, L. & Khanh, P. D. Preparation and characterization of zerovalent iron nanoparticles. **56**, 226–230 (2018).

195. Bhogeswararao, S. & Srinivas, D. Catalytic conversion of furfural to industrial chemicals over supported Pt and Pd catalysts. *J. Catal.* **327**, 65–77 (2015).

196. Chan, C. W. A. *et al.* New environmentally friendly catalysts containing Pd-interstitial carbon made from Pd-glucose precursors for ultraselective hydrogenations in the liquid phase. *Chem. Commun.* **47**, 7971–7973 (2011).

197. Ryu, J. C. *et al.* Effect of additives on redox behavior of iron oxide for chemical hydrogen storage. *J. Ind. Eng. Chem.* **14**, 252–260 (2008).

198. Guerrini, E., Vallini, S., Colombo, A., Trasatti, S. P. & Trasatti, S. Anodic films containing zirconia nanoparticles for corrosion protection of AA1050 aluminum alloy.

1457–1468 (2014) doi:10.1007/s10008-013-2274-1.

199.   Vásquez, P. B. *et al.* Gas-Phase Catalytic Transfer Hydrogenation of Methyl Levulinate with Ethanol over ZrO2. *ACS Sustain. Chem. Eng.* **7**, 8317–8330 (2019).

200.   Tabanelli, T. *et al.* Transfer Hydrogenation of Methyl and Ethyl Levulinate Promoted by a ZrO2 Catalyst: Comparison of Batch vs Continuous Gas-Flow Conditions. *ACS Sustain. Chem. Eng.* **7**, 9937–9947 (2019).